Mapping Bushfire Distribution and Burn Severity in West Africa Using Remote Sensing Observations

Satellitengestützte Kartierung der Verteilung von Buschfeuern und ihrer Auswirkung auf die Vegetation in Westafrika

Dissertation zur Erlangung des
naturwissenschaftlichen Doktorgrades
der Julius-Maximilians-Universität Würzburg

A bushfire in Pendjari National Park (photo taken on February 3, 2008)

vorgelegt von

Noellie Ahou RÜTH geb. YAO
aus
Dimbokro (Elfenbeinküste)

Würzburg 2010

Mapping Bushfire Distribution and Burn Severity in West Africa Using Remote Sensing Observations

Satellitengestützte Kartierung der Verteilung von Buschfeuern und ihrer Auswirkung auf die Vegetation in Westafrika

Dissertation zur Erlangung des
naturwissenschaftlichen Doktorgrades
der Julius-Maximilians-Universität Würzburg

vorgelegt von

Noellie Ahou RÜTH geb. YAO
aus
Dimbokro (Elfenbeinküste)

Würzburg 2010

Eingereicht am: ……

Mitglieder der Promotionskommission:

Vorsitzender: …….

Gutachter: Prof. Dr. K. Eduard Linsenmair

Gutachter: Prof. Dr. Stefan Dech

Tag des Promotionskolloquiums: ……

Doktorurkunde ausgehändigt am: ….....

Je dédie cette thèse

A mon père défunt Yao Kouassi Siméon,
ma mère Kouassi Aya Rose pour son très grand amour maternel,
à mes frères et à mes sœurs.

ABSTRACT

Fire has long been considered to be the main ecological factor explaining the origin and maintenance of West African savannas. It has a very high occurrence in these savannas due to high human pressure caused by strong demographic growth and, concomitantly, is used to transform natural savannas into farmland and is also used as a provider of energy. This study was carried out with the support of the BIOTA project funded by the German ministry for Research and Education. The objective of this study is to establish the spatial and temporal distribution of bushfires during a long observation period from 2000 to 2009 as well as to assess fire impact on vegetation through mapping of the burn severity; based on remote sensing and field data collections.

Remote sensing was used for this study because of the advantages that it offers in collecting data for long time periods and on different scales. In this case, the Moderate Resolution Imaging Spectroradiometer (MODIS) satellite instrument at 1km resolution is used to assess active fires, and understand the seasonality of fire, its occurrence and its frequency within the vegetation types on a regional scale. Landsat ETM+ imagery at 30 m and field data collections were used to define the characteristics of burn severity related to the biomass loss on a local scale.

At a regional scale, the occurrence of fires and rainfall per month correlated very well (R^2 = 0.951, r = -0.878, $P < 0.01$), which shows that the lower the amount of rainfall, the higher the fire occurrence and vice versa.

In the dry season, four fire seasons were determined on a regional scale, namely very early fires, which announce the beginning of the fires, early and late fires making up the peak of fire in December/January and very late fires showing the end of the fire season and the beginning of the rainy season.

Considerable fire activity was shown to take place in the vegetation zones between the Forest and the Sahel areas. Within these zones, parts of the Sudano-Guinean and the Guinean zones showed a high pixel frequency, i.e. fires occurred in the same place in many years. This high pixel frequency was also found in most protected areas in these zones.

As to the kinds of land cover affected by fire, the highest fire occurrence is observed within the Deciduous woodlands and Deciduous shrublands.

Concerning the burn severity, which was observed at a local scale, field data correlated closely with the ΔNBR derived from Landsat scenes of Pendjari National Park (R^2 = 0.76). The correlation coefficient according to Pearson is r = 0.84 and according to Spearman-Rho,

the correlation coefficient is r = 0.86. Very low and low burn severity (with ΔNBR value from 0 to 0.40) affected the vegetation weakly (0-35 percent of biomass loss) whereas moderate and high burn severity greatly affected the vegetation, leading to up to 100 percent of biomass loss, with the ΔNBR value ranging from 0.41 to 0.99.

It can be seen from these results that remotely sensed images offer a tool to determine the fire distribution over large regions in savannas and that the Normalised Burn Ratio index can be applied to West Africa savannas.

The outcomes of this thesis will hopefully contribute to understanding and, eventually, improving fire regimes in West Africa and their response to climate change and changes in vegetation diversity.

ZUSAMMENFASSUNG

Feuer ist ein wichtiger ökologischer Faktor für die Biokomplexität und den Fortbestand der westafrikanischen Savannen. Feuer kommt in westafrikanischen Savannen - insbesondere wegen des hohen Bevölkerungsdrucks infolge des starken Bevölkerungswachstums – immer häufiger vor. Es wird sowohl zur Umwandlung natürlicher Savannen in landwirtschaftliche Flächen als auch als Energielieferant verwendet. Diese Studie wurde mit der Unterstützung des BIOTA-Projekts durchgeführt, das vom Bundesministerium für Bildung und Forschung, BMBF, gefördert wird. Ziel dieser Dissertation ist die Bestimmung der räumlichen und zeitlichen Verteilung von Buschfeuern während eines langen Beobachtungszeitraumes (2000-2009) sowie die Kartierung von Brandschäden zum Verständnis der Auswirkung von Feuer auf die lokale Vegetationsstruktur. Fernerkundungs- sowie Felddaten werden in dieser Arbeit verwertet.

Fernerkundungsdaten wurden für diese Studie verwendet, da sie größere Flächen abdecken und die Daten über längere Zeiträume in verschiedenen Maßstäben zur Verfügung stehen. Daten des Moderate Resolution Imaging Spectroradiometer (MODIS)-Satelliten mit einer Auflösung von 1 km wurden verwendet, um in regelmäßigen Abständen aktive Feuer zu kartieren und die saisonale Verteilung von Feuern, ihr Vorkommen und ihre Häufigkeit nach Vegetationstyp zu bestimmen. Mit Landsat ETM+ Satellitendaten (Auflösung von 30 Metern) und Felddaten wurden auf einem lokalen Maßstab Brandschadensklassen definiert. Mittels der Biomasse-Felddaten wurde dann der Biomasse-Verlust abgeschätzt.

Die Feuerhäufigkeit, mittels Satellitendaten ermittelt, und der Niederschlag pro Monat zeigen eine sehr gute Korrelation ($R^2 = 0.951$, $r = -0.878$, $P < 0.01$). Daraus lässt sich schließen, dass Feuer bevorzugt in den Monaten vorkommen, in denen es wenig Niederschlag gibt und umgekehrt.

Auf regionaler Ebene wurden innerhalb der Trockenzeit vier Feuer-Perioden identifiziert; ‚sehr frühe Feuer', die am Anfang der Feuersaison entstehen, ‚frühe bis späte Feuer', die den Höhepunkt der Feueraktivität im Dezember/Januar bilden, und ‚sehr späte Feuer' am Ende der Feuersaison bis zum Beginn der Regenzeit.

Es zeigte sich, dass eine beträchtliche Feueraktivität in den Vegetationszonen zwischen dem Regenwald und der Sahelzone vorherrscht. Besonders wiesen Teile der ‚Sudan-Guinea'- und der ‚Guinea'-Savanne eine hohe Feuerpixel-Frequenz auf, d.h. hier traten Feuer in vielen Jahren am selben Ort auf. Diese hohe Pixelfrequenz wurde auch in den meisten Schutzgebieten in diesen Savannen-Gebieten gefunden.

Was die Landbedeckung betrifft, so ergaben die Ergebnisse, dass das höchste Feueraufkommen in den laubabwerfenden Waldgebieten und im laubabwerfenden Buschland vorkam.

Die Brandschäden, bzw. der Einwirkungsgrad, wurden im lokalen Maßstab untersucht. Hier korrelierten die Felddaten zur Brandeinwirkung signifikant mit den sogenannten ΔNBR-Index-Werten, die von Landsat-Aufnahmen des Pendjari-Nationalparks hergeleitet wurden (R^2 = 0,76). Der Korrelationskoeffizient nach Pearson ist r = 0,84, und nach Spearman-Rho ist der Koeffizient r = 0,86. Bei sehr niedrigen Brandschäden (mit ΔNBR-Werten zwischen 0 und 0,40) war die Vegetation schwach beeinträchtigt (0-35 % Biomasseverlust), während die Vegetation bei mäßigen und hohen Brandschäden sehr beeinträchtigt war und bis zu 100 % der Biomasse verbrannt war; hier lag der ΔNBR zwischen 0,41 und 0,99.

Diese Ergebnisse zeigen, dass durch Satellitenbilder die Verteilung von Feuern über größere Flächen in der afrikanischen Savanne effektiv bestimmt werden kann, und dass der Normalized Burn Ratio-Index auf Westafrika zur Berechnung von Brandschadens-Klassen anwendbar ist.

Die Ergebnisse liefern einen entscheidenden Beitrag zum Verständnis von Feuer-Ausprägungen in Westafrika, um letztlich den Einsatz von Feuer, auch im Hinblick auf den Klimawandel und die Veränderungen in der Vegetationsdiversität, verbessern zu können.

ACKNOWLEDGEMENTS

This thesis could not have been written without the most valuable help and the co-operation of several people, to whom I want to express my sincere and heart-felt gratitude.

First of all, I want to sincerely thank the BIOTA project, which made it possible for me to write this thesis and to enrich my scientific knowledge. It is this project that permitted me to learn the intricate science of remote sensing which has given me great pleasure as I was making progress in it, and which is very useful today for explaining certain past and present phenomena for ultimately feeding prediction models. The financial support from this project throughout my stay in Germany was very valuable to me.

I want to express my gratitude to the German Federal Ministry of Education and Research (BMBF), which by financing this project, provided the means for building a bridge of co-operation between German and African students and, moreover, for enhancing our knowledge and creating an exchange between cultures. It will be of great importance to keep and maintain this connection, as this project represents a genuine perspective for Africa in the field of research.

I sincerely thank my supervisors of this thesis, Prof. Linsenmair (Coordinator BIOTA West Africa) and Prof. Dech (Director of DLR´s German and Remote Sensing Data Center (DFD) in Oberpfaffenhofen) for their support, their encouragement and especially for the patience they have shown with me.

I am very grateful to my mentors, Dr. Tobias Landmann, Dr. Michael Schmidt and Dr. Souleyman Konaté who gave me great amount of advice, help and support throughout the whole thesis.

I would like to extend my thanks to Minnattallah Boutros (Administrative Coordinator BIOTA West Africa), Tillman Konrad, Johannes Penner and Petra Kube, who led me during my first steps in Germany, who were always there for me when I needed their help and who helped me to gradually integrate into the country.

My grateful thanks go to all my colleagues from the Remote Sensing Department of Würzburg University for their valuable help, which was essential for completing this thesis.

I would also like to show my gratitude to Prof. Sinsin from Abomey-Calavi University (Benin), Prof. Thiombiano from Ouagadougou University (Burkina Faso), the director of Pendjari National Park, Mr Tiomoko Djafarou as well as Mr Aristide Tehou, all of whom facilitated my field work and supported me.

My thanks must also go to Dr. Konstantin König, the technician Yaméogo Coulibaly, the Pendjari National Park Ranger, Celestin, and the driver Jacouba, who gave me very valuable support while I was collecting the data in the field.

I would leave these acknowledgements incomplete without thanking my friends, Claude Hepp, Yvette Achi, Willy Koffi, Sandrine Link, my family-in-law and my husband who advised, supported and encouraged me in the efforts leading to this thesis.

LIST OF FIGURES

LIST OF TABLES

LIST OF ACRONYMS

ASTER: Advanced Spaceborne Thermal Emission and Reflection Radiometer

BIOTA: Biodiversity Monitoring Transect Analysis

BMBF: German Federal Ministry of Education and Research

CH_4: Methane

CMORPH: Climate Prediction Center Morphing

CO_2: Carbon dioxide

CO: Carbon monoxide

DFD: Deutsches Fernerkundungsdatenzentrum (German Remote Sensing Data Center)

DLR: Deutsches Zentrum für Luft- und Raumfahrt e. V. (German Aerospace Center)

E: East

ETM+: Enhanced Thematic Mapper Plus

FAO: Food and Agricultural Organization

Gb: Gigabite

GEM: Global Environment Monitoring

GLC: Global Land Cover

GLCF: Global Land Cover Facility

GPS: Global Positioning System

ha: Hectares

.hdf: Hierarchical Data Format

IGBP: International Geosphere-Biosphere Programme

.img: Image

K: Kelvin

km: Kilometer

km^2: Square kilometer

LCCS: Land Cover Classification System

MODIS: Moderate Resolution Imaging Spectrometer

m: Meter

Max: Maximun

MIR: Middle Infrared

Min: Minimum

mm: Millimeter

MOD14A2: MODIS/Terra Thermal Anomalies/Fire 8-Day L3 Global 1km

MYD14A2: MODIS/Aqua Thermal Anomalies/Fire 8-Day L3 Global 1km

N: North

NASA: National Aeronautics and Space Administration

Nb.: Number

NBR: Normalized Burn Ratio

NIR: Near Infrared

NMHC: Non-Methane Hydrocarbons

NO_X: Nitrous Oxides

NP: National Park

REMO: Regional Climate Model Technique

S: South

SLC: Scan Line Corrector

SPOT: Satellite Pour l'Observation de la Terre

Std.Dev: Standard Deviation

SWIR: Shortwave Infrared

TM: Thematic Mapper

TIR: Thermal Infrared

UMD: Land cover product

UNESCO: United Nations Educational, Scientific and Cultural Organization

USGS: United States Geological Survey

UTM: Universal Transversal Mercator

VIS: Visible Infrared

VNIR: Visible Near Infrared

W: West

WGS: World Geodetic System

WIST: Warehouse Inventory Search Tool

ΔNBR: Image differencing index between NBRpostfire and NBRprefire

µm: micro-meter

TABLE OF CONTENTS

CHAPTER 1: INTRODUCTION

Research context of the thesis

A bushfire is defined as an uncontrolled fire which occurs in vegetation (Whelan 1995; Scott & Glasspool 2006). This fire can be spread rapidly or slowly depending on the weather conditions prevailing in the area at that time, as well as on the state, quantity and distribution of vegetation (Trollope et al. 2004). Vegetation fires of natural origin do exist. They are caused by lightning, volcano eruptions or by sparks flying from a falling rock crashing on another (Goldammer & de Ronde 2004). However, these phenomena are very rare in Africa (Goldammer & de Ronde 2004). Most bushfires in Africa are of anthropogenic origin. Their dynamics in landscape is one of the most important topics that attract the attention of the scientific community, as fire has effects on all the hierarchical levels of the environment, as will be explained in chapter two. In the literature, fire is recognized as one of the most widespread ecological disturbances in the world besides natural disasters such as droughts, floods or hurricanes (Goldammer & de Ronde 2004).

From boreal forests to the tropical grasslands and savannas of the world, fire burns enormous quantities of plant biomass (Goldammer & de Ronde 2004). Thus, it was estimated that between 2700 and 6800 million tons of CO_2 are released every year by burning savanna vegetation and through the conversion of forests into arable land (shifting cultivation) (Goldammer & de Ronde 2004).

Previous studies on fire by Laris (2002); Clerici (2006); Devineau et al. (2010) and many other researchers have demonstrated that satellite remote sensing is the only tool that is able to detect fire and to collect the data on a variety of scales and for long temporal series. The uses of satellite imagery in recent analyses of fire has shown that the largest number of detected fires was found on the African continent (Dwyer et al. 2000), which is why Africa is also designated as the fire continent (Goldammer & de Ronde 2004), and African biomass burning accounts for around 35 percent of the global total (Goldammer & de Ronde 2004).

Furthermore, studies made by Van Wagtendonk et al. (2004) in the Sierra Nevada of California, Roy & Landmann (2005) in South Africa, Walz et al. (2007) in the Jarrah-Marri forest of southwest Western Australia and other researchers have proven the utility of remote sensing in assessing the burn area or mapping burn severity, both at a local and at a regional scale.

In West Africa fire has long been considered a permanent and essential element of savanna ecosystems, especially regarding its effect on the vegetation structure and for

maintaining the balance between grass and tree biomass in savannas. Savannas are known as an area of special interest with respect to fires, as large areas of the savannas are burned each year (FAO 2001). In fact, it has been shown that more than 80 percent of the total savanna area is affected by fire (Menaut et al. 1991). Man-made fires also occur in the protected areas, where they are considered an important tool in park management.

Whereas, as said before, many studies have been carried out on the fire regimes and burn severity in places such as Australia, South Africa and California, very few studies on fire based on satellite data have been made for West Africa. Therefore, the aim of this study is to contribute to filling this gap by focusing on three aspects of the fire regime. The first is the distribution of bushfires in West Africa over a long period of observation. The second is the analysis of fire activity as a function of land cover on a regional scale. The third is the characterization of fire severity through observations at a local scale and the categorization of damages done to the vegetation, which provides one means of assessing the impact of fire.

This study was developed in the context of the research activities of the Biodiversity Monitoring Transect Analysis in West Africa (BIOTA West Africa), which groups three African countries, namely Benin, Burkina Faso and Côte d´Ivoire. BIOTA West Africa is part of BIOTA Africa which started in 2000 as a co-operative and interdisciplinary research project and also includes BIOTA Morocco, BIOTA East Africa and BIOTA Southern Africa. The project was initiated and funded by the German Federal Ministry of Education and Research (BMBF). It has developed into a unique network of German and African scientists aiming at a holistic contribution towards sustainable use and conservation of African Biodiversity, which is threatened by population growth, the unsustainable use of natural resources and by climate change[1].

The study areas of this thesis are located in West Africa (regional scale) and in three protected areas (local scale), namely Comoé National Park in Côte d´Ivoire, Bontioli Reserve in Burkina Faso and Pendjari National Park in Benin, all of which will be described in more detail in chapter three.

This study is divided into seven chapters.

In this first chapter, the introduction, a research context and the aims of this study are presented.

The second chapter, which is based on literature, provides an overview of the research topic, namely the characteristics of bushfires, their environment in West Africa and the theoretical background of remote sensing in the study of fire dynamics.

[1]cf. www.biota-africa.org; information retrieved on July 2nd, 2010

Chapter three is dedicated to the description of the study area at regional and local levels.

The fourth chapter starts by describing the different methods used for the MODIS fire product, Landsat ETM+, ASTER data processing and analyses. This is followed by an explanation of the methods used during the field trip to analyse and verify the burn severity classes.

In the fifth chapter, the results concerning the three main research areas mentioned above are presented.

The sixth chapter comprises the discussion of the various results obtained throughout this study and a comparison with other studies made in South Africa, California and Australia.

General conclusions are outlined in the seventh chapter. The work finishes with an outlook on desirable future research.

CHAPTER 2: LITERATURE BACKGROUND

2.1 Characteristics of bushfires

2.1.1 Fire impact at different environmental levels

This section sums up the results of some previous studies which analyzed the impact of fire on the environment. These studies have shown that fires have a great impact on the ecology and that they are one of the global modification agents worldwide (Thonicke et al. 2001), as they have a variety of effects on all organizational levels in the environment. These effects are resumed in figure 1 and explained in detail below (Houghton et al. 1999; Tilman et al. 2000; Clerici 2006)

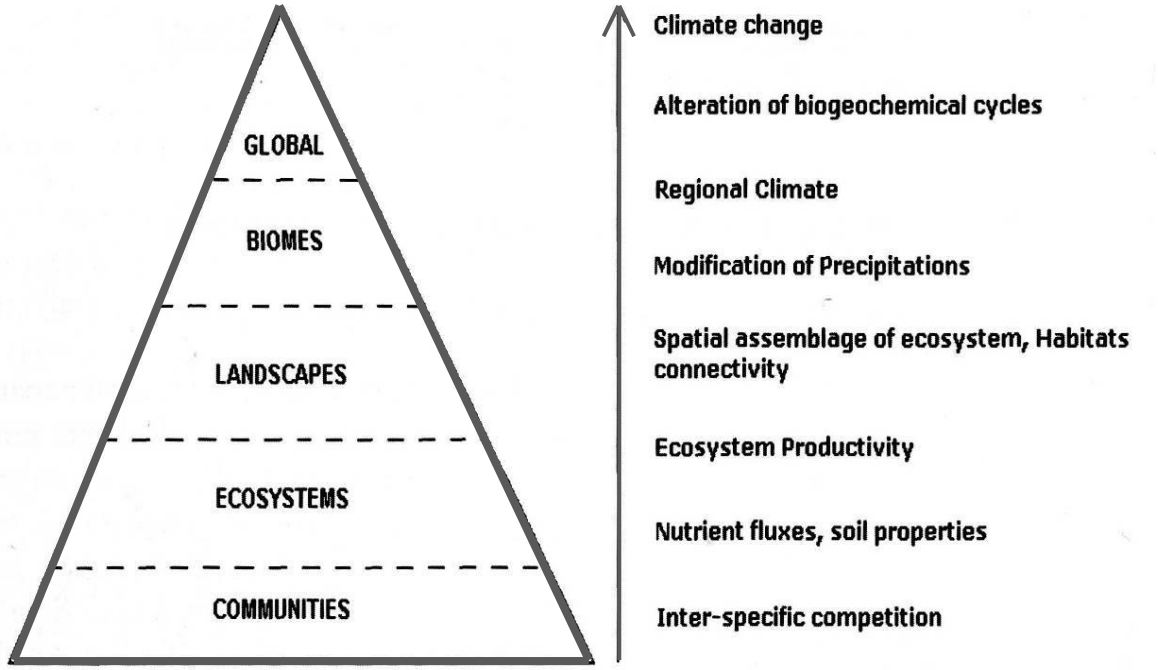

Figure 1: Environmental hierarchy levels (on the left) and the impact of fires on them (on the right), (Clerici 2006).

According to the above figure, at the communities level, for instance, fire can change the terms of competition between different plant species by giving plants adapted to fire an advantage over those that are not (Scholes & Archer 1997). At ecosystems level, if fires are suppressed over a long period in a savanna area, the so-called phenomenon of "bush encroachment" can occur. This means that the production of trees is increased, to the detriment of grass vegetation, as the tree cover can become so intense that eventually, hardly any sunlight reaches lower layers of vegetation such as the grass layer. Furthermore, the competition for nutrients will also be won by the trees. Therefore, in the long run, the quantity of grass will gradually diminish while the trees will spread, and thereby, where there is

enough water and suitable soil the savanna will progressively turn into shrubland or woodland (Scholes & Archer 1997; Roques et al. 2001; Dyer et al. 2001). This shows that fire plays an important role in maintaining savanna ecosystems (Sankaran et al. 2004).

Repeated fires reduce the organic matter in the soil by slowing the soil's enrichment with humus. After the fire has passed, the soil has become more strongly exposed to the direct action of the sun, the wind, and the rain. The consequence of this is often soil erosion. However, if fires do not occur too often, they have a direct positive impact on the soil by the mineralization of organic matter: The ash that is made soluble by the action of CO_2, transforms into soluble carbonate, which penetrates into the ground and makes it fertile. Another part of the ashes is washed away by the rivers and fertilizes their alluvia.

At the landscape level, tree growth is different in the presence or absence of fires, as is illustrated by figure 2. With fires occurring periodically (figure 2B), the size of trees and shrubs remains rather stable. By contrast, if fires do not occur during a period of more than ten years (figure 2A), the size of trees increases and a new type of vegetation takes hold.

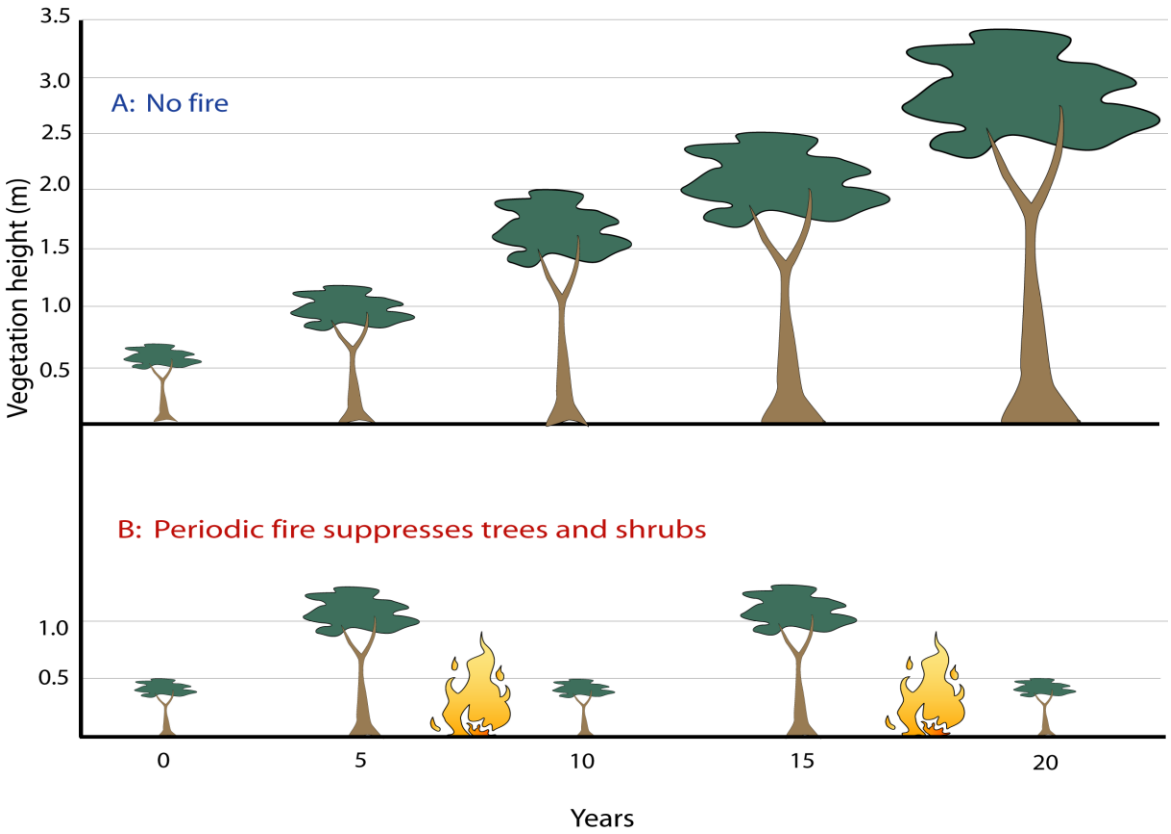

Figure 2: Evolution of tree height without (A) and with fire activity (B) in woody savannas; illustration adapted from (Dyer et al. 2001).

As the importance of the timing, intensity and frequency of fires in an area influences the competition between plants and ecological succession dynamics, a change in these factors can

have different effects on the make up of plant populations and the relative abundance of different species (Landsberg 1997; Dyer et al. 2001; Clerici 2006).

At biome levels, fire can modify the precipitation as the aerosols emitted by biomass burning hinder the formation of rainclouds, which has a great influence on both global and local rainfall patterns (Lacaux et al. 1992; Crutzen & Goldammer 1993).

At a global level, fire can affect the climate through the greenhouse gases and aerosols emitted into the atmosphere. Thus, biomass burning is seen as one of the principal causes of air pollution, as it releases a great quantity of CO_2, CH_4 and CO into the atmosphere (Andreae & Merlet 2001; Van Der Werf et al. 2003), namely 40, 16 and 43 percent of total emissions of carbon dioxide, methane and carbon monoxide caused by human activities (Grégoire et al. 2003; Clerici 2006). This quantity is comparable to that emitted by the combustion of fossil fuels (Crutzen & Andreae 1990; Keene et al. 2006). Moreover, between the years 1997 and 2001, CO_2 from biomass burning showed steady increases, i.e. growth rates in the excess of 66 percent during that time period (Van Der Werf et al. 2003). Besides emitting carbon, vegetation fires have also been shown to be an important source of trace-gases (such as NMHC and NO_X) and aerosols (Crutzen & Andreae 1990; Ward et al. 1996; Hao et al. 1991; Kauffman et al. 1998), which also act as greenhouse gases in the global atmosphere (Kauffman et al. 1989).

The equatorial and subtropical regions play a major role in this context as they account for 70 to 80 percent (Crutzen & Andreae 1990), and Africa alone for 35 to 37 percent, of the total biomass burned worldwide (Keene et al. 2006).

2.1.2 Fire regimes

The term “fire regime” is defined as the pattern of fires occurring in an area over long periods of time and their behaviour in the ecosystem in which they occur (Brown 1995).

The behaviour of fires can be characterised by their spread, the size of the flame fronts (Whelan 1995; Trollope et al. 2004) as well as the frequency of their occurrences, their intensity and the amount of biomass fuel they consume (Bond & Keeley 2005).

Climate is considered to have an important influence on the fire regime that prevails in any given region (Williams & Cook 2001). Another important variation factor is the make up of the landscape, as natural topographic components such as rivers, lakes, gallery forest, rocks or firewalls can be natural obstacles to fire. Further factors are the fuel productivity and the frequency of ignitions. Biomass fuel is produced both in the rainy season with its abundant growth of grasses and other herbs, and in the dry season, when leaves fall from the trees. Both grasses and leaf litter dry out during the dry season, providing fuels and an ignition source for

fires (Bowman 2001). To sum up, fire regimes depend on the climate, the quantity of fuel available, the probability of ignitions and the ignition type, the behaviour of fires, and the fire's capacity to spread through the landscape (Williams & Cook 2001).

Even though fire behaviour and its different parameters just mentioned are not within the scope of this work, the study of burn areas at a local scale can lead to some information about the characteristics of the fires.

2.1.3 Types of bushfires

Different types of fire to be found in different landscapes as they are presented in the literature are described below.

According to Monnier (1990) and Sonko (2000), **surface fires** or **soil fires** are very frequent, have a high intensity, and affect the whole grass and bush layer. They occur mainly in open grasslands, where there is abundant fuel and an uninterrupted cover of the herbaceous or gramineous layer. As the grass layer has a high ignitability, theses fires burn very fast, often have a considerable burn size and can also be transported over longer distances by sparks flying in the wind. These fires burn organic matter in the lower layers of vegetation, namely the surface of the humus and litter, as well as the grass layer and lower shrubs.

Litter fires, also called **crawling fires,** are quite frequent. They occur in woodland savannas and clear forests. In this vegetal formation, as herbaceous cover is missing or sparse, they consume the dead leaves on the ground and therefore, their spread depends on the presence of litter. Nevertheless, these fires can also continue their way by consuming dry shrubs and dead branches that they encounter. As litter easily ignites, these fires are the origin of many bushfires.

Crown fires occur in savanna formations such as clear forests and small clusters of shrubs and trees with interlaced branches. As the grass cover is often rather sparse in these formations, it is mainly the upper parts of trees or shrubs that burn. They spread by jumping from the dry branches of one tree or shrub to those of another and they can also use grass bridges. These fires occur less frequently than those mentioned before. They are rarely at the origin of a bushfire.

Concealed fires or **humus fires** are quite rare phenomena. They most often occur in gallery forests of the savanna, which are relatively humid. Therefore, if a fire does occur there, it remains confined to a dry humus layer, which it slowly consumes, and it hardly spreads to other layers of the vegetation.

As has been shown, each type of fire corresponds to one type of vegetation. When fire spreads from one type of vegetation to another, it will also change its character accordingly.

Thus, in the savanna, fire can successively take different forms, such as that of a surface fire in areas where grass cover is sufficiently thick, of a leaf fire under certain trees that form a thick layer of dead leaves, and sometimes of a crown fire.

Concerning the **direction of expansion**, fires going up a slope spread faster than those going down, as heat transfer through convection is greater the more the slope rises. On the other hand, fires going down can jump more easily to an opposite slope (Sonko 2000).

2.2 Fire environment in West Africa

Fire is one of the key factors influencing the vegetation of a savanna, and has played a great role in its evolution. The savanna biome is therefore the most frequently and extensively burned region of the earth (Eva & Lambin 1998; Barbosa et al. 1999). Human influence must not be underestimated in this context. As already mentioned, some literature has shown that while some fires have natural causes, the vast majority of burnings on the African continent are man-made (Schmitz 1996; Goldammer & de Ronde 2004). In fact, fire has been used by indigenous people for millions of years and continues to be used by them for many different purposes (Laris 2002; Bowman et al. 2009) such as hunting, maintaining food sources, clearing paths, communication, cleaning the surroundings of villages and hamlets, harvesting honey, making potassium and producing charcoal.

In African tribal societies, fire was also seen as a religious phenomenon. Even today, in certain West African peoples, it is linked with traditional beliefs. This is the case in the Baoulé country in central Côte d'Ivoire, where, for example, the smoke rising from early fires announces to the farmers that the time has come to prepare the fields for sowing (Paré 1992).

Likewise, for farmers in Burkina Faso, these fires have a purifying function. They accompany the transport of new crops into the villages. And it is only after these rites that the population can eat from the new crops. Fires are also used in religious rites whose function is to grant health, peace and to drive away misfortunes from the community. To this end, fires accompany the "going out" of masks and the purification of the souls. The latter, called fires of immunisation are lit to drive away certain diseases such as measles, the whooping-cough and many other children's diseases (Paré 1992).

Nevertheless, there are rare bushfires of natural origin, such as those caused by lightning. In fact, studies carried out by Philipps (1936), Tournier (1948), and quoted by Monnier (1990) on the high pastures of Mount Nimba between Côte d´Ivoire, Guinea and Liberia in West Africa showed that vegetation fires can under certain conditions be triggered by lightning. Another study made in Congo Brazzaville (Monnier 1990) showed that the

fermentation of grass after the first rainfall can trigger spontaneous fires in very thick vegetation that has not yet been affected by fires.

Fires have been found at all times of the year and in nearly every region of the earth. However, most fires worldwide, about 80 percent, take place in tropical countries (Cahoon et al. 1992; Williams & Cook 2001).

Recent estimates based on satellite imagery have shown that, depending on the year and the type of vegetation, between 25 and 80 percent of the wooded savanna burns in West Africa in the course of a year (Laris 2002). However, mosaic forests and gallery forest are less affected by fire. More specifically, Africa is the continent with the highest fire occurrence (Dwyer et al. 1998), as has also been confirmed more recently by global satellite fire products derived from Moderate Resolution Imaging Spectrometer (MODIS) of Rapid Response System Global Fire Maps (figure 3).

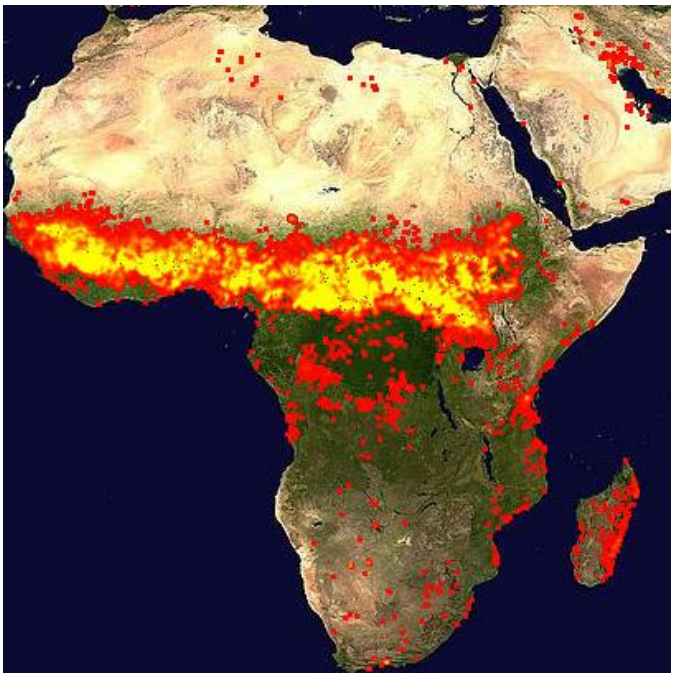

Figure 3: Fire map (active fires from the MODIS satellite for the period: 2008361-2009004), (NASA 2010a).

The vegetation formations in tropical Africa that show the greatest occurrence of fires are the savannas (Dwyer et al. 1999; Carmona-Moreno et al. 2005; Tansey et al. 2004), i.e. the vegetation formations ranging between dense forest and steppe. Here, bushfires take place every year, to the extent that satellite images from the fire season as the above show the pattern of a fire belt spreading from west to east in the savanna areas of the northern hemisphere of Africa.

2.3 Use of Remote Sensing for fire detection

2.3.1 Importance of Remote Sensing for fire studies

"Remote sensing is the science and art of obtaining information about an object, area, or phenomenon through the analysis of data acquired by a device that is not in contact with the object, area, or phenomenon under investigation" (Lillesand et al. 2004; Jensen 2005).

Beside being the only tool that allows to gather fire data time series at continental to regional and local scale (Walz 2004), satellite remote sensing is the only feasible means of observing and recording fuel combustion over large areas (Roy, Lewis, et al. 2002). Satellites can monitor small or large areas on the surface of the earth at a high temporal frequency. The data are relatively inexpensive for the scientist or even freely available for download. The MODIS sensors used for fire products quantify the thermal emissions of the burning process (Walz 2004). The data from these sensors are then processed by a detection algorithm that recognizes the active fires within each MODIS swath (Kaufman et al. 1998; Justice et al. 1998; Justice et al. 2000; Giglio et al. 2003). Thereby, MODIS can give information on the spatial distribution of active fires, the energy they emit, and the flaming and smoldering ratio; further MODIS sensors give indications about change in vegetation caused by fire (Justice et al. 2002; Justice et al. 2006).

Likewise, remote sensing can also detect and quantify electromagnetic energy reflected and emitted from the surface of the earth. On board of MODIS, there are different sensors responding to energy in the visible (VIS), near infrared (NIR), middle infrared (MIR), and thermal infrared (TIR) ranges respectively (Lillesand & Kiefer 2000). The information gathered from different sensors can be useful in different areas. For example, the shorter MIR and NIR are most sensitive to change in reflectance that is caused by variation in leaf water and dry matter content. The leaf water content and fuel moisture in a given area can then be calculated from the sensor data by using indices and models (Bowyer & Danson 2004).

2.3.2 Characteristics of MODIS active fire products

MODIS active fire products were used for the analyses on a regional scale carried out in this study. According to Justice et al. (2002), the MODLAND products are applicable to earth system science and global change research. Among these MODLAND products there are the land cover characteristics that contain thermal anomalies and fire, burned area, land cover, vegetation cover conversion and vegetative continuous fields (Morisette et al. 2002). The sensors on the Terra and Aqua platforms were launched in December 1999 and in May 2002 respectively (Morisette et al. 2002; Justice et al. 2002). MODIS Terra observes fires twice a

day (at 10:30 and at 22:30). The same goes for MODIS Aqua (at 13:30 and at 01:30). Each MODIS sensor furnishes daily coverage of almost the entire surface of the earth in the mid to high latitudes, making observations in 36 spectral bands at different scaling (see table 1).

Table 1: MODIS bands and their corresponding wavelengths with their pixel size and the areas of application (Lillesand et al. 2004).

Number of bands	Bandwidth (µm)	Spatial Resolution	Primary Use
1	0.620-0.670	250m	Land/Cloud/Aerosols
2	0.841-0.876	250m	Boundaries
3	0.459-0.479	500m	Land/Cloud/
4	0.545-0.565	500m	Aerosols
5	1.230-1.250	500m	
6	1.628-1.652	500m	Properties
7	2.105-2.155	500m	
8	0.405-0.420	1km	Ocean Color/
9	0.438-0.448	1km	Phytoplankton/
10	0.483-0.493	1km	Biogeochemistry
11	0.526-0.536	1km	
12	0.546-0.556	1km	
13	0.662-0.672	1km	
14	0.673-0.683	1km	
15	0.743-0.753	1km	
16	0.862-0.877	1km	
17	0.890-0.920	1km	Atmospheric
18	0.931-0.941	1km	Water Vapor
19	0.915-0.965	1km	
20	3.660-3.840	1km	Surface/Cloud
21	3.929-3.989	1km	Temperature
22	3.929-3.989	1km	
23	4.020-4.080	1km	
24	4.433-4.498	1km	Atmospheric
25	4.482-4.549	1km	Temperature
26	1.360-1.390	1km	Cirrus Clouds
27	6.535-6.895	1km	Water Vapor
28	7.175-7.475	1km	
29	8.400-8.700	1km	Cloud Properties
30	9.580-9.880	1km	Ozone
31	10.780-11.280	1km	Surface/Cloud
32	11.770-12.270	1km	Temperature
33	13.185-13.485	1km	Cloud Top
34	13.485-13.785	1km	Altitude
35	13.785-14.085	1km	
36	14.085-14.385	1km	

MODIS bands can be used for fire observations in the following way: Fires are detected in the wavelengths 3.9 µm (bands number 21 and 22) and 11 µm (corresponding to channel 31). The saturation point of those bands is reached at 500 K, 331 K and 400 K respectively. The Swath width of MODIS Terra/Aqua is 2330 km. The observations are made at 1 km

resolution and their revisit time is 4 times a day, thanks to which a regular monitoring of global fires is possible. The fire product is created by a detection algorithm (Giglio et al. 2003; Justice et al. 2006), which analyzes each pixel from MODIS and attributes it one of the following classes (Giglio 2005): *missing data, cloud, water, non fire, unknown and fire*. Table 2 shows the meaning of these classes.

Table 2: Classes values and meaning in the MOD14A2 and MYD14A2 Fire products.

Pixel Value	Meaning
0	Not processed (missing input data)
2	Not processed (other reason)
3	Water
4	Cloud
5	No fire
6	Unknown
7	Low-confidence fire
8	Nominal-confidence fire
9	High-confidence fire

According to Giglio (2007), pixels tagged as *missing data* are those that do not furnish valid data. The *cloud* and *water* classes are assigned to pixels that are determined as cloud and water masks. The class named *no fire* corresponds to background. The class defined as *unknown* groups the pixels whose data is not identified. As to the *fire* classes, they are identified by using the spectral signature of the pixels in the 3.9 and 11 μm channels. A few tests are then carried out on pixels which have thus been chosen. The purpose of these tests is to eliminate possible false detections that can be caused by sun glint, desert boundaries and errors in the water mask. The susceptible fire pixels that have not been removed during these tests are considered fire pixels.

2.3.3 Burned area mapping

Whereas MODIS data were used for studies at a regional scale, Landsat ETM+ and ASTER scenes, which have a higher resolution, were used for mapping the burn area at a local scale in Pendjari National Park, Comoé National Park and Bontioli National Park. These satellites are described in the following sections.

2.3.3.1 Characteristics of the Landsat ETM+ sensor

Landsat ETM+, also called Landsat 7, was launched on 15th April 1999 (Jensen 2000; Chandrashekhar et al. 2003). It has similar characteristics as Landsat TM or Landsat 5, which

was launched in March 1984 (Barsi et al. 2003). Table 3 contains the characteristics of Landsat ETM+:

Table 3: Landsat ETM+ channels and its characteristics (NASA 2010b).

Bands number	Spectral Range (µm)	Resolution (m)	Quantization (bits)
1 (blue)	0.45-0.515	30	8
2 (green)	0.525-0.605	30	8
3 (red)	0.63-0.690	30	8
4 (near-infrared)	0.75-0.90	30	8
5 (shortwave infrared)	1.55-1.75	30	8
6 (thermal infrared)	10.40-12.5	60	8
7 (shortwave infrared)	2.09-2.35	30	8
8 (panchromatic)	0.52-0.90	15	8

Landsat 7 orbits the earth at an altitude of 705 km. The orbit has a sun-synchronous inclination of 98.2 degrees with a descending equatorial crossing time of 10:00 a.m on each pass. The data storage on board of Landsat 7 is around 3.8 Gb for each scene. The temporal resolution (repeat cycle) of Landsat 7 on the earth surface is every 16 days (NASA 2010b).

The permanent failure of the Landsat ETM+'s scan line corrector, a hardware component of the instrument, which occurred in May 2003, has to be taken into consideration in this study (Chuvieco et al. 2008). The consequences of this failure are shown in figure 4.

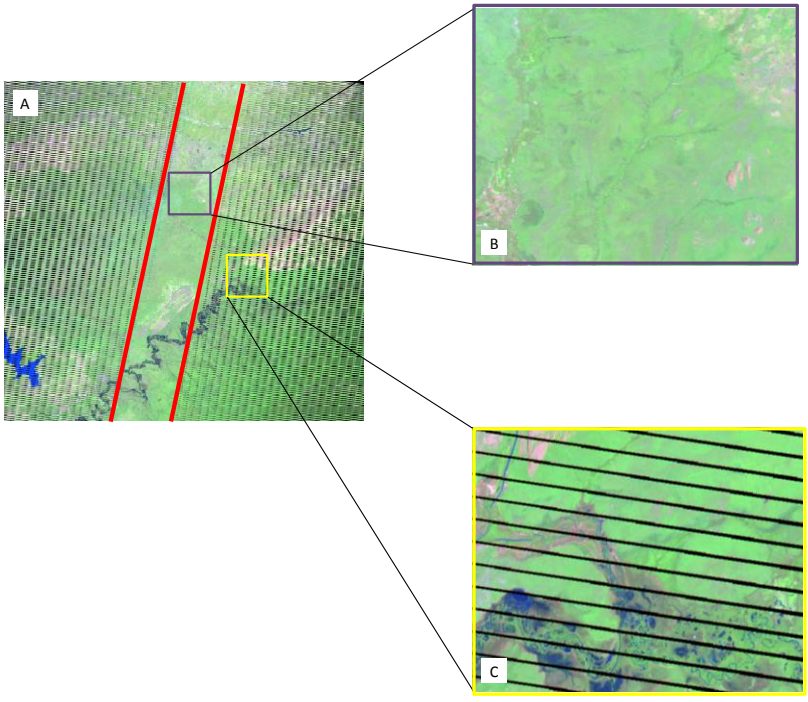

Figure 4: A) Landsat ETM+ scene in SLC-off mode with bands 5-4-3 (NASA 2010c).
B) The central part of the Landsat image is without data gaps.
C) Missing data occur in black parallel lines on the right and left of the scene.

Like MODIS products, Landsat ETM+ data are freely available and can be downloaded on the Glovis website (NASA 2010c) through USGS Global Visualization Viewer or on the Earth Explorer website (GLCF 2010) by using the Global Land Cover Facility site.

2.3.3.2 Characteristics of the ASTER sensor

The Advanced Space Thermal Emission and Reflection Radiometer (ASTER) was launched on board NASA´s Terra platform on 18th December 1999. "ASTER is an advanced multispectral imager, covering a wide spectral region with 14 bands from the visible to the thermal infrared with high spatial, spectral and radiometric resolution." Stereo coverage is provided by an additional backward-looking near-infrared band (Abrams et al. 1999). Each ASTER scene spans an area of 60 x 60 km. The ASTER bands and their characteristics are shown in table 4.

Table 4: ASTER bands (Abrams et al. 1999).

Subsystem	Band number	Spectral Range (µm)	Spatial Resolution (m)	Quantization levels
VNIR (Visible Near Infrared)	1	0.52-0.60	15	8 bits
	2	0.63-0.69		
	3N	0.78-0.86		
	3B	0.78-0.86		
SWIR (Shortwave Infrared)	4	1.60-1.70	30	8 bits
	5	2.145-2.185		
	6	2.185-2.225		
	7	2.235-2.285		
	8	2.295-2.365		
	9	2.360-2.430		
TIR (Thermal Infrared)	10	8.125-8.475	90	16 bits
	11	8.475-8.825		
	12	8.925-9.275		
	13	10.25-10.95		
	14	10.95-11.65		

2.3.3.3 Characteristics of the Normalised Burn Ratio index (NBR)

Since the first studies assessing burned areas through remote sensing, the term burn severity has been defined as the index calculated from satellite sensors (Van Wagtendonk et al. 2004). Different sensors such as MODIS, Landsat Thematic Mapper, ASTER and AVIRIS have proven their capacity to relate field measurements to burn severity from spectral data

(Brewer et al. 2005; Cocke et al. 2005; Epting et al. 2005; Chuvieco et al. 2006; Roy et al. 2006; Kokaly et al. 2007). With these satellite data sets, an index called Normalized Burn Ratio (NBR) is calculated (Keeley 2009), which is frequently used as a measure of burn severity and has been used in some burned area studies (Key et al. 2002; Van Wagtendonk et al. 2004; Key 2005; Zhu et al. 2006; Walz et al. 2007). Work by Key & Benson (1999) and Walz et al. (2007) show that the NBR index is most sensitive to landscape change caused by fire. The bands used for the NBR are centred in the Near Infrared (NIR) wavelength between 0.7µm to 0.9µm and in the Shortwave Infrared (SWIR) between 2.0µm to 2.4µm. This corresponds to bands 4 and 7 of Landsat TM and ETM+, bands 2 and 7 of MODIS and the index can also be applied to ASTER data using band 3N (VNIR) and one of the bands [5:8] of the SWIR spectral region.

The spectral bands of different satellites can be matched. Figure 5 gives the example of the relation of spectral bands between Landsat 7 Thematic Mapper and ASTER.

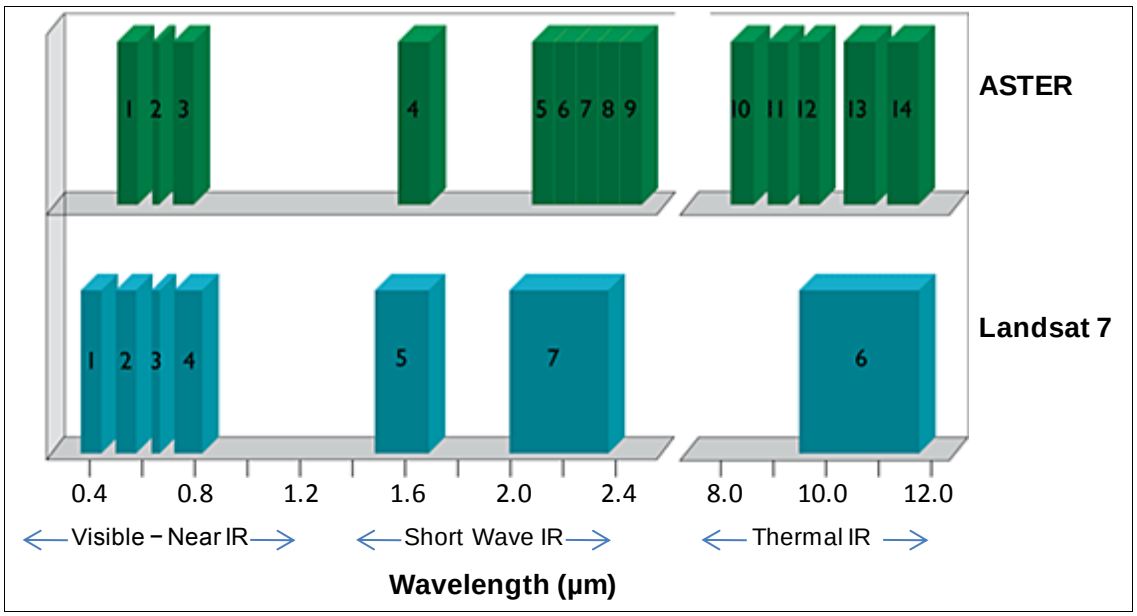

Figure 5: Comparison of spectral bands between ASTER and Landsat 7 Thematic Mapper (Abrams et al. 1999).

The NIR reflectance provides the most reliable indicator for loss of biomass, as dense vegetation leads to high reflection in this band, whereas sparse or removed vegetation leads to low reflection. Contrarily, at SWIR wavelengths, the presence of vegetation is shown by a low reflection, whereas reflectance increases when soil is exposed or leaf water content is low (Key & Benson 1999; Jensen 2000). Therefore, reflection increases with fire on band 7 of Landsat, while it decreases on band 4. In the same way, ASTER reflection on band [5:8] increases with fire, while that for band 3N decreases. The normalized burn ratio proposed by Key et al. (2002) can be written as follows:

$$\mathbf{NBR = (NIR - SWIR) \Big/ (NIR + SWIR)}$$

Results are in a range between -1.0 to 1.0. Positive values correspond to high quantities of biomass, whereas negative values are related to exposed soil and reduced leaf moisture.

The vegetation change caused by fire can be assessed through the image differencing index ΔNBR (delta NBR), which is calculated by subtracting the NBR derived post-fire from the NBR calculated from pre-fire data (Key & Benson 1999). Thus, burn severity is connected with the pre-fire vegetation conditions and the difference between pre-and post-fire NBR values (ΔNBR), as was suggested in some studies (García-Haro et al. 2001; Key et al. 2002; De Santis & Chuvieco 2007);

$$\mathbf{\Delta NBR = NBR_{prefire} - NBR_{postfire}}$$

Results range between -2.0 and 2.0. The ΔNBR value shows how much the vegetation of a landscape has changed, with high positive or negative values signaling a higher magnitude of change (Key & Benson 1999).

CHAPTER 3: STUDY AREA

3.1 Study area at regional scale

The study area is located in the West African savanna. In general, "savannas are grassy landscapes — woodlands with a grassy ground layer, or grasslands — that occur in tropical areas where the climate is seasonally dry" (Williams & Cook 2001). This vegetation type comprises several kinds of savanna. They range from wooded savanna to desert with changing grass coverage, the vegetation corresponding to the rainfall gradient from south to north and also depending on the soil types existing in different areas (Williams & Cook 2001), with precipitations and soil properties gradually decreasing as one gets closer to the desert (Laris 2002; Baxter & Getz 2005). The key characteristic of the savanna climate is the alternation between hot wet and warm dry seasons. This cycle of seasons, which is caused by the monsoon's movement between the northern and southern hemispheres, has a great influence on fire weather in the course of the year, and thereby on fire regimes. The climate in this area is favourable to bushfires, as the annual dry period generally lasts between 4 and 8 months (Cole 1987; Stott 1991).

Due to their long evolution, savanna ecosystems show a high complexity and diversity. Despite their simple structure, they are rich in species, communities of plants, habitats and both vertebrate and invertebrate animals. Their numerous plant life forms (e.g. trees, shrubs, grasses, herbs) have evolved many different ways to cope with the strongly varying climate (Williams & Cook 2001). Savannas cover about 20 percent of the earth's land surface (Williams & Cook 2001) and about 60 percent of sub-Saharan Africa (Baxter & Getz 2005).

In West Africa, the different types of savannas succeeding each other from north to south are, according to Lerebours & Ménager (2001) and Arbonnier (2002), the Sahara region, Saharo-Sahelian, Sahelian, Sahelo-Sudanian, Sudanian and Sudano-Guinean savannas. The following description of these types of savanna is based on these authors.

In the **Sahara zone**, rainfall is both very low and irregular. The soils are generally skeletal, consisting of sands more or less covered by pebbles. The bush vegetation primarily consists of *Acacia tortilis raddiana* and *A. ehrenbergiana*, *Balanites aegyptiaca*, *Maerua crassifolia*, *Salvadora persica* and *Leptadenia pyrotechnica*. In mountain areas, temperatures are lowered by height and the climate is less arid. The flora in such areas is of Mediterranean, Sahelian or Sahelo-Sudanian type. The *Acacia tortilis raddiana*, A. *laeta*, *Boscia senegalensis*, *Maerua crassifolia* and *Grewia tenax* species predominate in this area and are often associated with it.

The **Saharo-Sahelian zone** is characterised by a set of dunes alternating with depressions

covered by sand or with low vegetation cover and sometimes bare rock appearing. The bush layer is poor and takes the form of a steppe dominated by *Balanites aegyptiaca*, *Acacia tortilis raddiana*, *A. ehrenbergiana*, *Combretum glutinosum* and *C. micranthum*, *Boscia senegalensis* and *Leptadenia pyrotechnica*.

In the **Sahelian zone**, the annual rainfall levels are below 600 mm. The dry season is very long, lasting about 10 months. The type of vegetation found is arboraceous and/or scrubland steppe, with small trees or shrubs, which are often thorny and stunted due to the harshness of the climate and to overgrazing. In general, the grass cover is patchy and essentially made up of annual species, which are occasionally touched by bushfires.

In the **Sahelo-Sudanian zone**, the different types of vegetation are arranged in a mosaic form and depend on the relief and the type of soil. In these areas, one can find shrub steppes, tree savannas and groves, as well as gallery forest near waterbeds. Furthermore, there are agro-forest parks originating in natural vegetation that was reworked by man and also contains the village plantations.

The **Sudanian zone** is characterized by the abundance of grasslands. The height of the herbaceous cover ranges from 20 cm to 1.5 m. It consists particularly of Andropogons and Pennisetum, which are regularly affected by bushfires. Beside these grasslands, other vegetation formations such as shrubs, open woodlands savannas, clear forests, gallery forests, croplands or fallow lands can be found.

The **Sudano-Guinea zone** is constituted by a varied mosaic of different type of vegetations including those just mentioned as well as groves or wood islands of a height of 3 to 8 metres. The clear forests are made up of trees whose crowns almost join and below which land cover and herbaceous cover are very sparse. The wooded savannas and open woodland savannas are formed of dense trees or sparse trees and high grass (especially of the Andropogon species) that are easily affected by bushfires. The gallery forests are located along the perennial rivers and in the permanently humid valleys or gullies.

3.1.1 MODIS tiling

The study area extends over four MODIS product tiles located in West Africa between -10° W and 10° E and between 20° N and 0°S (figure 6). This area covers approximately 4,572,033 km^2. MODIS fire products are adequate for the goal of this study to match fire occurrences and their distribution within the vegetation at large scale.

In general, biomass burning can be monitored with MODIS in two different ways, namely by using either MODIS burn area products or MODIS fire products (Eva & Lambin 1998). In this study the latter will be used, as they give more precise temporal information about fires,

which also permits to analyse fire seasonality by using the approach of Clerici (2006).

The period of analysis covers the two seasons in West Africa (i.e. the dry season and the rainy season) to determine fire occurrences from 2000 to 2009 as well as the fire seasonality and the percentage of fires found in different land cover classes. For this purpose, the Global Land Cover 2000 map was used.

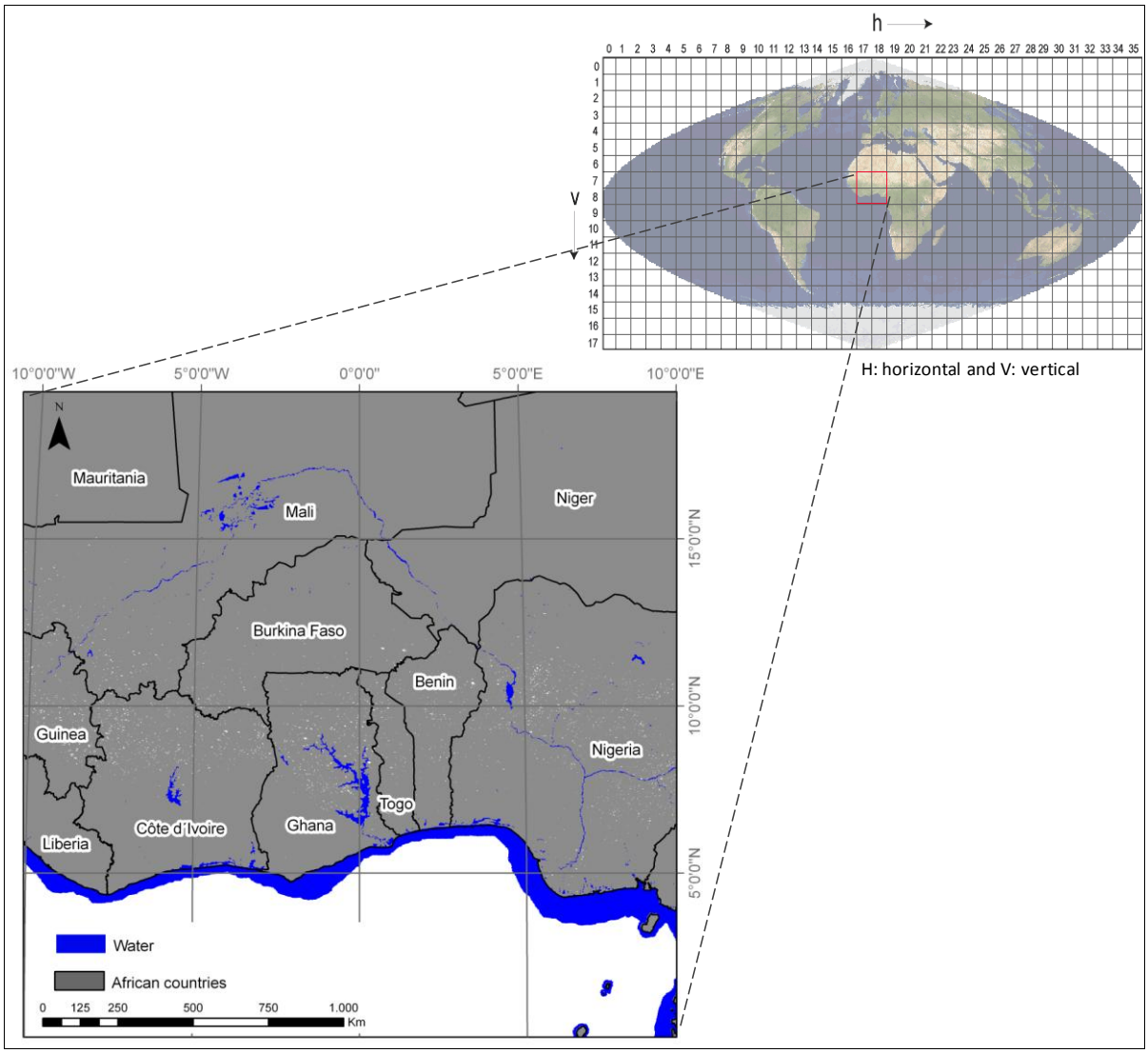

Figure 6: Study area in West Africa covered by MODIS tiling (h17v07, h17v08, h18v07 and h17v08).

3.1.2 The Global Land Cover 2000 maps

The maps created by Global Land Cover project, whose goal it is to create a better land cover product for the whole globe (Latifovic et al. 2004), show the different types of vegetation as well as the surfaces without vegetation to be found in Africa and elsewhere.

The data used for this map were acquired daily from the SPOT 4 satellite. The period of observation for the map used in this study covers the interval between November 1999 and December 2000 (Fritz et al. 2003; Fritz et al. 2004; Mayaux et al. 2003). The vegetation and

non-vegetation classification for this map was based on the Land Cover Classification System (LCCS) of the FAO (Di Gregorio 2005). Each class is specifically connected with one landcover type falling into the following categories: forests, woodlands, shrublands, grasslands, agricultural lands, bare soil, cities and water bodies. These classification results are used in many ecological applications (Defries & Townshend 1999; Kerr & Ostrovsky 2003; Lu & Weng 2007).

Global land cover 2000 (Bartholome & Belward 2005) is a vegetation classification map with a 1 km resolution (figure 7). It is available for free download on the Global Environment Monitoring website (GEM). In order to respond to the dynamics of land cover in a changing environment, other maps of this kind have been published, however using different methods and satellite data from different sensors (Herold et al. 2008). These maps are: IGBP Discover (Loveland et al. 2000), the MODIS land cover product (Friedl et al. 2002) and UMD land cover product (Hansen & Reed 2000).

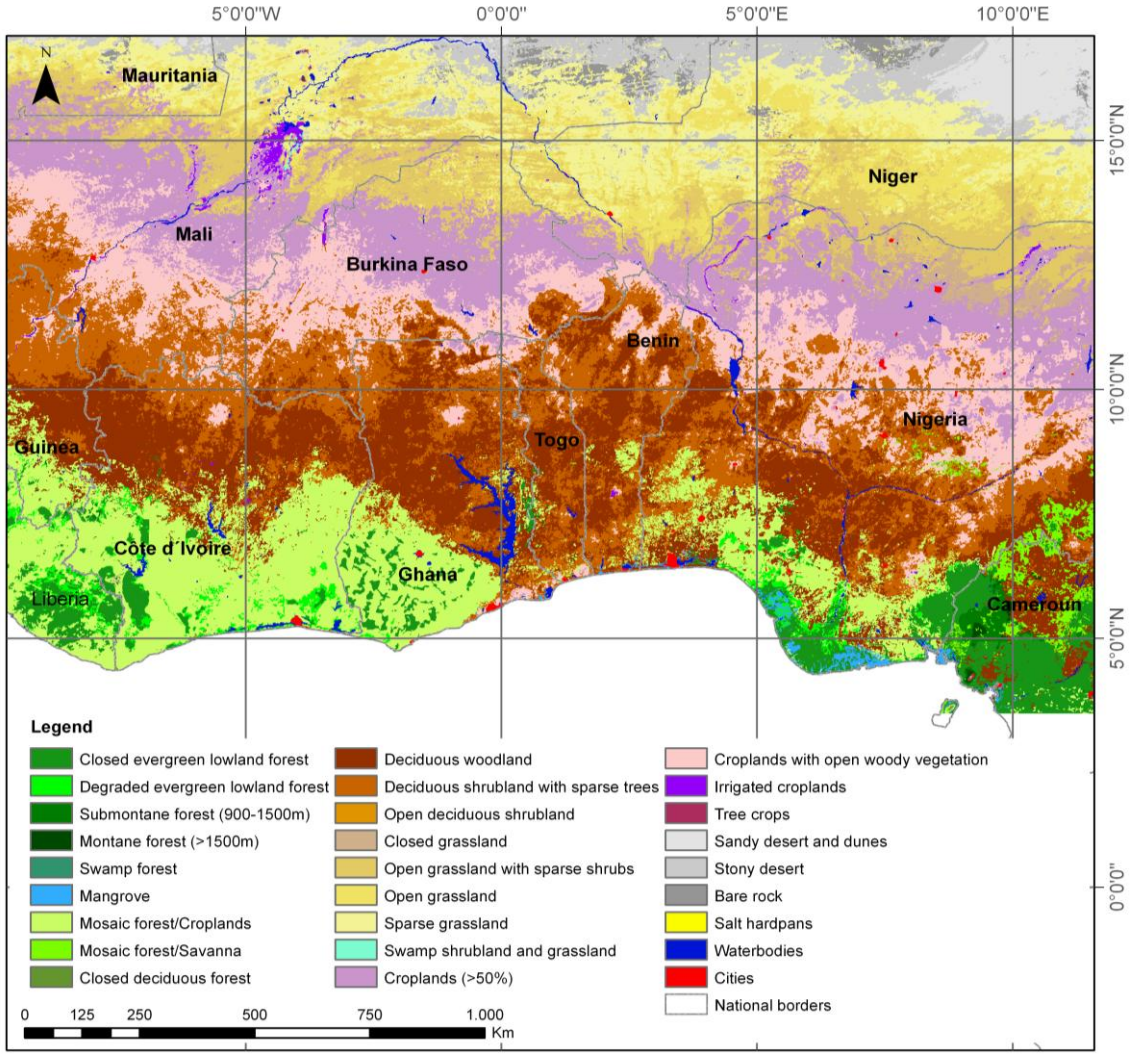

Figure 7: Land Cover map of West Africa at 1 km resolution using the SPOT 4 satellite (Mayaux et al. 2003), modified).

3.2 Local scale study area

At a local scale, three National Parks covered by the study area at the regional scale were chosen. They are all located in the savanna area. Parts of each of these parks had been designated as observatories by BIOTA West Africa. Whereas the goal of the regional study is to analyse the spatial and temporal distribution of fires, the fire analyses at the local scale will help to understand the effects of fire on vegetation, which is expressed by the degree of burn severity. This part gives a short overview of the geographical position, the climate, the vegetation and the fauna of each protected area.

3.2.1 Pendjari National Park

Pendjari National Park was created in 1961 and was classified as Pendjari national biosphere reserve by the UNESCO (Kassa 2008; BIOTA 2010). The park is located in the tropical zone of Sudanian type in the north-west of the Republic of Benin. It covers a surface of 2755 km^2 and is located between 10°30'N and 11°30'N and between 0°50'E and 2°00'E (figure 8). The park borders on the Arli-W-Singou complex, a vast reserve in Benin, Burkina Faso and Niger. It comprises two cynegetical zones, that of Atacora and that of Pendjari. It is limited by the Atacora range and the Pendjari river.

Two seasons of unequal length characterize the climate of this zone:

- The rainy season lasts for about five months, from May to September. Annual rainfall varies between 900 and 1200 mm, with a yearly means of 919.77 mm (Kassa 2008). During the rainy season, temperature varies between 25 and 30 degrees, with a relative humidity that can reach up to 97 percent in August.
- The dry season lasts for seven months, from October to April. Between March and April, the temperature reaches a maximum of between 42 and 45 degrees. The relative humidity throughout the season is between 25 percent and 55 percent.

The vegetal formations to be found are gallery forests along the rivers, bush savannas, tree savannas, grassland savannas, dry forests and clear forests. Every year, the vegetation is submitted to bushfires so as to maintain the dynamics of the savannas by assuring a good regrowth of gramineous plants for the animals and to prevent the pastures from being cluttered by shrubs. The fires that are lit by the park management are maintenance fires, mainly early fires that are lit between November and December in order to improve visibility for tourists. By contrast, the late fires, which occur regularly, are lit by poachers or breeders who do not respect the recommended times for setting fires.

As to the different species of animals to be found in the protected areas, only a brief

synthesis without any details will be given in this work: The fauna of Pendjari National Park consists of great mammals, rodents and a diversity of birds, of great reptiles and of several species of fish (Lalayé 2001; Nago et al. 2006; Mensah et al. 2006; Mensah et al. 2007; Kassa 2008).

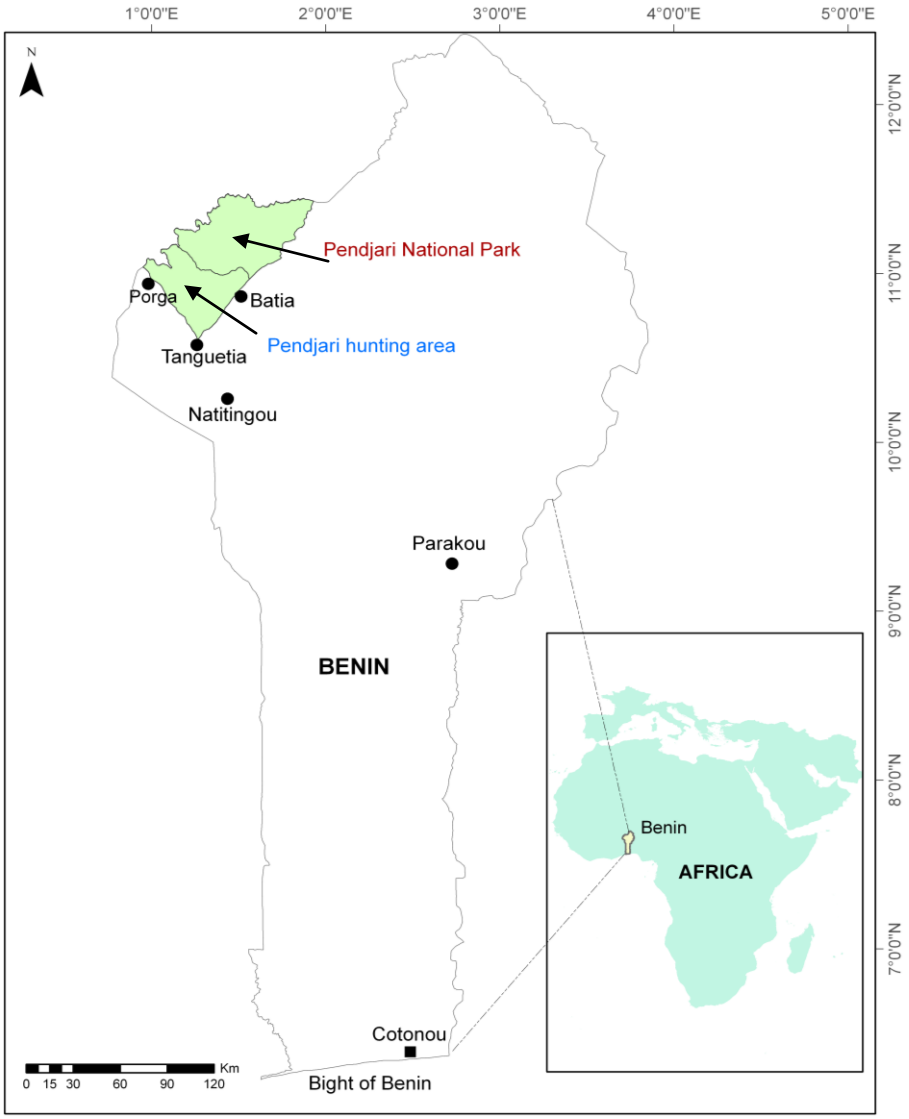

Figure 8: Pendjari National Park in Benin.

3.2.2 Comoé National Park

Comoé National Park (figure 9) is located in the north-east of Côte d'Ivoire, in the Zanzan region. It covers a surface of 11,500 km^2 and it is located between 8°32'- 9°32'N and 3°01'-4°24'W. It was founded in 1968 under the name Bouna Reserve. Since 1983, it has been inscribed on the World Heritage List of the UNESCO because of the diversity of its flora and fauna (Fischer & Linsenmair 2001). In 2003, it was declared an endangered world heritage site due to the intense poaching, which made use of fire, and the lack of management (UNESCO 2010). In fact, due to the unfortunate political situation in Côte d'Ivoire since 11th

September 2002 and the civil war in the country, the park has ceased to be managed; this has again led to an intensification of poaching.

The climate is characterised by two seasons:

- The rainy season, where annual rainfall varies between 1000 and 1400 mm. It lasts from April to October (Dugué et al. 2003).
- The dry season from mid October to mid April.

The yearly mean temperature is of 28 degrees, with a relative moisture of 40 to 50 percent in the dry season (Traoré 2009).

The local vegetation is of Sudanian type and it shows the same vegetal formations as Pendjari Park. Just like in Pendjari National Park, the savannas with vegetation ranging from woodland and shrub to grass are often affected by fire (N´Klo 2001).

Notable animals of its fauna are antelopes, buffalo, elephants, monkeys, crocodiles, hippopotami, migrating birds and several species of fish.

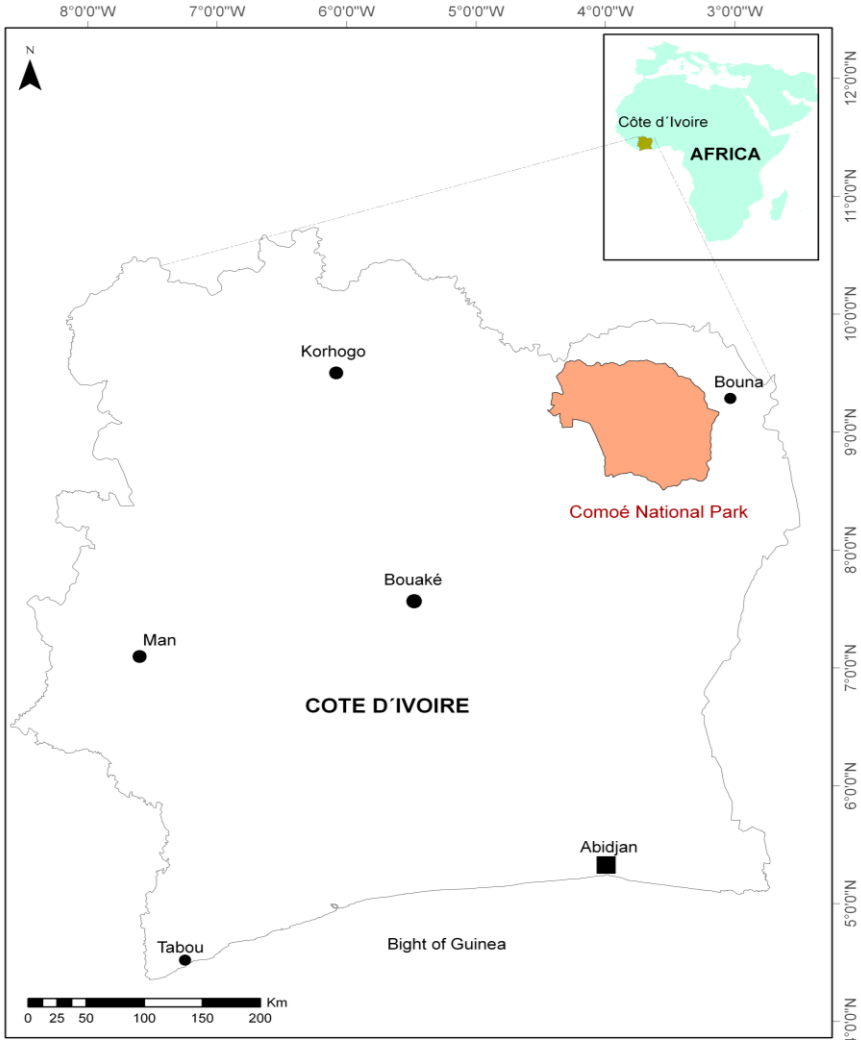

Figure 9: Comoé National Park in Côte d´Ivoire.

3.2.3 Bontioli Reserve

Bontioli National Park (figure 10) is in the Bougouriba province in south-western Burkina Faso, located at 11°10' N and 3°00' W. It covers a surface of 127 km^2. It was created in 1957. The reserve consists of two parts, the Bontioli total fauna reserve and the Bontioli partial reserve (Cord 2007). Bontioli National Park is 40 km south of Dano. "This protected region serves as a near-natural reference area for the anthropogenically heavily disturbed region of Dano" (BIOTA 2010). Nevertheless, this reserve, of small size in comparison to Comoé and Pendjari National Parks, is very much influenced by human land use.

The climate is characterized by two seasons, namely the rainy season from May to September, with an annual rainfall varying between 900 and 1000 mm and the dry season from October to April. The latter is characterised by a heightened temperature, which can reach a maximum of 45°C in March and April and a relative moisture of between 25 and 60 percent (Yahmed 2005). The vegetation, of Sudanian type, consists of woodlands and shrub savannas, grass savannas and gallery forests along the rivers.

The Fauna consists, among others, of elephants, crocodiles, hippopotami, migrating birds and several species of fish, various species of monkeys and antelopes (Ouédraogo 1999).

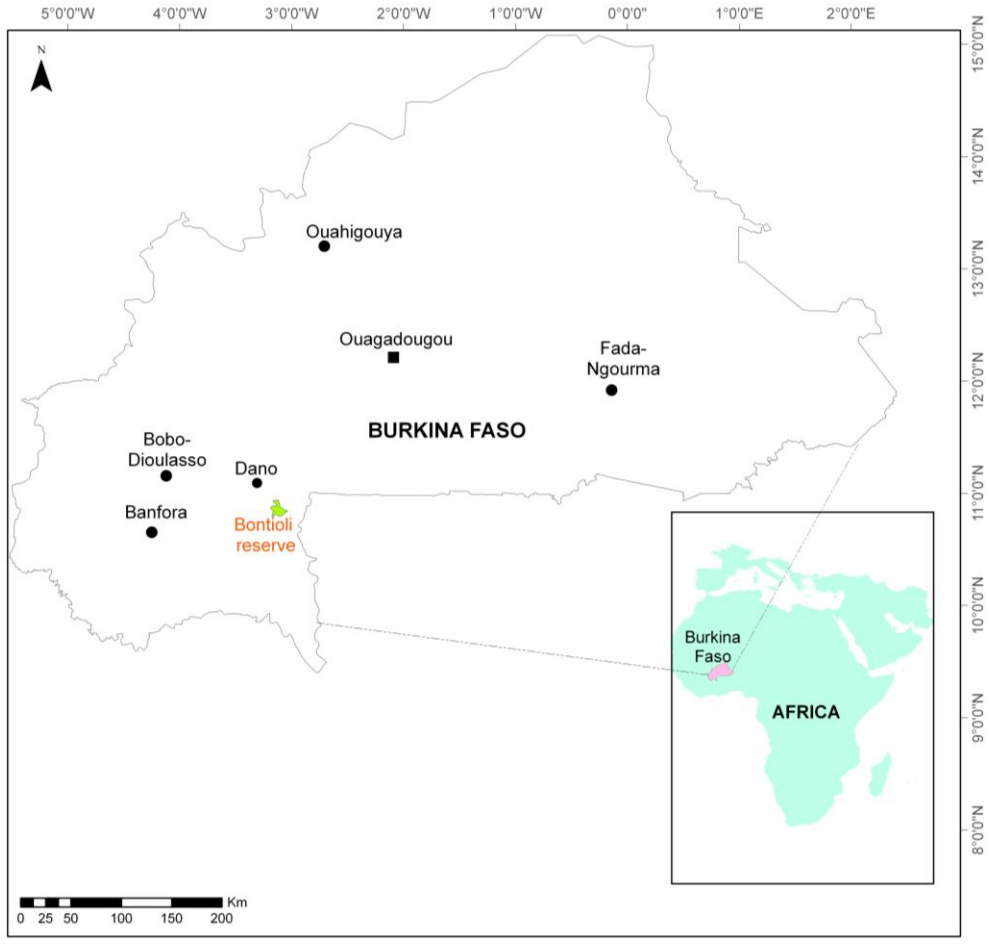

Figure 10: Bontioli Reserve in Burkina Faso.

CHAPTER 4: METHODS OF PROCESSING DATA AND DATA ANALYSES

4.1 Regional scale analysis

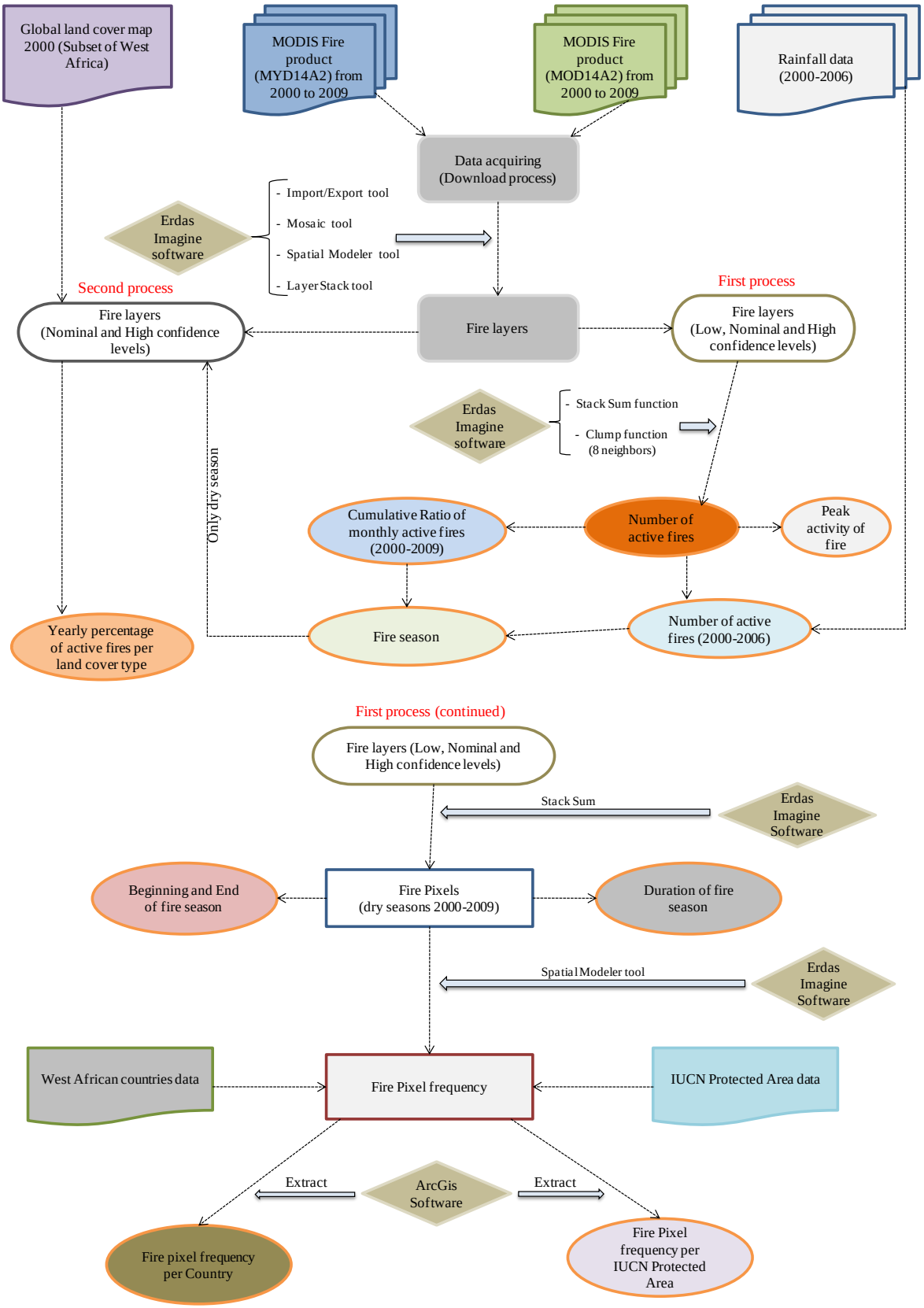

Figure 11: Workflow for the regional scale analysis.

This section will explain every step of the processing chain which was used for performing the regional scale analysis based on the MODIS data as illustrated in the above figure (figure 11).

The MODIS fire products on board of Terra and Aqua were acquired freely and downloaded through the websites of NASA, namely the USGS Global Visualization Viewer site (NASA 2010c) and the Warehouse Inventory Search Tool (WIST) site (NASA 2010d). The data are a sampling of MODIS 8-Day summary fire products MOD14A2 and MYD14A2. Each product is a composite of fire pixels detected at a 1 km spatial resolution over a period of 8 days.

The data cover a period from 2000 to 2009, which corresponds to 46 data layers each year, except when data layers are missing, which is the case for some years (see section 5.1.1). Each of the data layers represents the aggregation of the fires detected.

Two ways of processing the data were used. In both of them, the ERDAS Imagine software version 9.1 was used in the whole processing chain; ARGIS software version 9.3 was also used at certain points. In processing of the data, the fire pixels were assigned class 1 and the non fire pixels were assigned 0.

In the first process, all pixels classified as fire were used, i.e. pixels with three detection confidence levels, namely low, nominal and high confidence fires. The detection confidence is an estimation of the probability, ranging between 0 and 100 percent, that a fire pixel detected represents an actual fire on the ground, as opposed to a false alarm. All pixels in the fire mask with a confidence below 30 percent are classed in the “low confidence” group, those with a confidence greater or equal to 30 and lower than 80 percent are designated as “nominal confidence” fire pixels, whereas the “high confidence” group contains all the fire pixels with a confidence between 80 and 100 percent (Giglio 2010). Using the fire pixels of the three confidence level classes permits to detect the maximum number of fire pixels in an observation period. This process makes it possible to calculate the total number of active fires on a regional scale that occurred between 2000 and 2009, the cumulative number of fires per month during these 10 years of observation and the fire seasonality in West Africa. The fire season thus determined will subsequently be used in the analyses of the spatial and temporal distribution of bushfires with parameters such as the peak of fire activities, beginning and end of the fire season, its duration and the frequency of fires. All the results of this analysis will be presented in section 5.1 and discussed in section 6.1.

The second process only considered the class of fires which regrouped the nominal and high confidence levels in order to obtain fewer false alarms (Giglio 2005). In this particular

case, the fire pixels of low confidence class were considered as non fire and were tagged 0. Subsequently, the subset of Land Cover Map 2000, which covers the West Africa region (see chapter 3, section 3.1.2) was linked with the active fire layers of each dry season. These layers contain the aggregation of fire pixels detected during the dry seasons from 2000 to 2009. The goal of this operation was to find out which kinds of vegetation were affected by bushfire activity during the observation period. The results are shown in chapter 5.2 and discussed in chapter 6.2.

After the download of the MODIS data, which were delivered by USGS in hdf format, they were imported into the ERDAS format (as an .img file) using the Import/Export dialog tool. The mosaic tool was used to put the four MODIS tiles of one product into one output image. Then, the Spatial Modeler dialog was used to select the fire pixels. This selection was made by assigning 1 to a pixel if its value was superior or equal to 7; otherwise, 0 was assigned (appendix 1). Where the low confidence fire class was not considered, a fire pixel was assigned 1 if its value was superior or equal to 8; otherwise, 0 was assigned (appendix 2). Then, all layers classified as fire were put together using the Layer Stack tool, so that there was one output layer for each input layer.

In the first process, whose goal it was to determine the number of active fires per year (appendix 3); all fire layers were summed by using the Stack Sum function of the Spatial Modeller dialog. The output of this function is a single layer which contains the sum of the pixel values for all the layers of the input. Then, the contiguous groups of fire pixels were aggregated using the Clump (8 neighbors) function. This function regroups fire pixels that are very close to one another and counts them as a single fire. This means that in this step, the number of fires for every month and year, not the number of fire pixels, was determined.

After this, the proportion of fires per months was calculated through the following equation:

$$\textbf{Cumulative proportion of fires per month} = \frac{\text{Cumulative sum of fires per month 2000-2009}}{\text{Total number of fires 2000-2009}}$$

This proportion lets us determine, in a first step, in which months the fire activity is greatest. Secondly, the cumulative proportion of fires per month from 2000 to 2006 was compared to the rainfall data from the same period in order to determine the season of bushfires in West Africa. Rainfall data were obtained from two climate data sets. The first is from REMO (Paeth & Hense 2005), covering a period from 2000 to 2003 and the second is

from CMORPH (Joyce et al. 2004), covering the period from 2004 to 2006. Only rainfall data from 2000 to 2006 were taken into consideration, as the REMO model results from 2007 to 2009 were not yet available at the time of this study.

For the statistical analyses, the SPSS software was used in order to determine if there is a relation between rainfall and fire occurrence.

The cumulative sum of fires detected by month between 2000 and 2009 made it possible to identify the peaks of bushfire activity.

In order to determine the beginning and end of the fire season, its duration and the frequency of fire pixels in the dry seasons between 2000 and 2009, the number of fire pixels was now considered. This was done by adding up the fire layers per month and year by using the Stack Sum function, without using the clump function, which merges neighbouring fires.

The length of a fire season during a dry season is worked out by using the "Natural Breaks (Jenks)" classification method in ArcGis, which is described in the software manual. In this method, the data are subdivided into several classes, so that each class regroups the elements that are relatively similar to each other, forming a cluster, and that the differences between the classes are as great as possible (Shaner & Wrightsell 2000).

The beginning and end of a fire season within a dry season was determined by identifying the first and last fires occurring within it. For this purpose, the weekly layers of fire pixels were grouped into data sets for each month by using the layerstack function.

In order to find out in how many years from 2000 to 2009 fires occurred in a given place, all the fire pixels within each dry season from 2000 to 2009 were added up (e.g. all fire pixels from October 2000 to April 2001), which led to a one output layer for each fire season of this observation period. After that, the spatial Modeler dialogue in Erdas Imagine was used to select the fire pixels that were detected in more than one dry season from 2000 to 2009. If a fire pixel was detected in one or more than one dry season, this pixel was attributed the respective class of frequency, if none was detected, it was given the attribute 0.

Subsequently, the frequency of fire pixels by country and protected area of the study area was determined by applying the extract by mask method (Spatial Analyst tool) in ArcMap. This method extracts the cells of a grid that correspond to the areas defined by a mask.

For the extraction of the fire frequency within a country, the fire pixels were displayed in the polygon map of the West African countries. Then, the features of a selected country and the grid containing the fire pixels were use as input data. In the output, the counts of pixels were classified by frequency. The same method was used to extract the frequency of fire pixels inside each protected area.

4.2 Local scale analysis

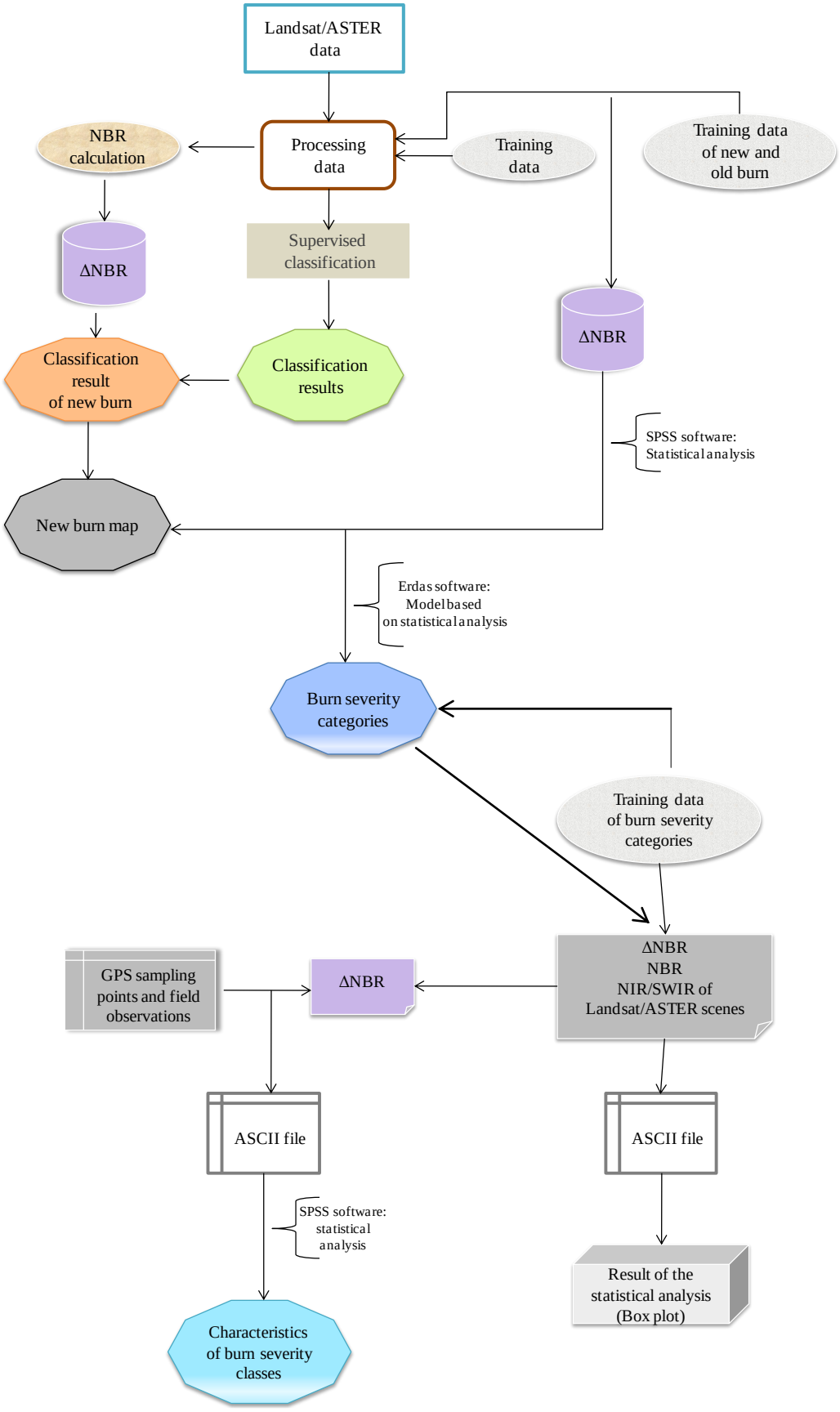

Figure 12: Workflow for the local scale analysis.

This whole processing chain for the local scale fire mapping is illustrated in the figure 12, and will be explained in detail in this section. For this analysis, high resolution satellite imagery was used to map the burn area and burn severity. The processing data were so-called "snap shot" data from Landsat ETM+ and ASTER. All the results from this section will be presented in chapter 5.3 and discussed in chapter 6.3.

4.2.1 Landsat ETM+ data

Burn area and burn severity for Comoé National Park, Pendjari National Park and Bontioli Reserve were mapped using multispectral Landsat ETM+ imagery at 30 m resolution.

The Landsat data used in this work are shown in table 5. Landsat scenes from different dates and years are listed below and were downloaded and processed for the pre fire and post fire severity analysis. The imagery is provided in a UTM projection, zone 30 and zone 31 and in the reference system WGS84.

Table 5: Overview of Landsat ETM+ data acquisition used for the local scale fire severity assessment.

Area name	Date of acquisition	Julian day	Path/Row	Spectral Bands	Projection	Reference
Comoé National Park	13th April 2000 25th December 2000	104 360	196/053 196/054	1-5 and 7	UTM	WGS84 Zone 30
Pendjari National Park	20th October 2001 5th October 2007 7th December 2001 26th February 2008	293 278 341 057	193/052 193/053	1-5 and 7	UTM	WGS84 Zone 31
Bontioli Reserve	25th October 2001 28th December 2001	298 362	196/052	1-5 and 7	UTM	WGS84 Zone 30

Landsat images used for the analysis of these three parks were taken in different years. The reason for this is that many images presented strong cloud cover, which made them unsuitable for analysis. Therefore, images which presented very little or no clouds cover had to be found.

Landsat imagery was imported into ERDAS Imagine version 9.1 and ENVI software version 4.4, where all further data processing was completed. The data processing consisted of the following steps:

- Satellite image data processing
- Calculation of the Normalized Burn Ratio
- Classification

These steps will now be described in detail.

4.2.1.1 Satellite image data processing

The Landsat data were delivered by USGS in a Geo Tiff format, with each data band saved in another Tiff file. This means that, at first, there are nine single Tiff files used for the data layering, namely channels one (blue), two (green), three (red) four (near infrared), five (middle infrared), six.1 and six.2 (thermal channels) seven (middle infrared) and eight (panchromatic). In order to process the files in the ERDAS Imagine software, they first were imported into the ERDAS format (as an .img file). Second, all band layers were stacked into one image and saved as an img file. Third, all images were subsetted to bands 1 to 5 and 7 and quantized as 8-bit data. The AOI (areas of interest) tool was used to select, create and edit only the relevant part of the satellite image, which contains the whole study area at each respective site for the local scale analysis.

4.2.1.2 Calculation of the Normalized Burn Ratio

A band ratio was calculated from both images (pre and post fire) using the SWIR (2.09 - 2.35 µm) and NIR (0.75 - 0.90 µm) channels, since these have been shown to be most responsive to post fire conditions. This index is calculated by subtracting the reflectance of band 7 from band 4 in Landsat.

$$\mathbf{NBR_{(TM/ETM+)} = (band\ 4 - band\ 7) \,/\, (band\ 4 - band\ 7)}$$

This equation is made using a model function of ERDAS software, which is called the Spatial Modeler Language. The NBR derived post fire was subtracted from the NBR calculated from pre-fire data to obtain the differencing index (ΔNBR).

4.2.1.3 Image classification

The multispectral classification is the process of sorting pixels into a finite number of individual classes based on their data values. If a pixel satisfies a certain set of criteria, this pixel is assigned the class that corresponds most to those criteria (ERDAS Incorporation, 1997). There are two different ways of classifying pixels into different categories: the unsupervised and the supervised classification method. Supervised classification has stronger user control than the unsupervised classification. In the former procedure, pixels are chosen which represent a pattern that is known or that can be identified with other sources. Previous knowledge about the data, the classes desired and the algorithm to be used is necessary before selecting the training areas. By identifying patterns from the satellite image, one can train the program to identify pixels with similar features. If the classification is correct, every resulting class will show a pattern that had first been assigned by the user.

Unsupervised classification is more automatized. It allows to set parameters which the computer uses as a guideline for detecting statistical patterns in the data.

In the first step, the supervised classification was used to define the burnt and unburnt areas. Before deriving the classification, it was important to do some training on data in order to determine the spectral signature of each element on the Landsat scene. The signature editor was used to create the signatures of older burn scars, new burn scars, vegetation and bare soil on the Landsat imagery, which were saved as .sig files. Each Landsat image and the corresponding signature file were use as input for the supervised classification dialog to create the classes.

In the second step, with the record function, only the new burn class derived from the classified image was considered. This class was filtered using the statistical filtering with the majority function of the kernel window 7x7 to remove small polygons for producing a generalized burn severity map. After this, the mask dialog was used to create a map of new burn areas by first selecting, as input mask the new burn class .img file and then as input .img file the ΔNBR.

Now the ROI (Region of Interest) tool of the ENVI software was used for a second data training on the Landsat image which only considers new and old burn. After this, the training data was imported into the ΔNBR image to create a distribution histogram for new and old burn using the SPSS software. This statistical analysis shows the min, max and Std.Dev. for each distribution. Following Landmann (2003), the histogram distribution of new burn will be considered in the rest of the process to create the burn severity categories.

A model was then worked out by using the Spatial Modeler dialog of ERDAS to edit the burn severity category values. In this model, the input is the map of new burn areas, on which a function based on the result of the distribution histogram of new burn was performed. The result of this model was rescaled in 8 bit and recoded according to the pixel values in order to obtain the burn severity categories.

In a third step, training data for each category were made from a classified image by using the ROI tool. These ROI points were imported into the ΔNBR image, NBR image and the NIR/SWIR of Landsat scenes and exported as ASCII file. The SPSS software was used to create a box plot.

In the fourth step, the GPS sampling points were imported into the ΔNBR image (map of new burn areas img file) and exported as an ASCII file. The ground truth data was only collected in Pendjari National Park in February 2008; the collecting method will be detailed in

section 4.2.3. The SPSS software was used to analyse the field data and the map of new burn areas.

4.2.2 ASTER data

ASTER data have a higher spectral resolution than the other satellite data used in this work, with nine bands from Visible Infrared to Shortwave Infrared. It also has a higher, 15 meter, spatial resolution in the Visible Near-Infrared. ASTER data sets, unlike MODIS products and Landsat data, are not free. ASTER data are acquired as on demand data by acquisition requests. For more information see the ASTER web page (NASA 2010e).

In this part, only Pendjari National Park in Benin was considered. ASTER scenes pre and post fire were processed. The data used was acquired on 8th December 2007 (pre-fire) and on 26th February 2008 (post-fire). The ASTER imagery was provided in a UTM projection with zone 31 and in the reference system WGS84. The processing was the same as with the Landsat imagery. A short description of each step follows.

First, the images were imported into ERDAS Imagine. Only the VNIR and the SWIR channels were grouped into one image file. The AOI and subset image tools were used to select and create new image subsets, which contain only the study area.

Second, the NBR band ratio was calculated using the Shortwave Infrared (SWIR: 2.14 to 2.36 µm) and Near-infrared (NIR: 0.78 to 0.86 µm) channels. Here, the index is calculated by subtracting reflectance of band 8 and band 3N in the ASTER data.

$$\mathbf{NBR_{(ASTER)} = (band\ 3N - band\ 8) / (band\ 3N - band\ 8)}$$

Third, the ΔNBR image was derived from pre and post fire data.

4.2.3 Field verification

The field protocol used to estimate the biomass loss related to the burn severity will now be described.

In a given savanna type, a transect is made to establish the biomass loss. Therefore, the coordinates of some burned surfaces are determined by using GPS. Then, in order to make a visual description of biomass loss by fire, the biomass that must have been there before the fire is visually estimated based on the type of surrounding vegetation. Then, the biomass burned by the fire is estimated by looking at what has remained in the zone after the fire. These latter estimations were made in percent values of between 0 and 100, with the maximum value of 100 percent signifying that the whole pre-existing vegetation has been consumed and that the soil is completely exposed after the fire. By contrast, if the vegetation

has remained intact after the passage of the fire or if no fire has scorched the vegetation, the value was estimated to be 0 percent.

The state of the burned area made it possible to determine whether the fire had occurred early or late in the season. Within this study, the thickness of the ashes was not estimated because they had been largely dispersed by the wind. It is important to note that the month of the field trip (February) is characterised by a dry wind called Harmattan which blows at a very high speed and thereby quickly disperses the ash. Finally, two photos were taken to characterize the burned area from two different angles.

In total, 329 points were collected on the ground. However, due to the problems connected with Landsat's scan line corrector, only 149 points could be used in the analysis and verification of the remotely sensed results.

CHAPTER 5: RESULTS

5.1 Spatio-Temporal analysis of active fires on a regional scale

From the various approaches that exist to characterize fire patterns temporally (Clerici 2006), some indicators were selected that can be deemed appropriate to the data availability and to the goal of representing the broad scale fire activity in West Africa. These indicators are: fire occurrences, beginning and end of the fire season, peak activity of the fires, fire season duration and the frequency of fires (revisit cycle).

5.1.1 Fire occurrences

MODIS Aqua and Terra datasets were analysed to obtain the total number of active fires detected per year from 2000 to 2009 in West Africa, with observations beginning on Julian day 057 of 2000. From 2000 to 2009, a rising number of fires detected can be observed, with 38,594 active fires detected in 2000 and 138,974 fires detected in 2009. A total of 1,172,191 active fires were detected during these ten years. Figure 13 shows a steady increase in the number of fires detected by the MODIS sensors at 1 km resolution during the observation periods. However, in year 2009, the number of fires detected (138,974) was lower than that detected in 2008 (146,463). An explanation of this decrease could be that the data observed on Julian day 337 of the year 2009, which corresponds to the 8 day summary fire product of Aqua and Terra from 26th November to 2nd December could not be taken into account, as they were not available on the website. A visual assessment of the active fire image sent to the author of this study by the NASA in jpeg format showed great fire activity. It can therefore be expected that the actual number of fires occurring in 2009 was not significantly lower than that in 2008.

The great increase in active fires detected between 2000 and 2001 (from 38,594 to 63,261) might mainly be due to the fact that two of the months with greatest fire activity are completely (January) or mostly (February) missing from the data. Similarly, the further drastical increase between 2001 and 2003 (131,028 active fires) could be explained by the fact that MODIS Aqua began to acquire fire data from Julian day 185 of 2002, which corresponds to the 8 day summary product from 27th June to 4th July 2002, whereas before, only MODIS Terra had been active. Therefore, the number of fires detected in 2000 and 2001 is only based on the MODIS Terra data, the number for 2002 (95,478 active fires) also contains some data from MODIS Aqua (starting on Julian day 185), and the numbers for 2003 to 2009 were calculated from the data provided by both sensors.

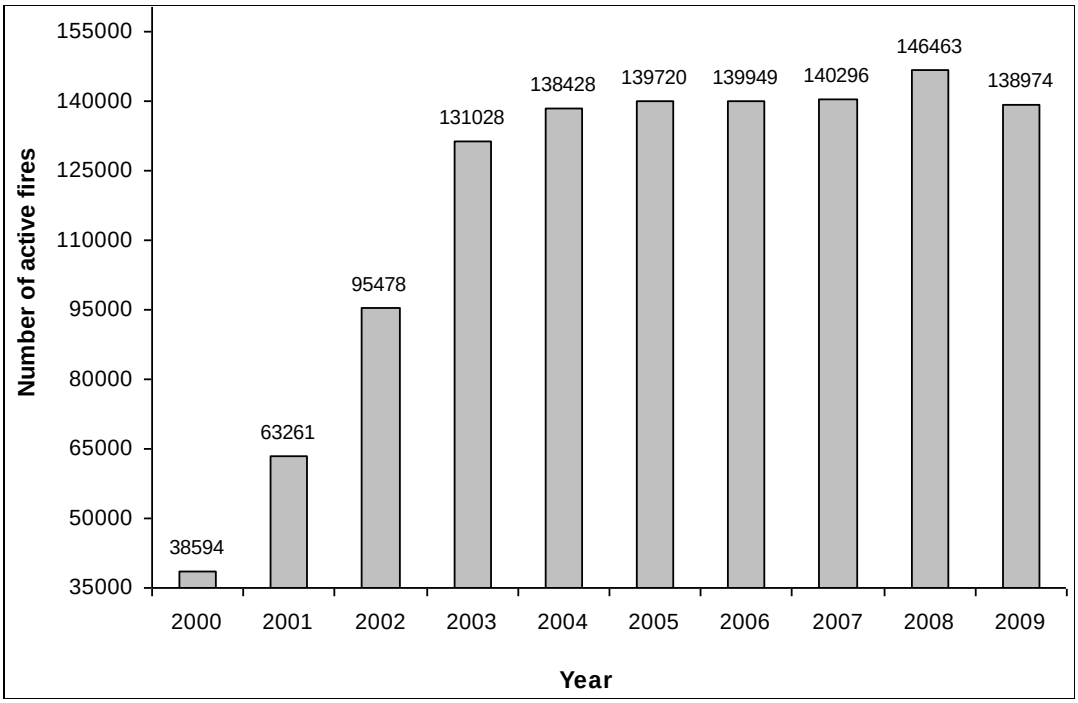

Figure 13: Steady increase in fire activity detected by 1 km MODIS satellite observations between 2000 and 2009 in the study area. MODIS Terra observations started on Julian day 057 of 2000, MODIS Aqua data are only included from Julian day 185 of 2002 onwards, all data for Julian day 337 of 2009 are missing.

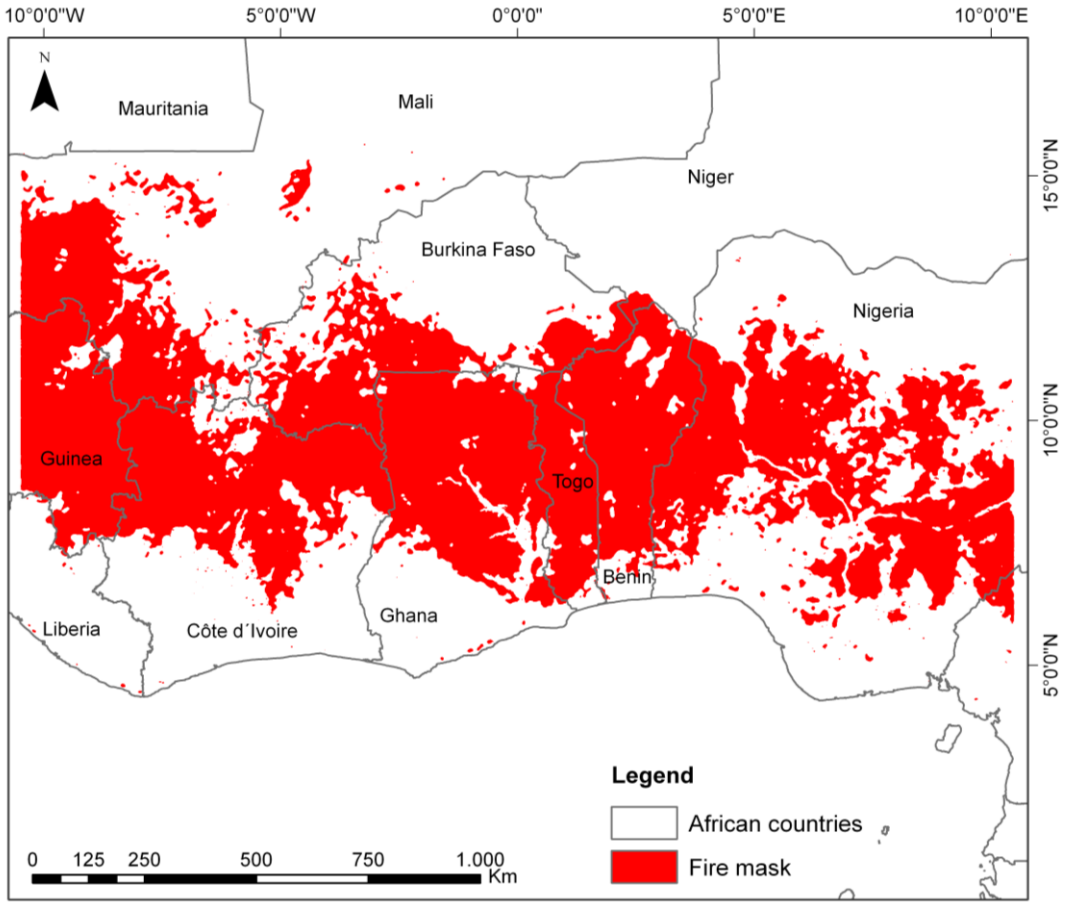

Figure 14: Map of cumulative fires detected by MODIS from 2000 to 2009 in West Africa.

Figure 14 shows the cumulative distribution of active fires detected by MODIS sensors from 2000 to 2009 in the study area. The fire activities took place in the savanna formations between the limits of dense forest and steppe, which are located between 5° and 15° of Northern latitude.

The active fires during the observation period were extracted per country to show the number of fire occurrences during the ten years in these countries. Only the countries completely covered were taken into consideration, namely Côte d'Ivoire, Ghana, Togo, Benin and Burkina Faso and also the countries of which at least two thirds are covered by the four MODIS tiles. These countries are Mauritania, Mali, Nigeria, Liberia, Guinea and Niger. The results are presented in table 6. If one considers the occurrence of fires detected per country, one notices that the accumulation of the number of fires dectected is highest in Nigeria, which is followed, in descending order, by Côte d´Ivoire, Ghana, Mali, Bénin, Guinea, Burkina Faso, Togo, Niger and Liberia, and lowest in Mauritania. However, the density of fires in the various countries, which is obtained by dividing the total number of fires detected in a country through its surface, it is greatest in Benin, which is followed, in descending order, by Togo, Ghana, Côte d´Ivoire, Guinea, Burkina Faso, Nigeria, Mali, Liberia and Niger. In Mauritania, whose surface is greatest and which has a very low number of fires detected, the fire density is extremely low.

Table 6: Cumulative number of active fires occurrences and their density (Nb. active fires/km^2) in 11 countries within the study area as detected by the MODIS sensors (2000-2009).

Country	Number of active fire detected by MODIS sensors	Country surface (in km^2)	Density of fire [Cumulative nb. of active fires (2000-2009)/km^2]
Côte d´Ivoire	175,735	322,462	0.545
Ghana	164,510	238,540	0.690
Benin	112,994	112,620	1.003
Burkina Faso	106,748	274,200	0.389
Togo	56,184	56,785	0.990
Mauritania	6	1,030,700	$5.8213*10^{-06}$
Mali	132,233	1,241,238	0.110
Nigeria	302,265	923,768	0.327
Liberia	1,523	111,370	0.014
Guinea	112,280	245,857	0.460
Niger	3,289	1,267,000	0.003

In order to check if there is a relation between the surface and the cumulative number of fires detected per country, the SPSS statistic software was used to determine the so called square curve of regression (appendix 4) and the Pearson correlation test. The square regression test shows a very weak positive relationship, with $R^2 = 0.198$. The results of the Pearson test are summed up in the table 7.

Table7: Relation between the surface of the country (in km^2) and the cumulative number of fires detected during the observation period (2000-2009).

Variables	N (quantity)	r (Correlation coefficient according to Pearson)	Significance level with P > 0,05
Surface in km^2	11	-0.004	0.99
Cumulative number of active fires detected (2000-2009)			

The statistical analysis shows that r = -0.004 is negative, with a value between -0.99 and 0.00, which means that there is no relation between the surface and the number of fires detected per country. The value for P = 0.99 is significantly higher than 0.05, which shows that the results are not significant.

However, if Mauritania, Mali and Niger are removed, 2/3 of which are located in the desert, where – due to the absence or discontinuous distribution of fuel biomass – no fires occur, the square curve of regression shows a very strong correlation, with $R^2 = 0.94$ (appendix 5). The results of this analysis are summed up in table 8.

Table 8: Relation between the countries of which 2/3 of the surface are located in savanna zones and the cumulative number of fires detected in them during the observation period (2000-2009).

Variables	N (quantity)	r (Correlation coefficient according to Pearson)	Significance level with P < 0.01
Surface in km^2	7	0.943**	0.001
Cumulative number of active fires detected (2000-2009)			

** Correlation is significant at 0.01 level (2-tailed)

r = 0.943** shows the existence of a strong correlation between the surface of the countries in which more than 2/3 are covered by savanna, and the number of fires detected. P<0.01 shows that the relationship is highly significant.

5.1.2 Fire season

Fire season is defined as the season where fire activity is very high. This season was determined from the cumulative number of active fires detected during each month across the ten years of observation and the proportion of this number to the overall number of fires

(figure 15). As evident from figure 15, virtually all fires detected during the ten years took place in the months from October to April. The sum of all fires observed in the months between October and April (from 2000 to 2009) makes up 98.75 percent of all fires detected by MODIS sensors during these years.

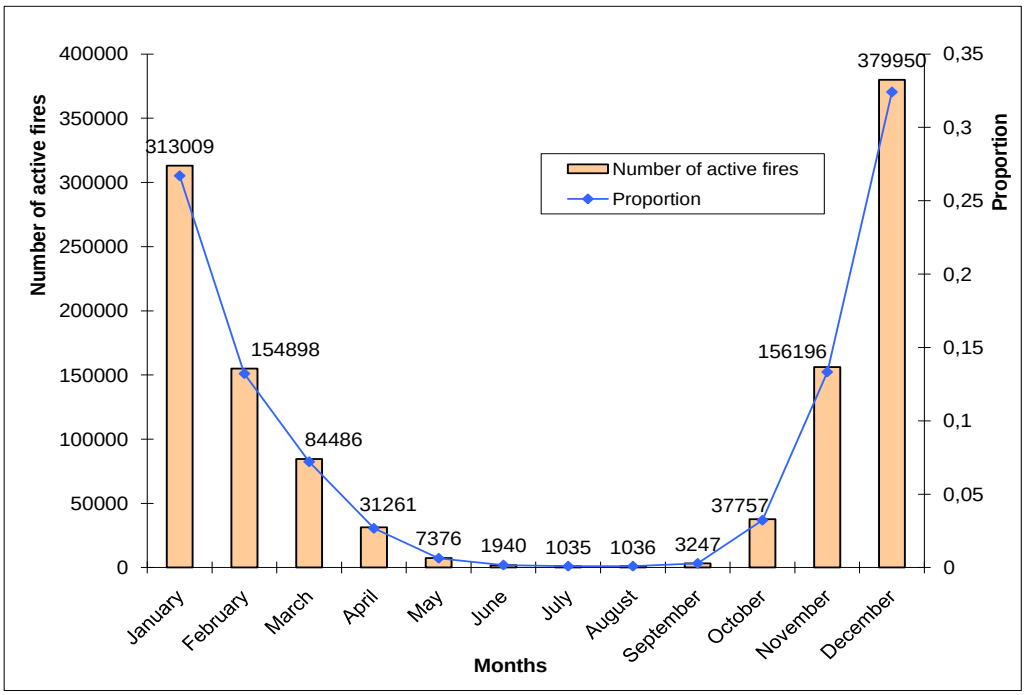

Figure 15: Accumulation of active fires per month detected by 1 km MODIS satellite between 2000 and 2009 and their proportion (in %).

In a further step, the fire curve was compared to rainfall (monthly precipitation in mm) observations from 2000 to 2006 (Figure 16). The comparison shows that the two curves move in opposite directions, with fires being proportionally very rare from May to September (1.34 percent of all fires observed), whereas the proportion of rainfall amount is high (66.50 percent of the all the precipitation occuring throughout these observation months).

Conversely, the proportion of fires detected from October to April is very high (98.66 percent), whereas the rainfall amount is proportionally low, with only 33.50 percent of all precipitation occuring throughout these months.

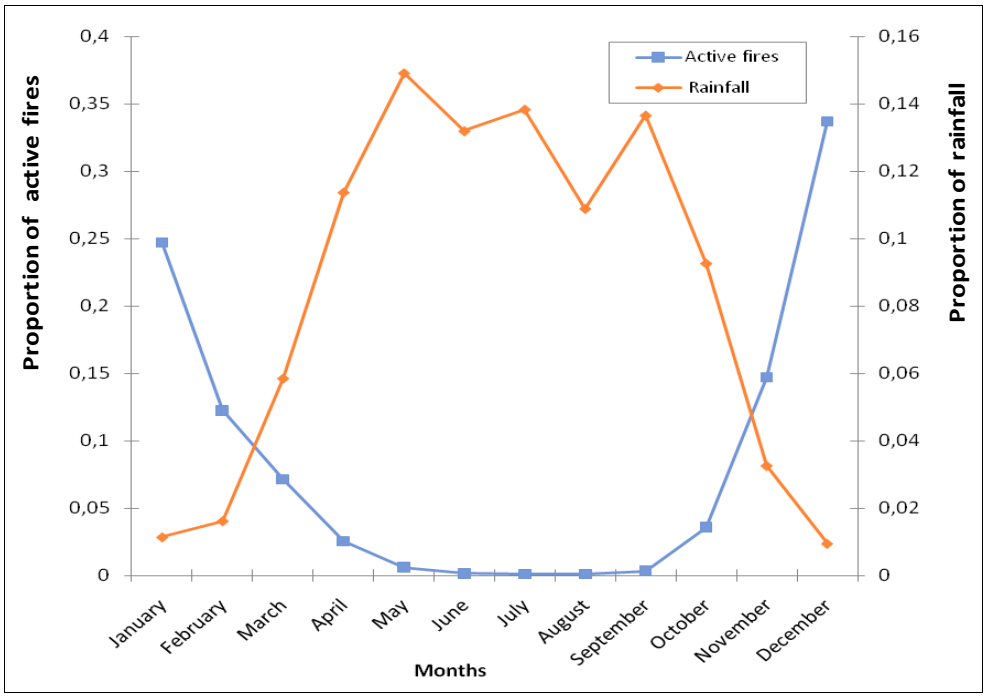

Figure 16: Cumulative proportion of rainfall amount and number of active fires (in %) detected per month from 2000 to 2006.

In order to find out if there is a relation between the proportion of fires detected and the proportion of rainfall amount, the Pearson and Spearman-Rho statistical tests were carried out on these data. Figure 17 shows the correlation curve obtainted between the cumulative proportions of fires detected and rainfall amount per month between 2000 and 2006. The cubic curve was chosen because it best shows the line of regression that models the data points. The result is a cubic curve of negative regression with $R^2 = 0.951$. The Pearson and Spearman-Rho correlation tests were carried out to test the correlation coefficient (r) between these two variables. The result of this analysis is summed up in table 9.

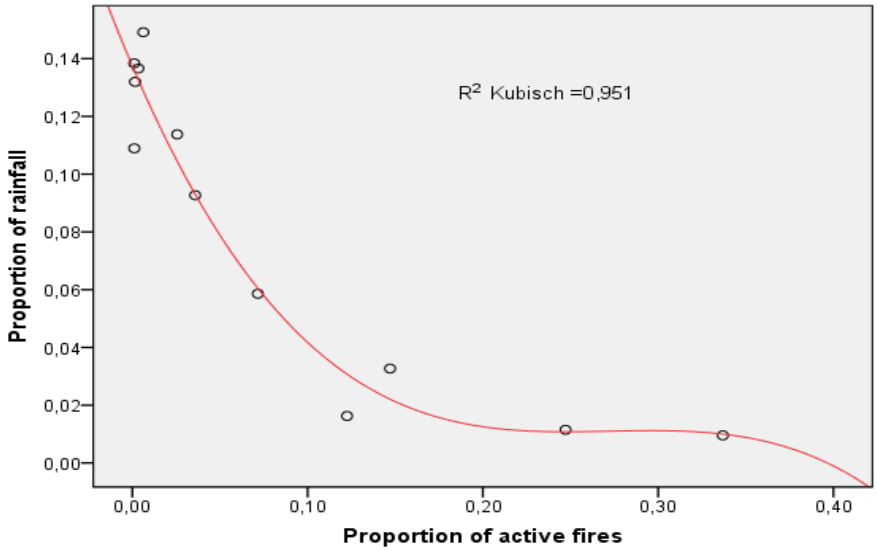

Figure 17: Curve of correlation between the monthly cumulative proportions of rainfall amount and the number of active fires detected from 2000 to 2006.

Table 9: Relation between the monthly proportions of the number of active fires detected by MODIS and the rainfall amount during the observation period from 2000 to 2006.

Variables	N (quantity)	r (Correlation coefficient according to Pearson)	r (Correlation coefficient according to Spearman-Rho)	P < 0.01 value
Cumulative monthly proportion of number of active fires detected (2000-2006)	12	-0.878**	-0.867**	0.000
Cumulative montly proportion of rainfall in mm from 2000- to 2006				

** Correlation is significant at 0.01 level (2-tailed)

The analysis of these variables shows that there is a very strong negative relation (r = -0.878 and -0.867) between the cumulative monthly proportion of the number of active fires detected and rainfall amount. The significance level P < 0.01 shows that this result is highly significant, which means there is a correlation between monthly fire occurrence and rainfall. This result confirms the curves obtained in figure 16, which shows that the occurrence of fires in a month varies depending on the rainfall quantity of this month. This variation means there is a high number of fires detected by MODIS in the months where rainfall amount is low, and vice versa. All the results of this subsection show that, as far as fire activity is concerned, there are two seasons in West Africa. In the dry season, from October to April, there is a high occurrence of bushfires and very low rainfall. Therefore this dry season is also the season of bushfires. Conversely, in the rainy season from May to September, the occurrence of fires is very low whereas the amount of rainfall is much greater.

5.1.3 Peak activity of fire

The peak of the fire season is referred to as the time of the season corresponding to the maximum fire activity, which is herein represented by the month in which most active fires have been detected. This peak was identified by establishing the cumulative sum of fires detected during the dry seasons from October to April from 2000 to 2009 (figure 15). The month characterized by greatest fire activity, in terms of the number of fire counts detected, is December (379,950 active fires detected). This phenomenon could be found in every year of this study's observation period. Between October and December, there is a rapid increment in fire occurrences, followed by a decrease in activity starting in January and continuing up until April. The fire season begins in October with 3.26 percent of fires detected. The number of fires progressively grows to 13.49 percent of fires detected in November and reaches a peak of 32.82 percent of fires detected in December. The percentage of fires detected in January is

still high, with 27.04 percent and goes down to 13.38 percent of all fires detected in February, followed by March, where 7.30 percent of all fires took place and finally April where the proportion of fires is low, with 2.70 percent off all fires detected occuring in this month.

5.1.4 Temporal and spatial distribution of fires in West Africa

The topic of this section is the temporal and spatial distribution of fires, i.e. the question as to where fires take place at what time during a dry season in West Africa. For this purpose, active fire counts for two dry seasons, October 2002 to April 2003 and October 2005 to April 2006 (figures 18a and b) were assessed.

This active fire count showed that fire activity generally starts earlier at higher latitudes (14°-12° N) and, with the proceeding of the dry season, goes southwards (as far as 6° N) and intensifies. As to vegetation zones, areas where fire activity starts early (i.e. in October and November) are mainly located in the Sahelian, Sahelo-Sudanian and Sudanian regions, which can be found in the south-west and center of Mali, the north-west, south-west, center and south-east of Burkina Faso, northern and central Benin and Togo, north-eastern central Guinea, north-eastern and north-western Côte d´Ivoire, northern Ghana, north-western, northern and central Nigeria and one area in the south-west of Niger.

Fire activity is greatest and very widespread in December, when it occurs in all countries cited above, also in many areas where no fires took place in October and November. December fires begin at 12° N and progressively advance to 6° N. Fires now also take place in Sudano-Guinean and Guinean savanna.

January fires occur roughly in the same areas as December fires, but these fires are fewer compared to those in December and generally occur more towards the south while they are now rare towards the north.

The February, March and April fires are comparatively rare and dispersed in different areas between 15° and 5° N. They mainly occur in the forest zones and in the transition zone between Guinean savannas and forests. In Liberia, it is only in this period that fires are observed. There is a strong concentration of these fires in the forest region in southern Guinea. They are also observed near the Inner Niger Delta in Mali and in the irrigated croplands around it.

In the coast area of the observation zone, the only fires to be observed were very few and dispersed, and occured mainly from February to April.

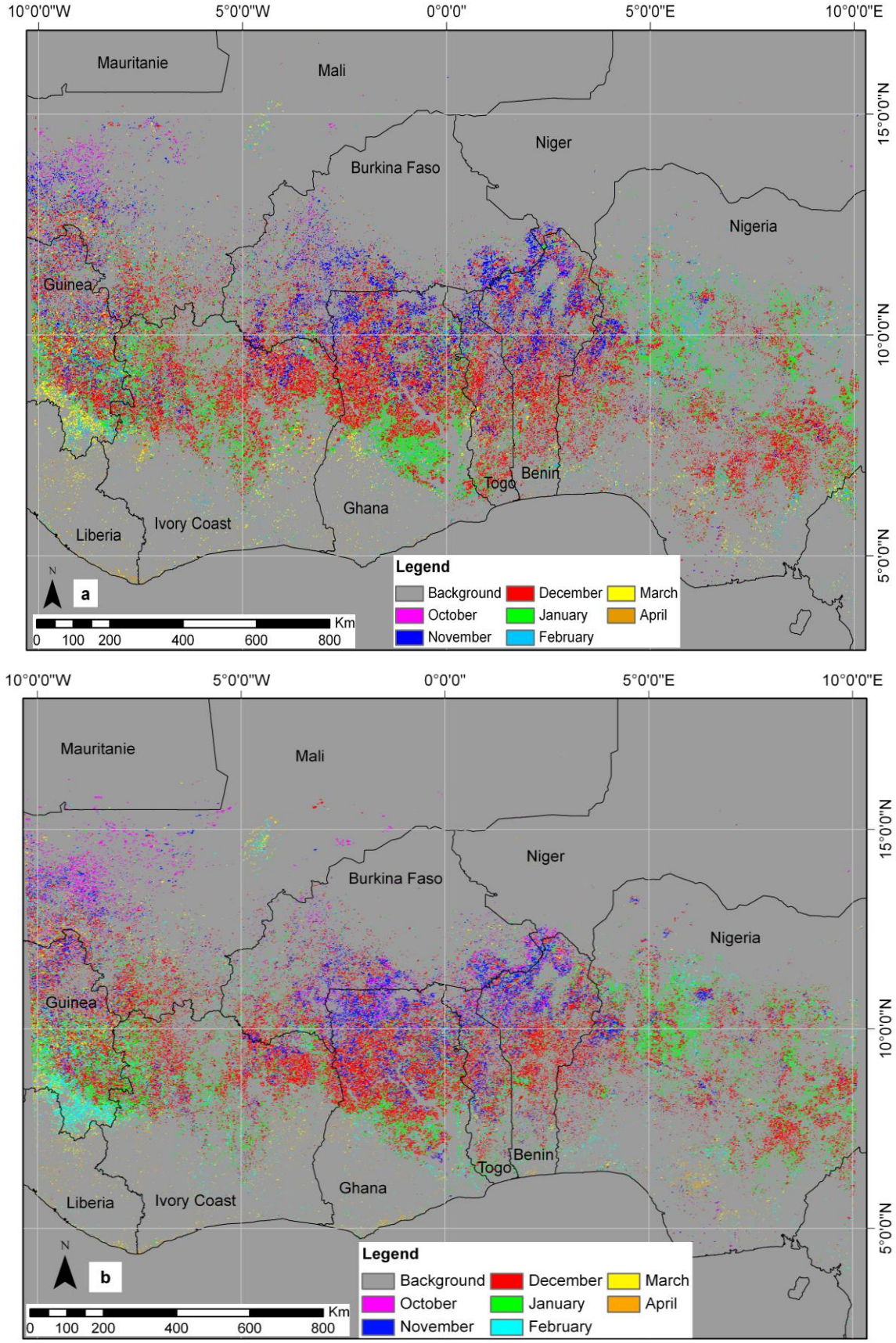

Figures 18 a and b: Monthly distribution of active fire during the dry season in West Africa. a) Dry season October 2002 to April 2003 and b) Dry season October 2005 to April 2006.

5.1.5 Fire season duration

Fire season duration is the total length of time between the start and the end of the fire season (from October to April, which is the main fire observation season), that means from the moment when 2 percent of fire pixels have been detected to the moment when 100 percent of pixels have been detected. For obtaining the fire season duration, only two dry seasons (those from October 2003 to April 2004 and from October 2004 to April 2005) were used as observation period because the fire season duration is virtually the same for all dry seasons during the ten years of fire observations. Figures 19a and 19b show that the duration of the fire season is prolonged at higher latitudes.

In general, very early fires, which appear in the first month of the fire season, i.e. October, start at high latitudes and advance towards lower latitudes which are characteristic for late fires, appearing in the 6^{th} or 7^{th} month.

Very early fires announce the beginning of the fire season and represent about 3 percent of the fire pixels detected, corresponding to 2,891,370 ha of affected area. These fires were observed in the north-west of Mali and in some areas in northern Burkina Faso. In October 2003, a very early fire was also observed in central Niger.

Early fires, which occur in the 2^{nd} and 3^{rd} month of the fire season, i.e. November and December, make up about 51 percent of fires detected, affecting an area of 49,153,290 ha. They are more concentrated between 12° and 8.5°N. The great majority of them was observed in northern Ghana, in central, southern and southern-central Burkina Faso, in northern and central Benin, in the north-east of Côte d'Ivoire, in eastern and western Nigeria and in eastern Guinea.

Late fires occur in the 4^{th} and 5^{th} month of the fire season, i.e. January and February. They make up 40 percent of fires detected, which corresponds to an area affected of 38,551,600 ha. These fires could be observed mostly in the region of the Baoulé V and in north-western Côte d'Ivoire. In Ghana, these fires are located in the area around Lake Volta. They are also widespread in the center of Nigeria. In Benin, Togo and Burkina Faso, there are fewer of these fires compared to the early fires occuring in these countries. In Guinea, these fires are concentrated in the center-east. Most of these late fires take place in a transition zone between the savanna and the forest.

Very late fires are fires occuring in the 6^{th} to 7^{th} month of the fire season, i.e. March and April, i.e. towards the end of the fire season. They make up 6 percent of the fires detected, corresponding to 5,782,740 ha of area affected. These fires are concentrated in southern Guinea, in the Inner Niger Delta in Mali, and they are dispersed in the forest zone in West

Africa. They can be found in various places around Comoé National Park and in the very north of Benin. In sum, most fires appear in the 'early fire season' (November-December) and the 'late fire season' (January-February).

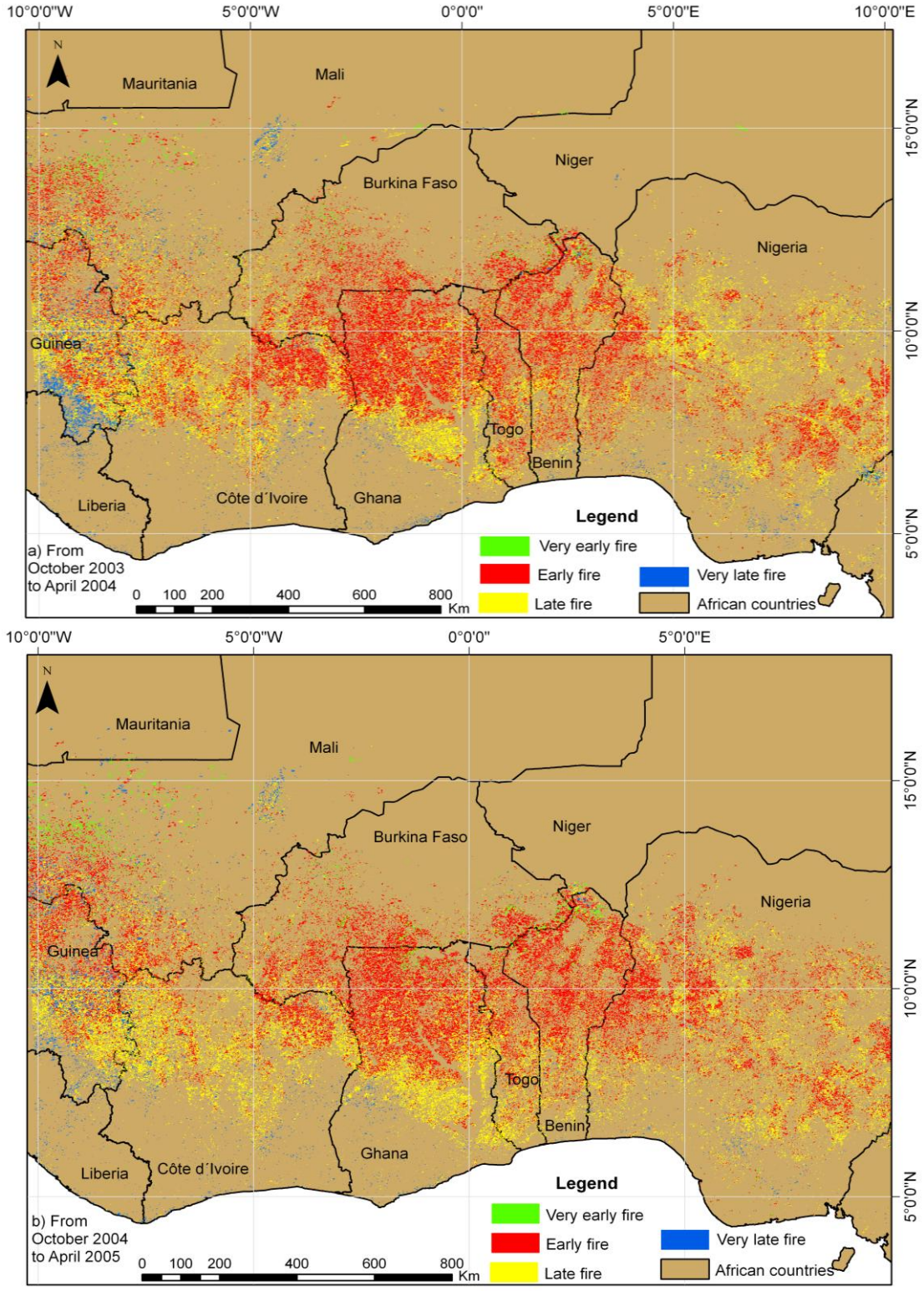

Figures 19: Spatial distribution of fire season duration: Example of two dry seasons, a) October 2003-April 2004 and b) October 2004-April 2005. Very early fire (273-304); Early fire (305-365); Late fire (001-059) and Very late fire (060-121).

5.1.6 Fire frequency

Fire frequency refers to the fire revisit cycle that is the number of times an area is burnt (Williams & Cook 2001). In this thesis, this frequency concerns the number of times a fire pixel occurs within the observation period of 9 dry seasons (October 2000 to April 2009). To determine the fire pixel frequency during this period, a threshold was defined, which was set at 1 (in this case an area could be burnt in more than one season). Figure 20 shows where burning occurred at least in one of the dry seasons during the observation period.

The fire frequency map reveals that the fire pixels at the margins of the fire belt are detected once or twice. Most of these pixels are found in the Saharo-Sahelian and Sahelian zone towards the north and in the transition zone between forest and Guinean savanna towards the south of the observation zone. Towards the center of the fire belt, i.e. in the Sahelo-Sudanian, Sudanian and Sudano-Guinean savanna, one can find fire pixels that were detected in 3 or more dry seasons, up to nine dry seasons. One remarkable exception is the area with oil fields in Nigeria, in the southern part of the forest zone around 5°N. Fire pixels that can be detected more than 6 times, up to 9 times are concentrated in this zone. This is an expression of the permanent fires occurring on the oil fields.

Another remarkable exception is the Inner Niger Delta in Mali, where fire pixels with a frequency of up to 5 can be detected in an area that is located in the Sahelian savanna. This could be explained on the one hand by the availability and continuity of biomass in this area, and one other hand by the intense agricultural activity (which includes clearing fields with fire) made possible by the fertility of the soil and the availability of water.

Table 10 sums up the frequency of fire pixel occurrences detected by country of the study area (figure 20). Whereas in Mauritania, Liberia and Niger, the maximum fire pixel detection frequency is 3, 5 and 7 seasons respectively, the other countries within the study area have a maximum of 9 fire pixels detected (i.e. a fire was detected in every season).

Frequency 0 represents the areas where no fire pixel was observed throughout the 9 fire seasons. The number of fire pixels and their frequency varies from one country to another, but in general, the greatest number of pixels is detected only in one season, except for Ghana and Guinea (in Togo and Benin, the number for one and two seasons are almost equal), and this number gradually diminishes towards the maximum frequency of 9. The cases of Ghana, Guinea, Togo and Benin could be explained by the fact that they contain great areas of savanna with available fuel, where fires frequently occur.

The number of pixels that were detected 9 times, i.e. in every dry season, is very low (41 fire pixels detected) compared to the total number of fire pixels detected in the other

frequency classes. This may be an indication that fires do not generally revisit the same area in many consecutive years.

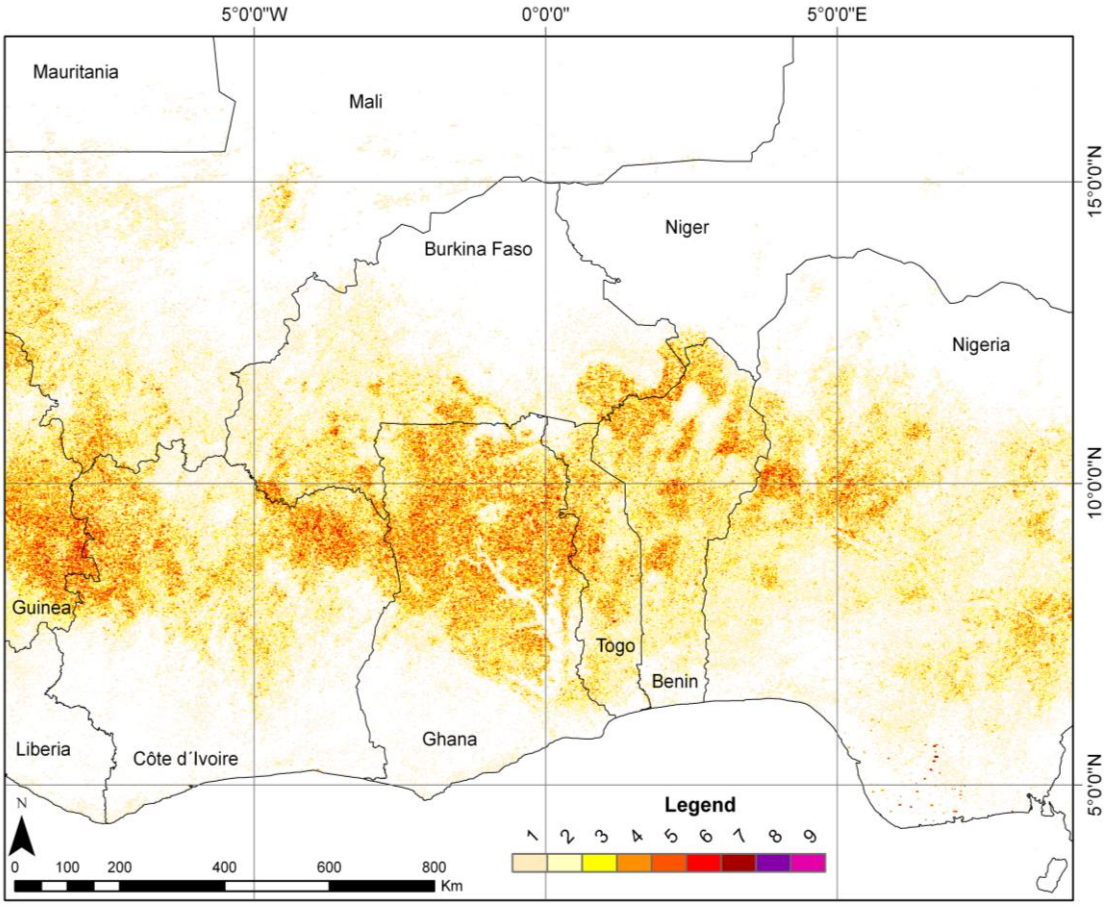

Figure 20: Spatial and temporal distribution of fire pixel frequency in the study area. Data compiled from October 2000 to April 2009. In West Africa fire pixels were detected one to nine times, i.e. in 1 to 9 out of the 9 dry seasons.

Table 10: The frequency of fire pixels detected during the 9 dry seasons (October 2000 to April 2009) per country within the study area.

Fire pixel frequency detected during the 9 dry seasons										
Country	**0**	**1**	**2**	**3**	**4**	**5**	**6**	**7**	**8**	**9**
Benin	27,582	30,854	30,123	23,299	13,857	6,140	1,870	390	56	1
Burkina Faso	200,710	54,047	31,660	18,454	9,670	3,928	1,301	285	55	4
Côte d´Ivoire	180,837	65,863	47,955	36,886	23,320	11,645	4,127	1,051	167	11
Ghana	101,349	39,125	39,060	40,923	31,421	16,656	5,938	1,381	205	9
Guinea	36,935	21,705	27,117	25,745	18,507	9,830	3,605	954	147	12
Liberia	90,088	9,730	997	88	9	5	0	0	0	0
Mali	920,788	78,629	42,776	22,852	9,935	3,487	798	151	14	0
Mauritania	311,684	2,474	133	9	0	0	0	0	0	0
Niger	853,030	2,072	827	595	273	122	35	9	0	0
Nigeria	589,118	165,129	95,498	50,436	22,133	7,978	2,284	549	53	2
Togo	13,558	15,433	15,273	11,288	6,551	2,800	900	202	37	2
Total	3,325,679	485,061	331,419	230,575	135,676	62,591	20,858	4,972	734	41

Figure 21 shows the protected areas and fire frequency occurring within them. In general, all protected areas located in the Sahelo-Sudanian, Sudanian, Sudano-Guinean and Guinean savannas have fire pixels that were detected in more than 3 seasons. By contrast, the protected areas located in the Saharo-Sahelian and Sahelian zone as well as those at the transition between the Guinean savanna and the forest area only have fire pixels that were detected in 1 or 2 of the 9 dry seasons of the observation period. Nini Suhien National Park in south-western Ghana is the only protected area where no fire pixel at all was detected during the observation period. It is obvious from this figure that in most Protected areas, fire frequency is equal to, and often even higher than, the fire frequency in the non-protected area surrounding it.

The fire pixel frequencies observed in all the protected areas, as shown in figure 21, are detailed in table 11.

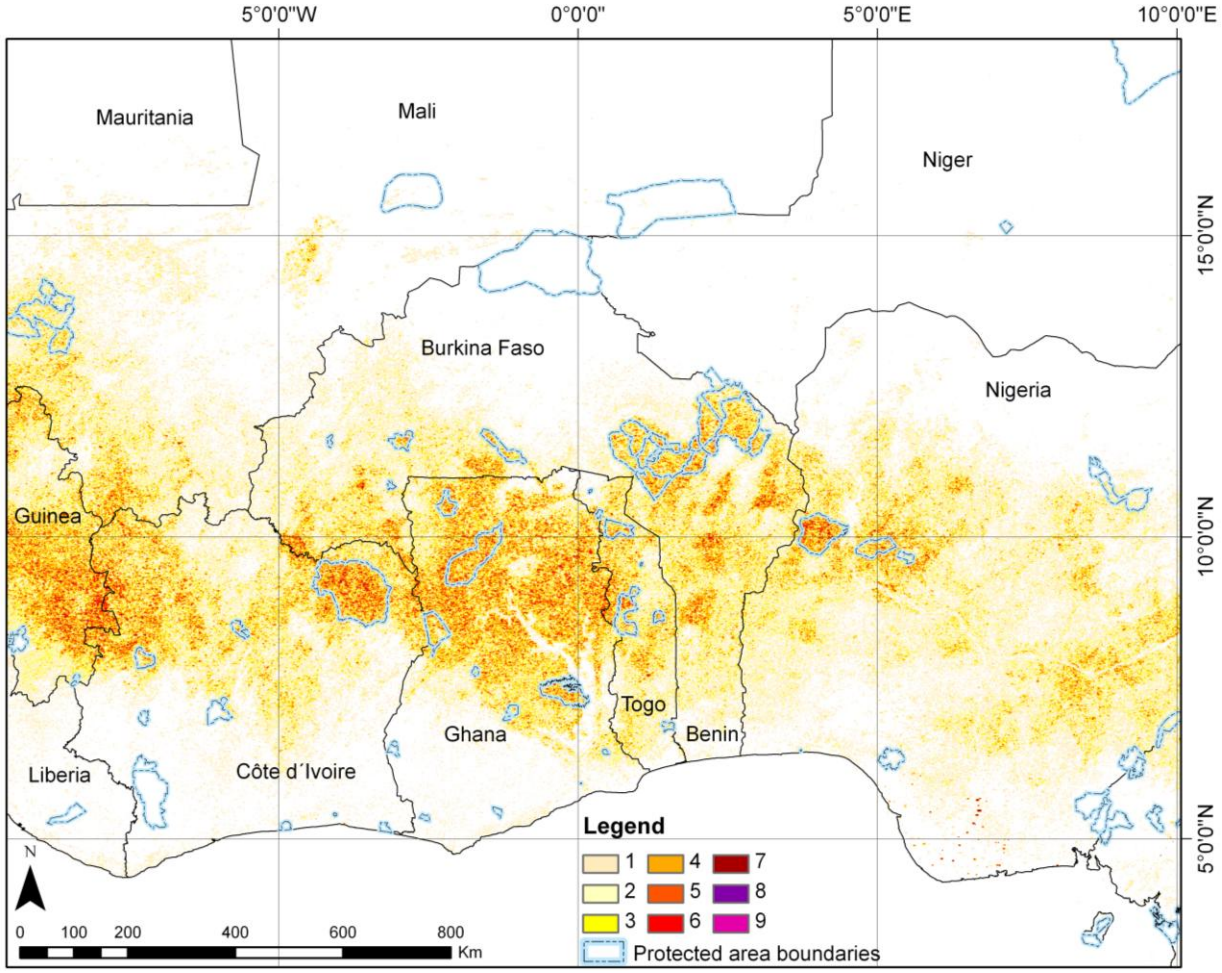

Figure 21: Spatial and temporal distribution of fire pixel frequency detected in the protected areas during the dry seasons (October 2000 to April 2009) inside the study area. In virtually all protected areas, fire pixels were detected at least once. Many protected areas show a high fire frequency. Protected areas are shown as grey outlined polygons.

Table 11: The frequency of fire pixels which were observed within the dry season observation periods (October 2000 to April 2009) in each protected area in the study area.

		Fire pixel frequency detected during 9 dry seasons									
Protected Area Name	**Country**	**0**	**1**	**2**	**3**	**4**	**5**	**6**	**7**	**8**	**9**
Hunting Zone Djona	Benin	118	231	319	333	235	117	32	4	1	0
Pendjari NP	Benin	111	526	1,145	1,515	1,233	663	176	34	13	1
Bird Reserve mare aux Hippopotames	Burkina Faso	6	21	50	47	29	16	4	3	0	0
Deux Bales NP	Burkina Faso	56	155	285	247	189	78	26	2	0	0
Faunal Reserve Bontioli	Burkina Faso	9	25	49	38	26	6	0	0	0	0
Faunal Reserve Singou	Burkina Faso	190	785	1,276	1,368	862	372	111	22	1	0
Kaboré-Tambi NP	Burkina Faso	76	215	460	505	321	135	47	9	3	0
Partial Faunal Reserve Ansongo-Menaka	Burkina Faso	16,408	259	12	0	0	0	0	0	0	0
Partial Faunal Reserve Arly	Burkina Faso	78	324	603	670	506	261	92	20	5	0
Partial Faunal Reserve Sahel	Burkina Faso	21,438	29	3	0	0	0	0	0	0	0
W du Burkina Faso NP	Burkina Faso	455	1,438	2,643	3,055	2,312	1,209	443	93	11	0
Azagny NP	Côte d´Ivoire	240	30	0	0	0	0	0	0	0	0
Banco NP	Côte d´Ivoire	21	9	0	0	0	0	0	0	0	0
Comoé NP	Côte d´Ivoire	139	745	2,006	3,275	3,415	2,436	1,122	319	69	8
Iles Ehotile NP	Côte d´Ivoire	290	2	0	0	0	0	0	0	0	0
Marahoué NP	Côte d´Ivoire	917	285	126	40	9	1	0	0	0	0
Mont Péko NP	Côte d´Ivoire	336	23	1	0	0	0	0	0	0	0
Mont Sangbé NP	Côte d´Ivoire	83	154	226	232	171	115	44	6	3	0
N´Zo Partial Faunal Reserve	Côte d´Ivoire	797	6	0	0	0	0	0	0	0	0
Tai NP	Côte d´Ivoire	5,006	11	0	0	0	0	0	0	0	0
Haut Bandama Fauna and Flora Reserve	Côte d´Ivoire	16	67	150	165	116	53	15	1	0	0
Bui NP	Ghana	67	250	492	571	476	221	81	14	4	0
Digya NP	Ghana	132	388	616	803	696	394	127	30	12	0
Game Production Reserve Bia	Ghana	391	1	0	0	0	0	0	0	0	0
Game Production Reserve Gbele	Ghana	8	39	144	282	303	173	82	15	5	0
Game Production Reserve Kalakpa	Ghana	5	13	23	30	11	8	0	0	0	0
Kakum NP	Ghana	202	2	0	0	0	0	0	0	0	0
Kogyae Strict Nat. Reserve	Ghana	18	109	131	118	68	27	11	2	0	0
Mole NP	Ghana	66	376	869	1,421	1,447	981	414	107	15	0
Nini-suhien NP	Ghana	168	0	0	0	0	0	0	0	0	0
Wildlife Sanctuary Boabeng-Fiema	Ghana	20	39	47	44	20	3	2	0	0	0
Strict Nature Reserve Massif du Ziama	Guinea	737	245	50	19	3	1	0	0	0	0
Strict Nature Reserve Mount Nimba	Guinea	93	47	23	11	0	0	0	0	0	0
Sapo NP	Liberia	1,096	4	0	0	0	0	0	0	0	0
Boucle du Baoulé NP	Mali	720	1,677	1,718	1,048	427	109	12	2	0	0
Fauna Reserve Fina	Mali	128	384	464	416	220	79	11	1	0	0
Faunal Reserve Badinko	Mali	438	756	642	404	184	57	8	1	0	0
Partial Faunal Reserve Gourma éléphant	Mali	6,395	366	23	0	0	0	0	0	0	0

Faunal Reserve Gadabedji	Niger	296	34	0	0	0	0	0	0	0	0
Faunal Reserve Tamou	Niger	903	802	789	587	271	122	34	9	0	0
Forest Reserve Okomu	Niger	1,009	247	22	2	0	0	0	0	0	0
Cross River NP	Nigeria	3,045	36	1	0	0	0	0	0	0	0
Cross River Takamanda NP	Nigeria	1,370	334	62	26	14	3	1	0	0	0
Game Reserve Dagida	Nigeria	33	89	144	96	42	14	4	0	0	0
Game Reserve Kashimbila	Nigeria	415	419	285	94	19	2	0	0	0	0
Game Reserve Lame-Burra	Nigeria	1,573	969	520	231	63	10	1	0	0	0
Kainji Lake-1 NP	Nigeria	75	260	697	1,153	1,234	843	470	138	21	2
Kainji Lake-2 NP	Nigeria	42	183	399	490	421	225	79	26	5	0
Strict Nat. Reserve Lekki	Nigeria	2	2	2	0	0	0	0	0	0	0
Faunal Reserve Abdoulaye	Togo	5	19	60	110	90	60	19	1	0	0
Faunal Reserve Djamdé	Togo	0	0	3	6	11	2	1	0	0	0
Faunal Reserve Galangashie	Togo	6	27	31	33	27	9	0	0	0	0
Faunal Reserve Togodo	Togo	25	83	106	69	26	4	0	0	0	0
Fazao-malfakassa NP	Togo	67	264	535	625	531	289	142	31	7	1
Fosse aux Lions NP	Togo	17	8	4	4	1	1	0	0	0	0
Kéran NP	Togo	33	146	293	388	328	138	57	13	0	0
Total		**66,390**	**13,958**	**18,549**	**20,571**	**16,357**	**9,237**	**3,668**	**903**	**175**	**12**

The total number of fire pixels detected with maximum frequency 9 is lowest (12 fires). Among these 12 fire pixels which were detected in every dry season of the observation period, 8 were detected in Comoé National Park (Côte d'Ivoire), 2 in Kainji Lake 1 National Park (Nigeria) and 1 in Pendjari National Park (Benin) and Fazao-malfakassa National Park (Togo). In all of the national parks, the total number of fire pixels that were detected at least once amounts to 83,430. The number of pixels considered as being without fire, with the fire frequency 0, is 66,390.The number of fire pixels detected with frequency 3 is 20,571, which is higher than the number of fire pixels detected with frequencies 1 and 2 as well as 4 to 9.

5.2 Fire activity by vegetation type

The number and distribution of active fire pixels in a given type of vegetation provides information that helps in the understanding of the spatial distribution of fire across different vegetation types.

By overlaying the land cover data with active fire pixel scores over a cumulative period of dry seasons from October 2000 to April 2009, land cover vegetation classes that are affected by fire can be assessed. Figure 22 shows that not all vegetations classes are affected by fire equally.

Whereas five classes of vegetation are greatly affected by the four parts of the fire season, namely Mosaic forest/croplands, Deciduous woodlands, Deciduous shrublands, Croplands and Croplands with open woody vegetation, the other classes of figure 22 are hardly or not at all affected by the fires in the fire season. Therefore, they are practically not visible in figure 22. Only 1.66 percent of the fire pixels are detected in these vegetation classes. These fires affect only 3,913,600 ha, compared to the 232,473,100 ha of area in the five vegetation classes that are greatly affected by the fires in the four parts of the fire season (Mosaic forest/croplands, Deciduous woodlands, Deciduous shrublands, Croplands and Croplands with open woody vegetation).

Fire seasonality is different between vegetation types as can be seen from figure 22 and appendix 6:

Most fires in Deciduous woodlands and Deciduous shrublands with sparse trees occur in December (45 and 42 percent respectively), and almost all of them are early fires (about 58 and 59 percent respectively) or late fires (38 and 34.5 percent respectively), whereas very early and very late fires are very rare in this vegetation class.

Croplands with open woody vegetation show a comparable fire seasonality: They also have their fire peak in December, and the percentage of fires occurring in the following months is almost the same as that for Deciduous woodlands and Deciduous shrublands with sparse trees, but the percentage of fires occurring in December is somewhat lower than for Deciduous woodlands (31.5 percent), whereas more fires occur in October and November (8.8 and 18.3 percent respectively).

By contrast, the fires occurring in Croplands are more evenly distributed across the months: A high percentage of fires already occur in October (18.5 percent), the peak occurs in November and December (about 22 percent for each month), and the rate of fires only gradually declines after that.

Whereas very early and early fires predominate in Croplands, the fires occurring in Mosaic forest/croplands are mainly late (52 percent) and very late fires (23 percent): Almost no fires occur in this vegetation type in October and November (2 percent in sum), December fires are propotionally important (22.2 percent), but the peak is reached only in January (27.8 percent), and fire activity still remains high in February and March.

These differences in fire seasonality between different vegetation types are also reflected in the vegetation types that are affected by fires in the different fire seasons: Most early and late fires occur in Deciduous woodlands and Deciduous shrublands. In fact, of the 1,265,679 fire pixels detected during the early fire season, 1,023,792 were observed in these two classes, whereas only 233,613 fire pixels are observed in the Croplands, Mosaic forest/croplands and Croplands with open woody vegetation and 8,274 in the other classes. Likewise, of the 888,111 fire pixels detected during late fire season, 635,835 were found in Deciduous woodlands and Deciduous shrublands, compared to 236,341 pixels found in Croplands, Mosaic forest/croplands and Croplands with open woody vegetation and 15,935 pixels in the other classes. By contrast, more than 50 percent of the very early fires occur in Croplands and Croplands with open woody vegetation, whereas fires occurring in decidous woodlands and Deciduous shrublands are proportionally (43 percent) and numerically (34,949 fire pixels) less important in this period. As to very late fires, they take place in many different vegetation classes: 43 percent of them occured in Deciduous woodlands and Deciduous shrublands, 48 percent were found in Croplands, Mosaic forests/croplands and Croplands with open woody vegetation, and 8 percent (10,494 fire pixels) in other classes, where hardly any fires occurred in very early to late fire season.

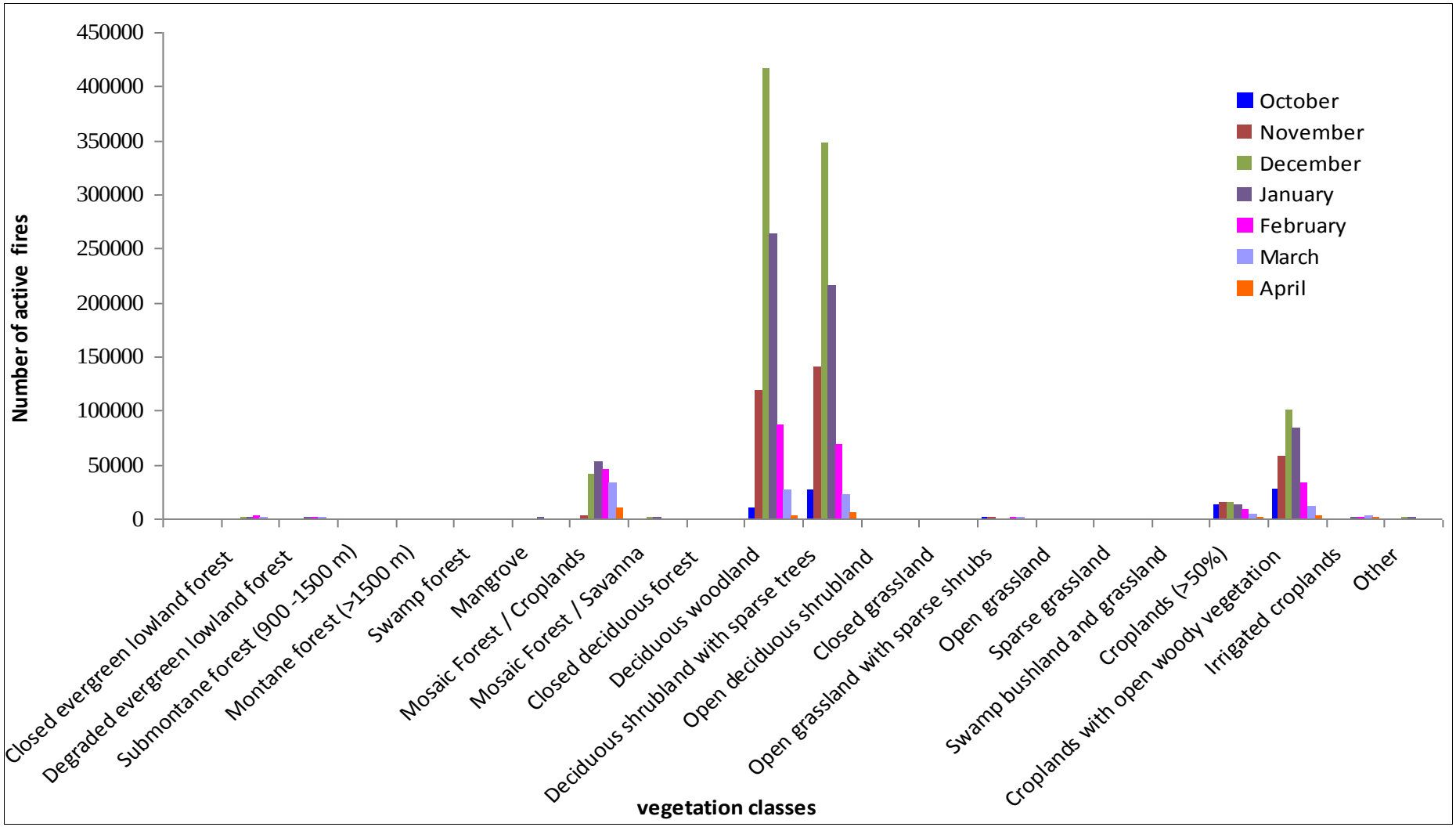

Figure 22: Number of active fires pixels detected by MODIS during the dry seasons (October 2000 to April 2009) by vegetation classes. The greatest occurrences of fire pixels are observed in Mosaic forest/croplands, Deciduous woodlands, Deciduous shrublands with sparse trees, Croplands (>50%) and Croplands with open woody vegetation.

Figures 23a to 23i below show the proportion of fire pixel occurrences within each land cover class for each dry season. The analysis of the dry season observation periods between October 2000 and April 2006 shows that between 40 percent and 42 percent of fire pixels (all fire pixels observed in very early, early, late and very late fire seasons) were observed in the Deciduous woodland class and between 34 percent and 36 percent occurred in the Deciduous shrubland with sparse trees class. Also, most fire counts per year detected by MODIS were within these two classes.

However, the observation of the percentage of fire pixels detected in the dry seasons between October 2006 and April 2009 shows that the proportion of fire pixels detected in Deciduous woodland fell by an average 11 percent of fires detected, in comparison to preceding fire seasons (October 2000/April 2006). By contrast, within the Deciduous shrubland class, there was a slight increase of about 2 percent of fire pixels detected in the October 2006/April 2009 period.

During the dry seasons between October 2000 and April 2006, lower fire pixels percentages (between 11 percent and 14 percent) of total fire pixel counts were detected within the Croplands with open woody vegetation class, between 6 percent and 11 percent of fire pixels were detected in the Mosaic forest/Croplands class and a very low percentage of fires pixels (between 1 percent to 2 percent) occurred in the Croplands class and the other classes.

By contrast, in the dry seasons between October 2006 and April 2009, a greater proportion of fire pixels was detected in certain classes: Between 19 percent and 22 percent of them were detected in the Croplands with open woody vegetation class, which is – on average - about 8 percent of fire pixels more than what was detected in the previous years. Between 7 percent and 10 percent of fire pixels were detected in the Croplands class, which is – on average – about 6 percent of fire pixels more than for the previous years. In the last three dry seasons observed, a much lower percentage of fire pixels (2 percent) was detected in the Mosaic forest/Croplands class than in the previous dry seasons (October 2000/April 2006), where the percentage of fire pixels detected in this class was about 7 percent higher on average. A low increment in the percentage of fire pixels was observed in the other classes; this percentage rose by about 1 percent on average.

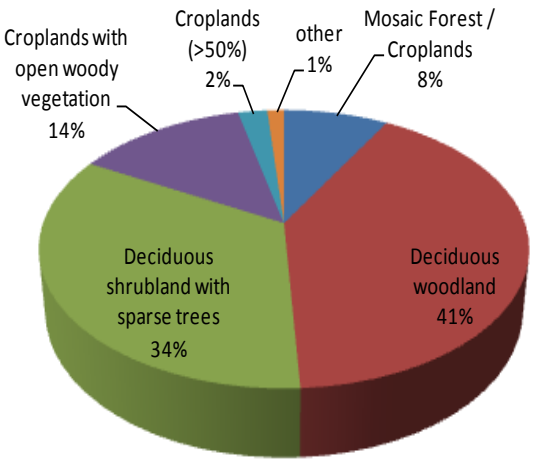

a) October 2000/April 2001

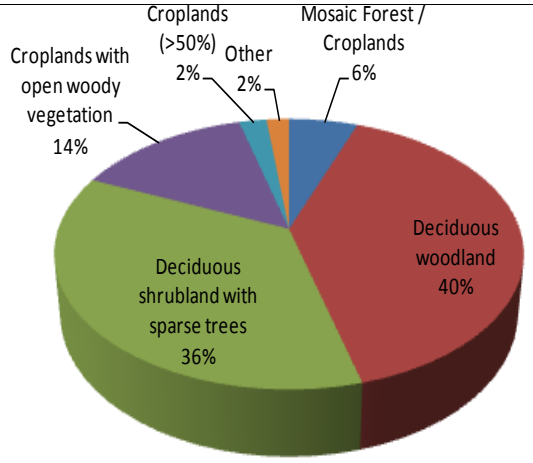

b) October 2001/April 2002

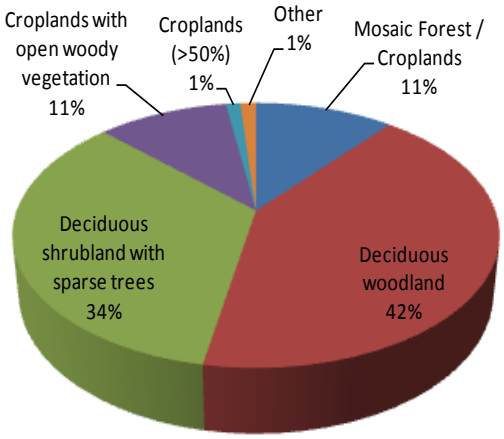

c) October 2002/April 2003

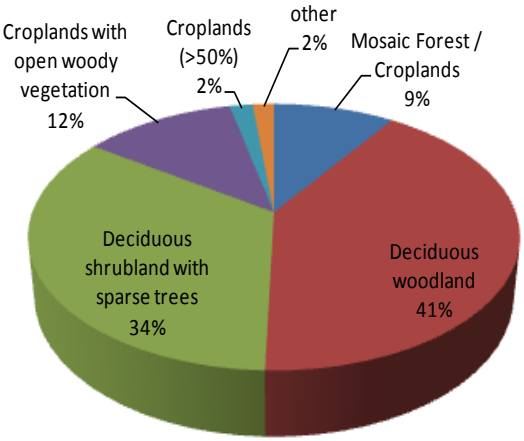

d) October 2003/April 2004

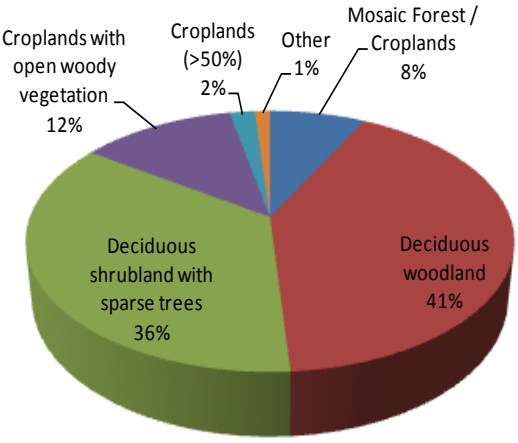

e) October 2004/April 2005

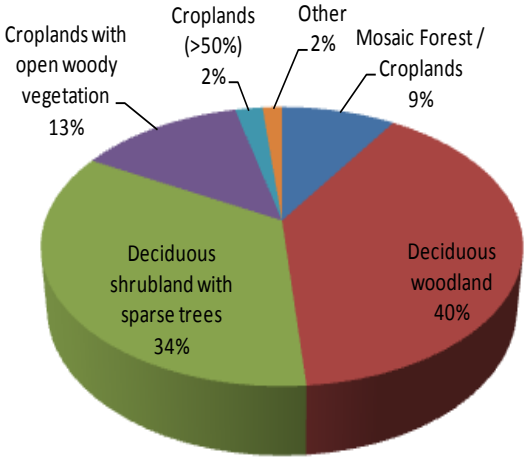

f) October 2005/April 2006

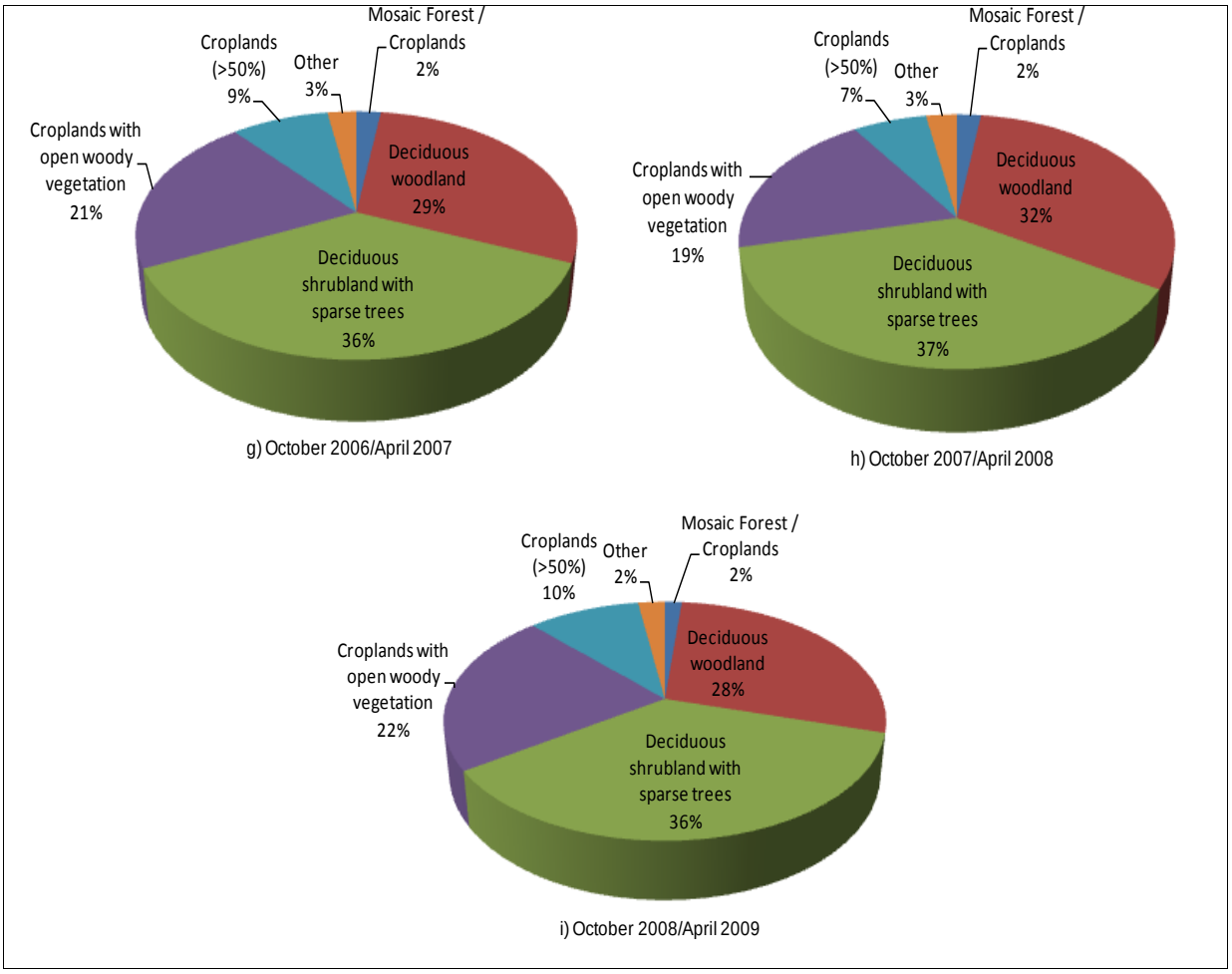

Figures 23 (a-i): Percentage of total fire pixel occurences in land cover types during the different dry seasons.

Figure 24 shows the average proportion of fire pixel occurrences as per land cover type over the 9 dry seasons. Throughout these years, the most frequent fires were observed within the Deciduous woodlands, with an average proportion of 37.18 percent of total counts of fire pixels detected, and in the Deciduous shrubland with sparse trees class with an average proportion of 35.29 percent of total yearly counts of fire pixels detected. On average, about 10,311,322 ha of Deciduous woodlands and 9,167,811 ha of Deciduous shrubland with sparse trees were affected by the yearly fire seasons. Fairly high occurrences of fires were observed within the various types of croplands (Croplands with open woody vegetation, Mosaic forest/ Croplands, Croplands (>50%)), with 25.72 percent of total counts of fire pixels detected across the whole observation period. The croplands area yearly affected by dry season fires is about 6,365,156 ha on average. Infrequent fires pixels, making up 1.82 percent of total counts of fire pixels detected in all observation years was detected in the other classes, where an average of 421,700 ha were affected by fire every year.

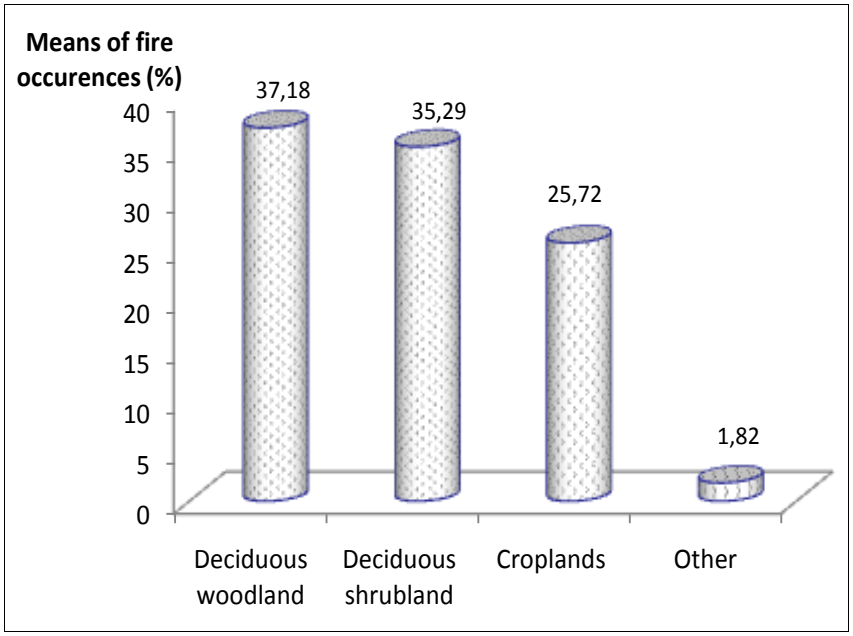

Figure 24: Fire occurrences in the dry seasons from 2000 to 2009 expressed as an average percentage of total fires and as a function of land cover.

5.3 Burned area and burn severity mapping at a local scale

The results of this chapter are presented in two parts. The first part gives the results concerning the burned area and burn severity mapping for Comoé National Park and Bontioli Reserve. The second part presents the results for Pendjari National Park, followed by the validation of burn severity results with data collected during field work in this park.

5.3.1 Landsat imagery suitability

5.3.1.1 Comoé National Park and Bontioli Reserve

Figures 25 and 26 are subset images of Comoé National Park and Bontioli Reserve respectively acquired from Landsat ETM+ at a 30 m resolution from the days 2000360 (25/12/2000) and 2001362 (28/12/2001) respectively. In these figures, it is possible to see the difference between old and new burn scars as well as an unburned area. This difference becomes apparent when one uses the spectral band combination of 5 (1.55-1.75 µm), 4 (0.75-0.90 µm) and 3 (0.63-0.69 µm), corresponding respectively to shortwave infrared, near-infrared and visible (red) of Landsat ETM+ channels. In figures 25 and 26, an old burn scar is represented by pink to clear purple colours. A new burn scar is visible by the flame, the smoke and is characterised by ash and/or charcoal with dark colours in the visual to near IR Landsat wavebands. An unburned area is represented in the vegetation in green colors; bare soil appears in white colors.

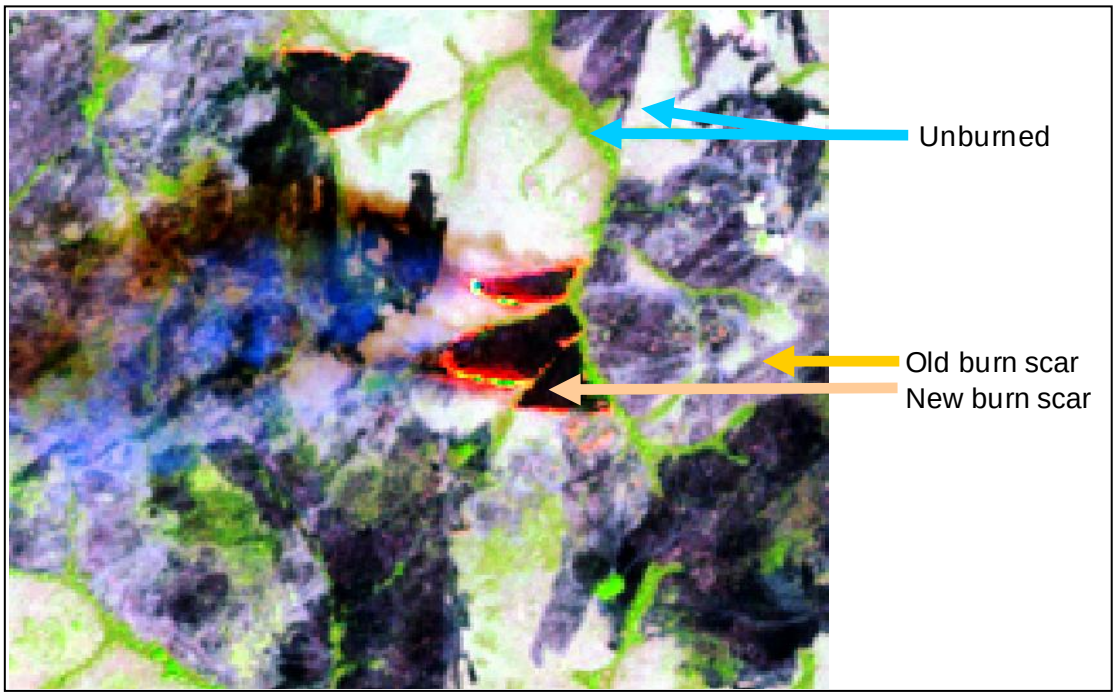

Figure 25: Landsat ETM+ subset image of Comoé National Park (25/12/2000) using bands 5-4-3.

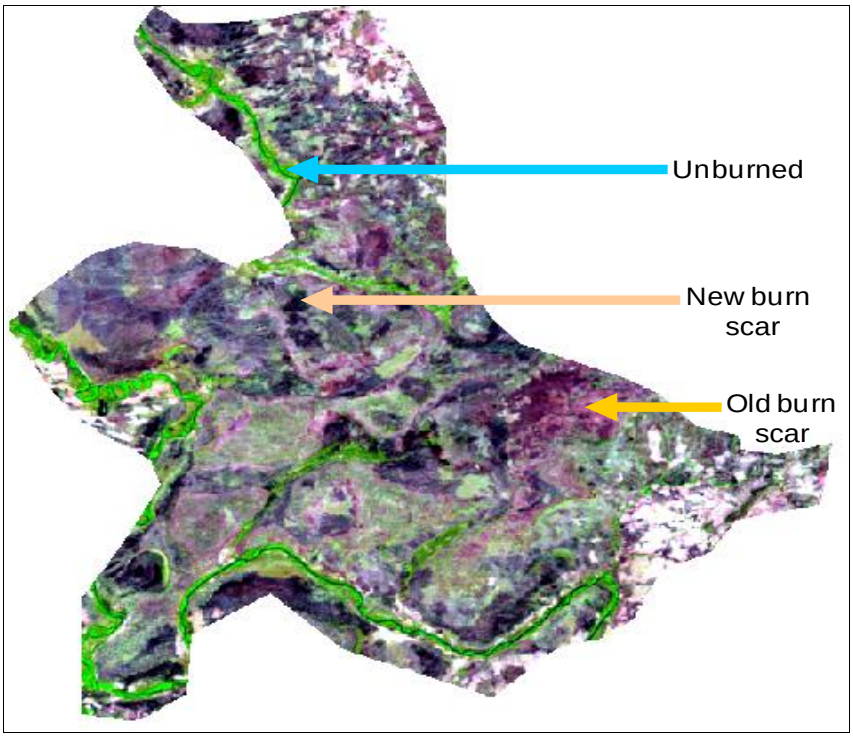

Figure 26: Landsat ETM+ image of Bontioli Reserve (28/12/2001) using bands 5-4-3.

The spectral signature of burned areas at different temporal stages (in figures 27 and 28) shows a low reflectance in the near infrared wavelength, corresponding to band 4 (0.75-0.90 µm) and an increase of reflectance in the shortwave infrared wavelength, represented by band

7 (2.09-2.35 µm). By contrast, the spectral properties of unburned area (figures 27 and 28) show a high reflectance in the near infrared (band 4) and a low reflectance in the shortwave infrared (band 7).

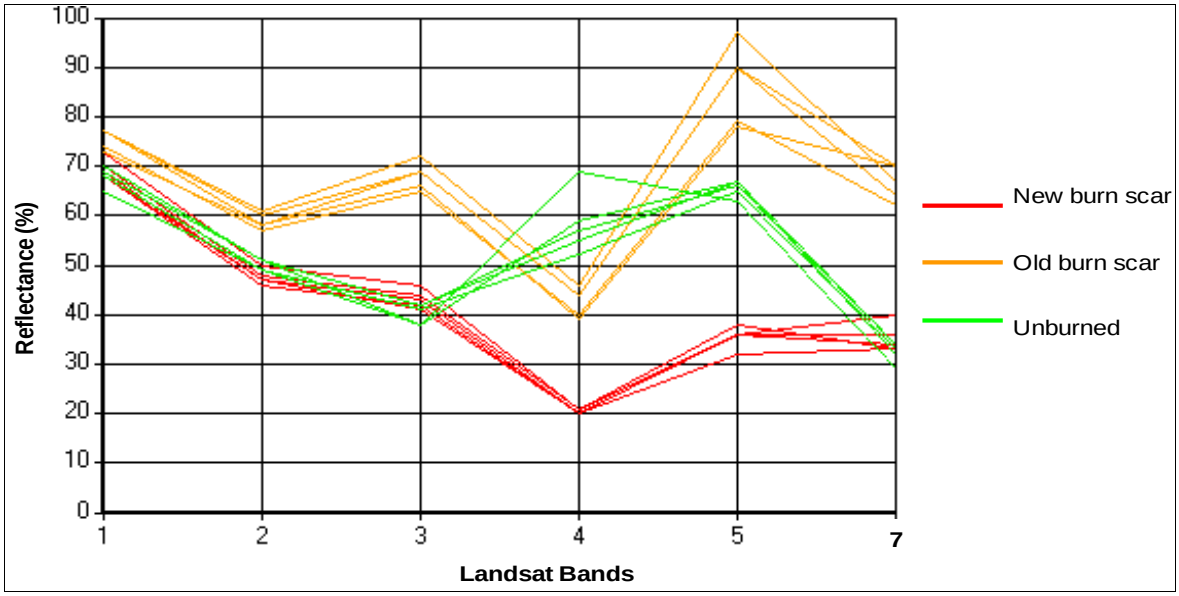

Figure 27: Spectral properties detected in bands 1 to 5 and 7 of Landsat ETM+ for unburned area, new and old burn scars from subset image of Comoé National Park (25/12/2000).

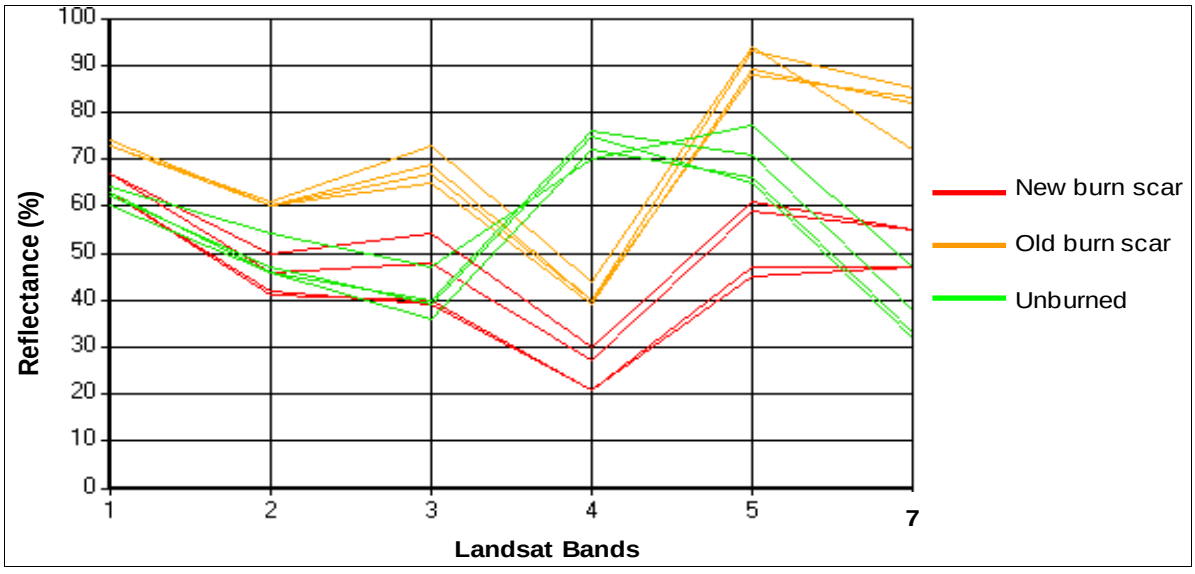

Figure 28: Spectral properties detected in bands 1 to 5 and 7 of Landsat ETM+ for unburned area, new and old burn scars from subset image of Bontioli Reserve (28/12/2001).

To create the burned area mapping for each protected area, the Landsat scenes of Comoé National Park (25/12/2000) and Bontioli Reserve (28/12/2001) were classified by using the supervised classification algorithm, which resulted in discriminating five classes (figures 29b and 30b) namely the water class, the vegetation class (with active chlorophyll), old burn scar, new burn scar and bare soil.

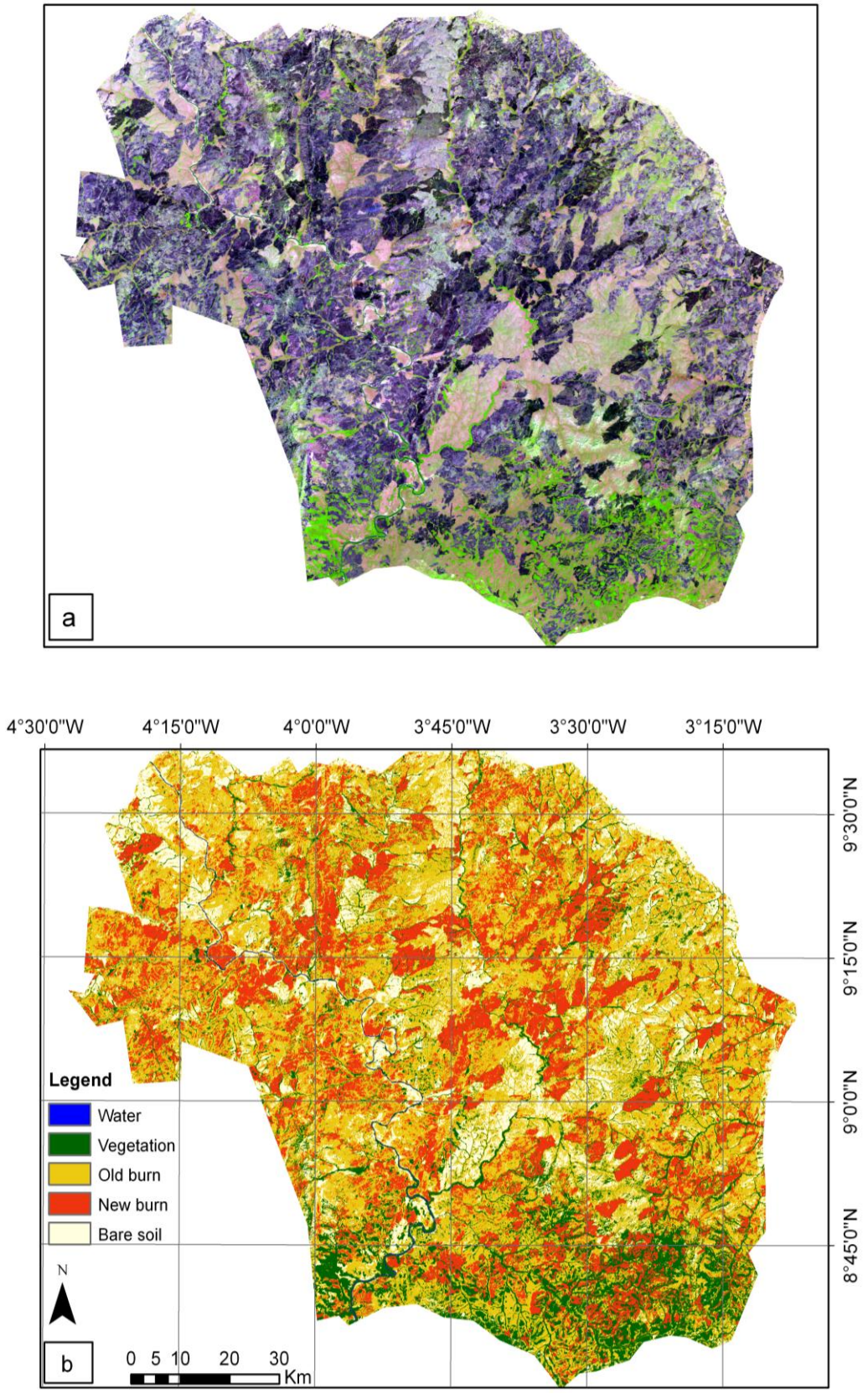

Figures 29: a) Landsat ETM+ subset image (25/12/2000) using bands 5-4-3 and b) Classified image showing burned and unburned areas in Comoé National Park (Côte d´Ivoire).

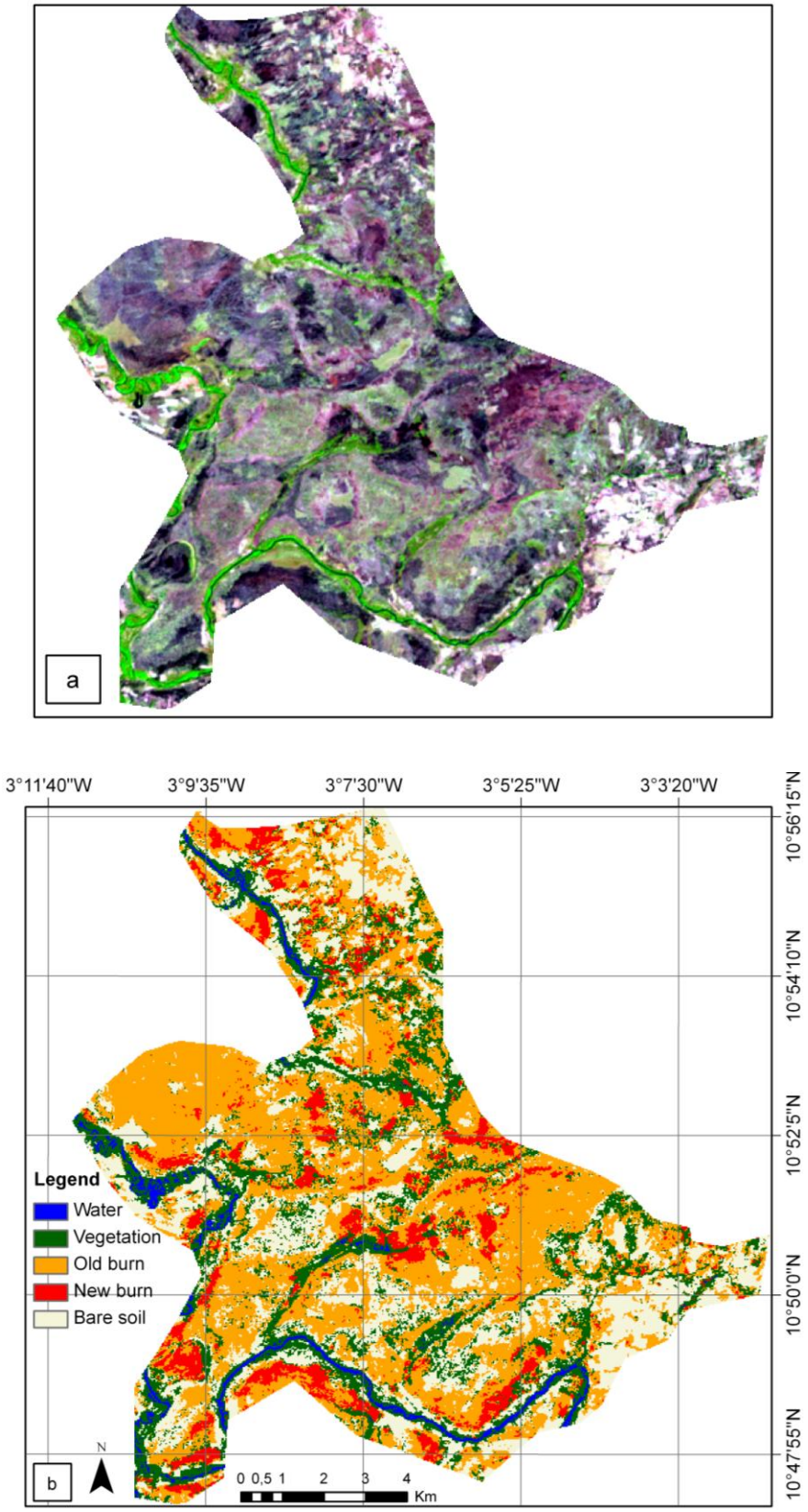

Figures 30: a) Landsat ETM+ subset image (28/12/2001) using bands 5-4-3 and b) Classified image showing burned and unburned areas in Bontioli Reserve (Burkina Faso).

In a next step and as part of the classification process, the Normalized Burn Ratio index of pre-fire ($NBR_{prefire}$) and post-fire ($NBR_{postfire}$) for each protected area was calculated using the sensitive wavebands of Landsat ETM+. The equation was already shown in section 4.2.2. Subsequently, the difference image (ΔNBR) between the two indexes ($NBR_{prefire}$ and $NBR_{postfire}$) was derived for Comoé National Park and Bontioli Reserve.

This second classification process is used to understand through burn severity how the fire affects the vegetation. To create the burn severity mapping, only new burn scars were considered. According to Landmann (2003), only new burn scars are suitable for fire severity mapping since older burn scars show a significant increase in reflectance Std.Dev., causing spectral confusion with unburned areas. Furthermore, the dispersion of ash on new fires is significantly lower compared to older burn scars. One example of the distribution histogram for old burn and new burn scars in Bontioli Reserve (figure 31) shows a high Std.Dev. (0.19) for old burn and a low Std.Dev. (0.05) for new burn.

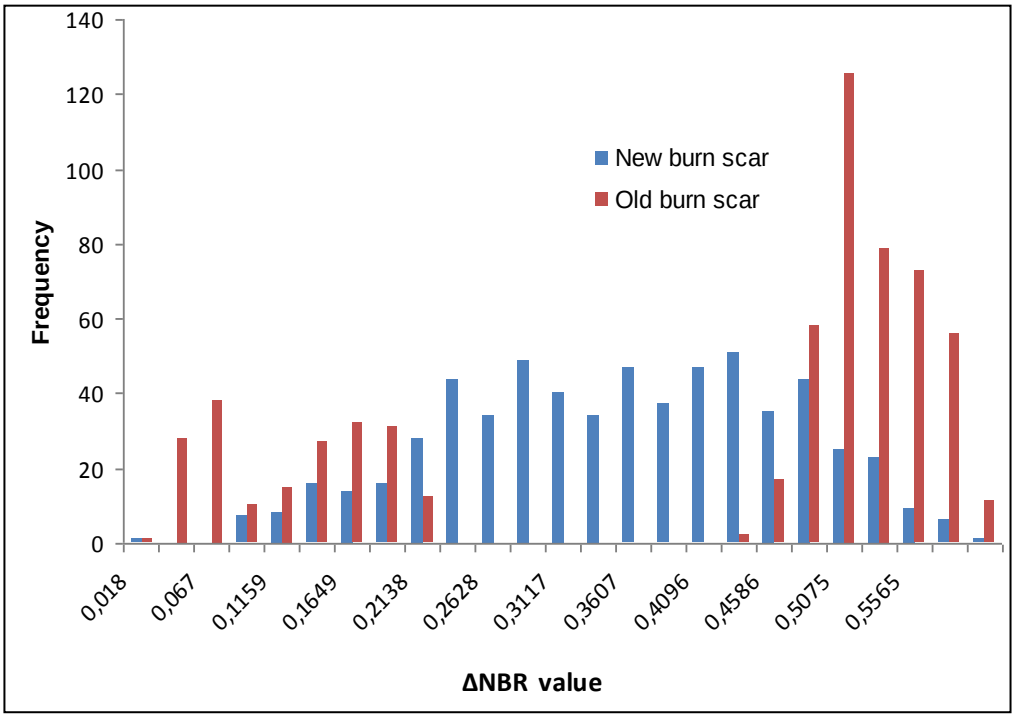

New burn scar	Min 0.323874	Max 0.588370	Mean 0.468731	Std.Dev. **0.051780**
Old burn scar	Min 0.018009	Max 0.605440	Mean 0.387574	Std.Dev. **0.192525**

Figure 31: Distribution histogram for new burn and old burn scars according to ΔNBR value in Bontioli Reserve (Burkina Faso).

Therefore, a mask derived from the new burn scars (figures 32 and 33) was considered for the analysis.

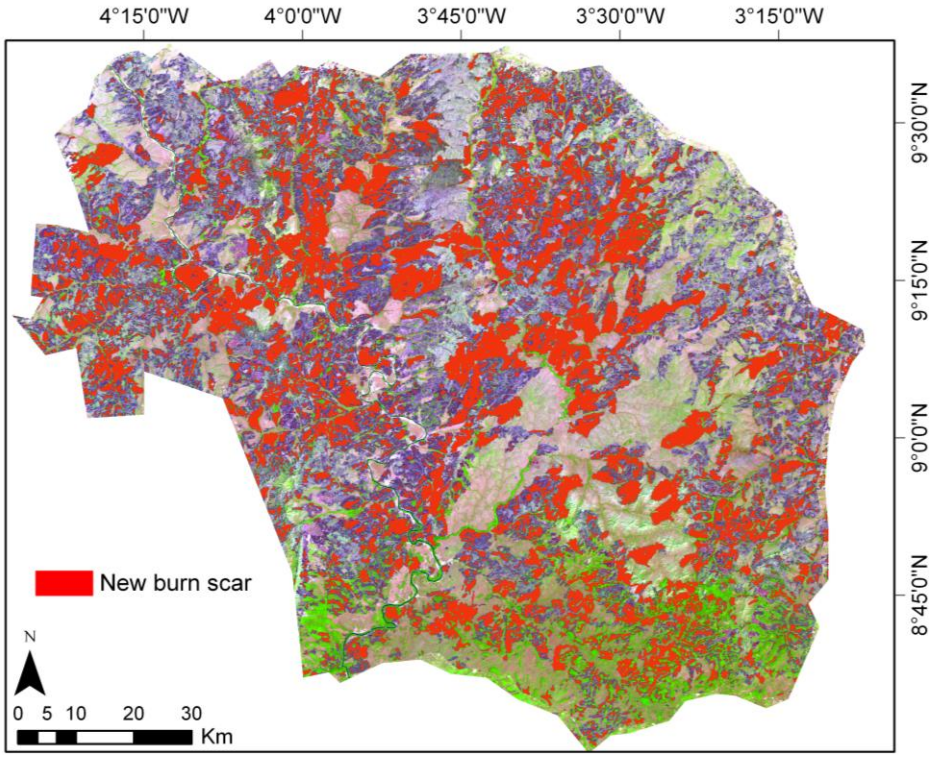

Figure 32: New burn scar mask superimposed on the Landsat ETM+ subset image (25/12/2000) of Comoé National Park (Côte d´Ivoire).

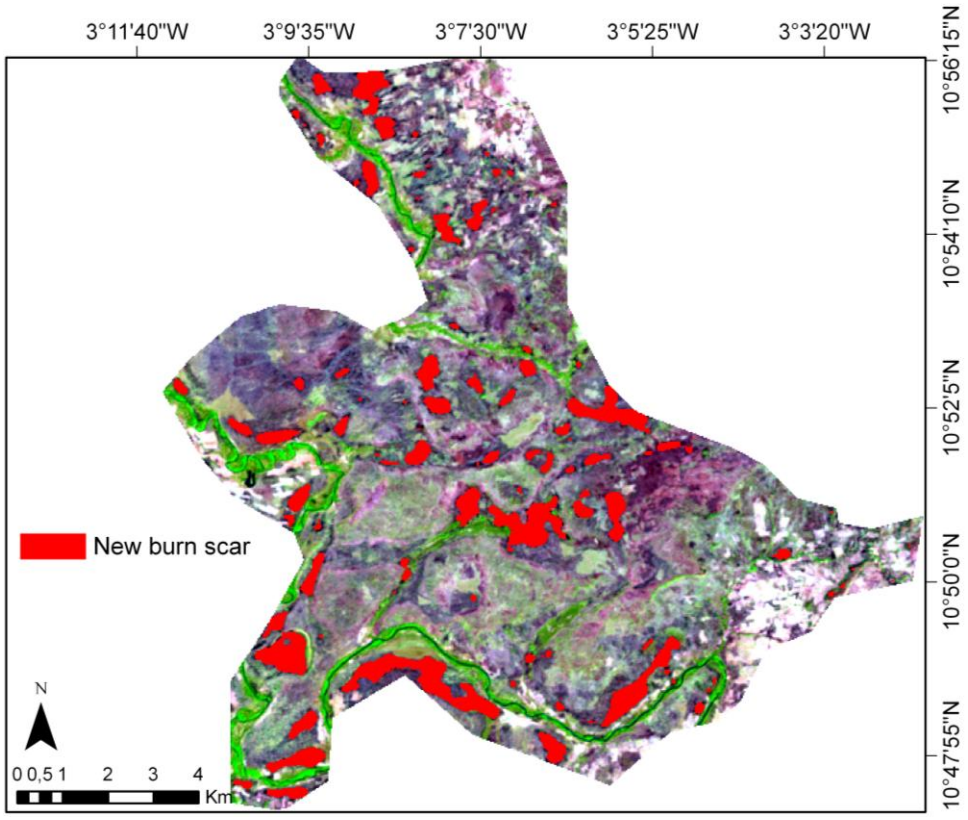

Figure 33: New burn scar mask superimposed on the Landsat ETM+ subset image (28/12/2001) of Bontioli Reserve (Burkina Faso).

The new burn mask for each protected area was combined with the corresponding ΔNBR values to create another burn map which shows the ΔNBR for new burn areas. This burn map was classified using the histogram distribution of new burn already obtained in Comoé National Park and in Bontioli Reserve. After the classification, the different results were rescaled to 8 bit and recoded according to the ΔNBR values, which resulted in four burn severity categories, namely: very low burn, low burn, moderate burn and high burn. The figures 34 and 35 show these categories which were observed in Comoé National Park and Bontioli Reserve. The comparison of these two figures shows that the burn scars observed in Comoé National Park are more numerous and more aggregated than in Bontioli Reserve. Additonally, the repartition of the different burn severity categories is not the same in the two protected areas.

In Comoé National Park (figure 34), very low and low burn severity is more concentrated in the northern part and in one area in the south of the park. Large scars caused by fires of moderate severity can be observed between 9° and 9°20´ N, right in the center of the park. High burn severity is more concentrated in the very south of the park. In the whole park, for this observation period, very low burn severity occurred on 67,085.3 ha, low burn severity was found on 65,121.1 ha, moderate burn severity was found on 122,836 ha and high burn severity occurred on 6,408 ha. In total, if one considers only the new burn scars, 23 percent of the total surface of the park were burned, which amounts to 261,450.4 ha of surface area.

In Bontioli Reserve (figure 35), in this observation period, high burn severity is very weakly represented, with only 1.53 ha. The dominant category is low burn severity, with 625.77 ha, followed by moderate burn severity, which was found on 184.23 ha. Very low burn severity occurred on 56.16 ha. All in all, if one considers the new burn scars, 6.83 percent of the total surface of the reserve was affected by fires of the different severities, which corresponds to a burned surface of 867.69 ha.

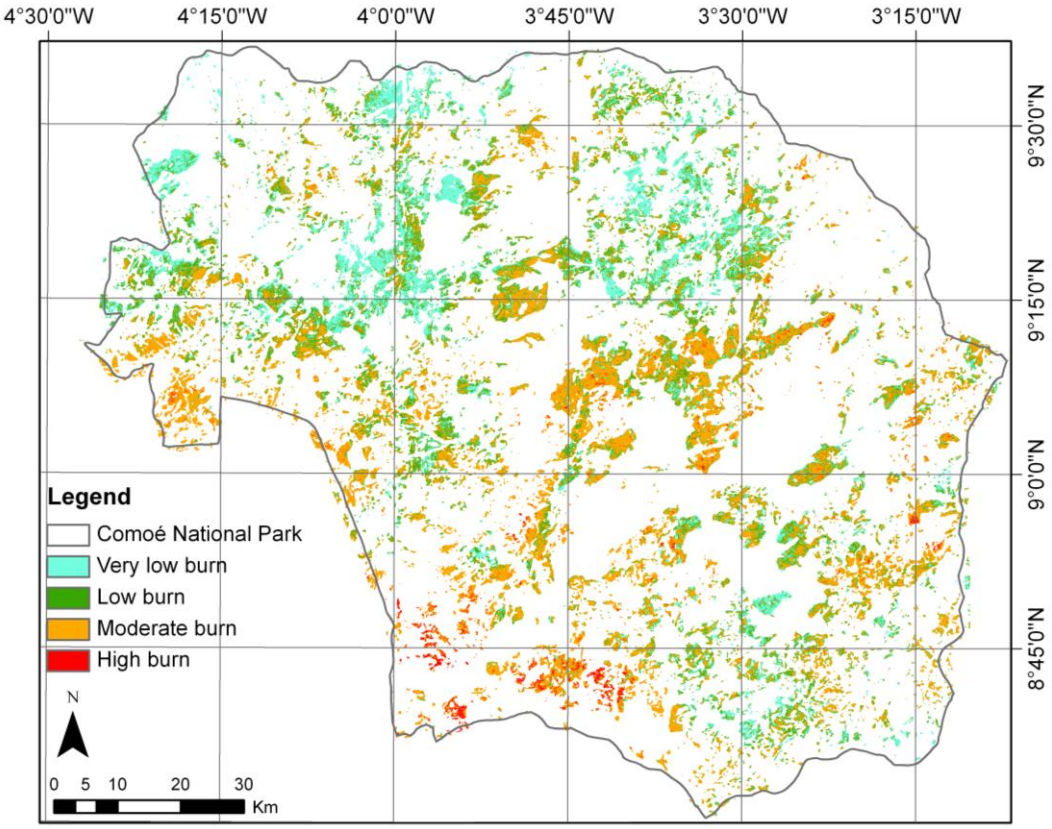

Figure 34: Burn severity map using ΔNBR value derived of Landsat ETM+ scenes from pre-fire (2000104) and post fire (2000360) observation period in Comoé National Park (Côte d´Ivoire).

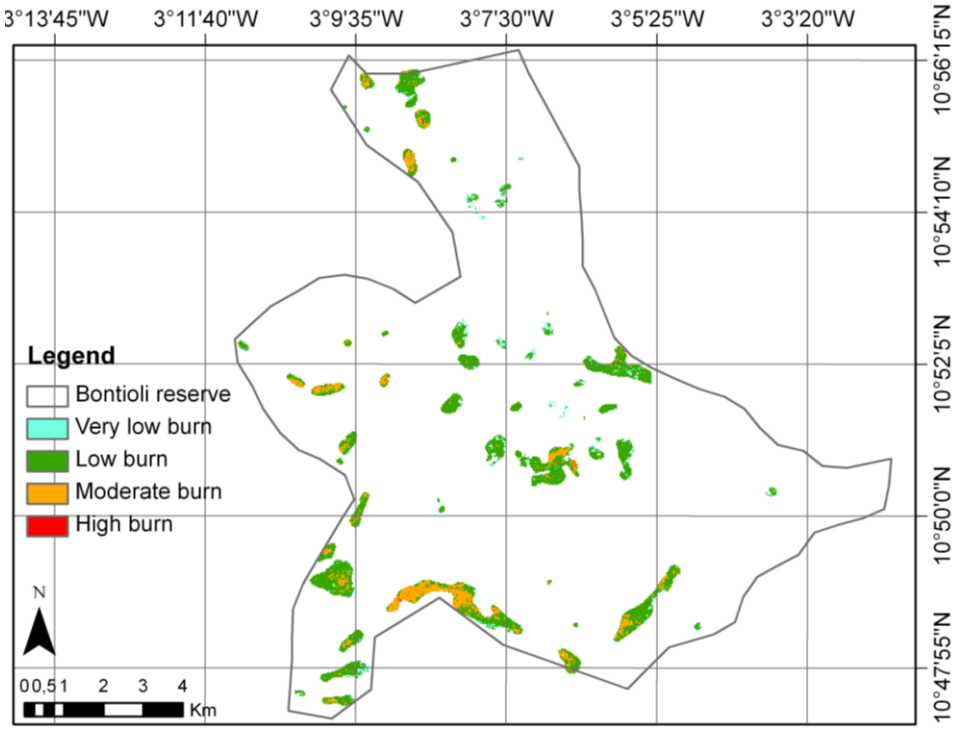

Figure 35: Burn severity map using ΔNBR value derived of Landsat ETM+ scenes from pre-fire (2001298) and post fire (2001362) observation period for Bontioli Reserve (Burkina Faso).

The statistical analyses of the four burn severity categories were made using the box plot of SPSS software. The result for each protected area is show in figures 36 and 37.

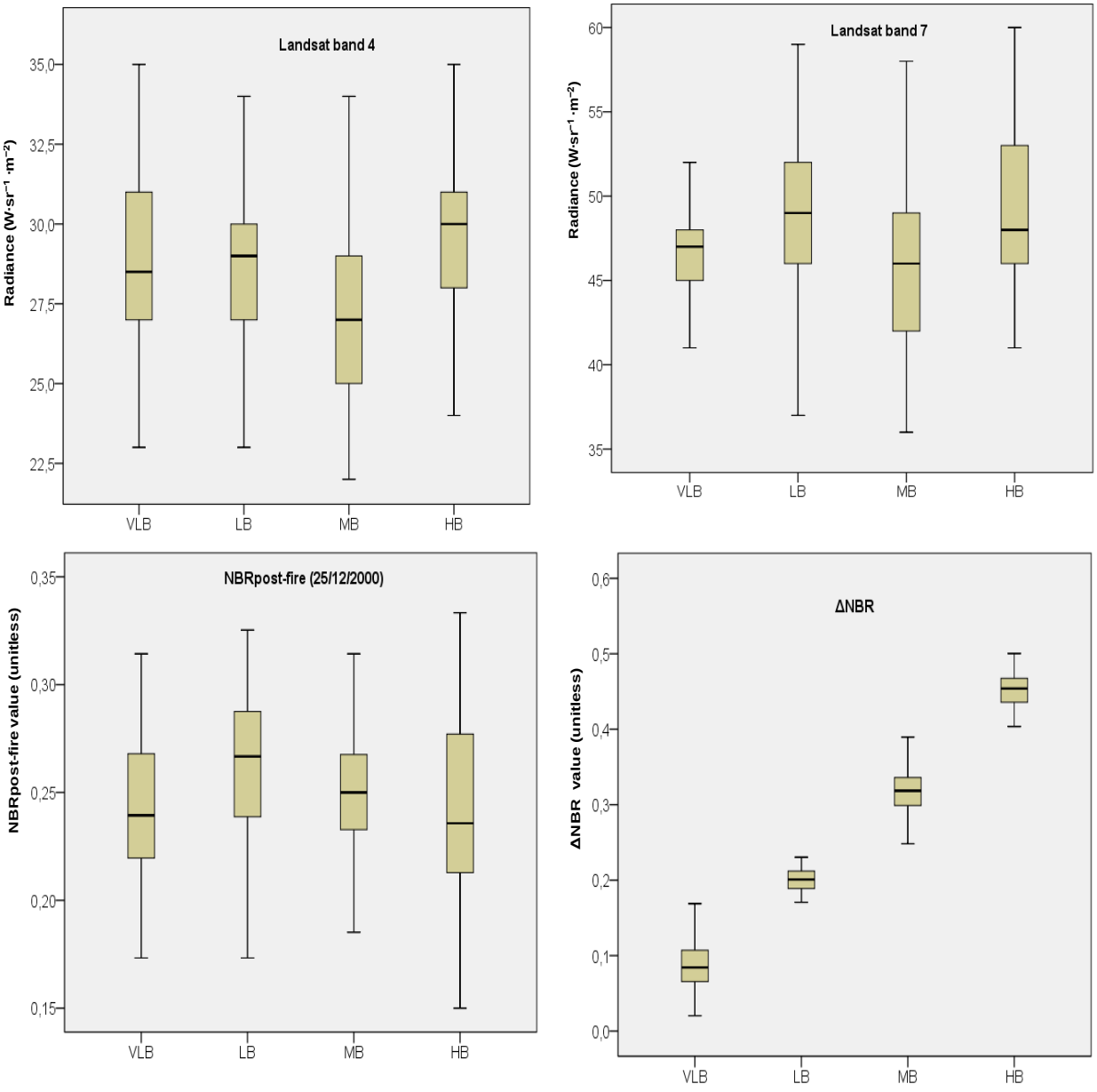

Figure 36: Box plots of the band $4_{post\text{-}fire}$, band $7_{post\text{-}fire}$, $NBR_{post\text{-}fire}$ and $\Delta NBR_{(prefire\text{-}postfire)}$ of Landsat scenes according to burn severity categories (Very low burn: VLB, low burn: LB, moderate burn: MB and high burn: HB) in Comoé National Park (Côte d´Ivoire).

Figure 36 shows how the burn severity categories can be distinguished using the bands 4 and 7 of Landsat ETM+ image (2000360), the Normalised Burn Ratio post fire (2000360) and the differencing image index (ΔNBR) between the Julian day 2000104 and 2000360. Unlike the box plot of the ΔNBR index, the other box plots show very little difference between the different categories of burn severity. This is shown by the position of the median line for each category of burn severity. Likewise, there is a strong variance between the radiation values for the bands 4 and 7 and the NBR post fire values for each category. This can be seen from the

great variance between the values due to a high Std.Dev. for each category.

By contrast, the burn severity categories are very well distinguished and separated with the ΔNBR index. The median lines of the different categories are far apart, and the variance between the values is low within each category, which leads to a very low Std.Dev. value.

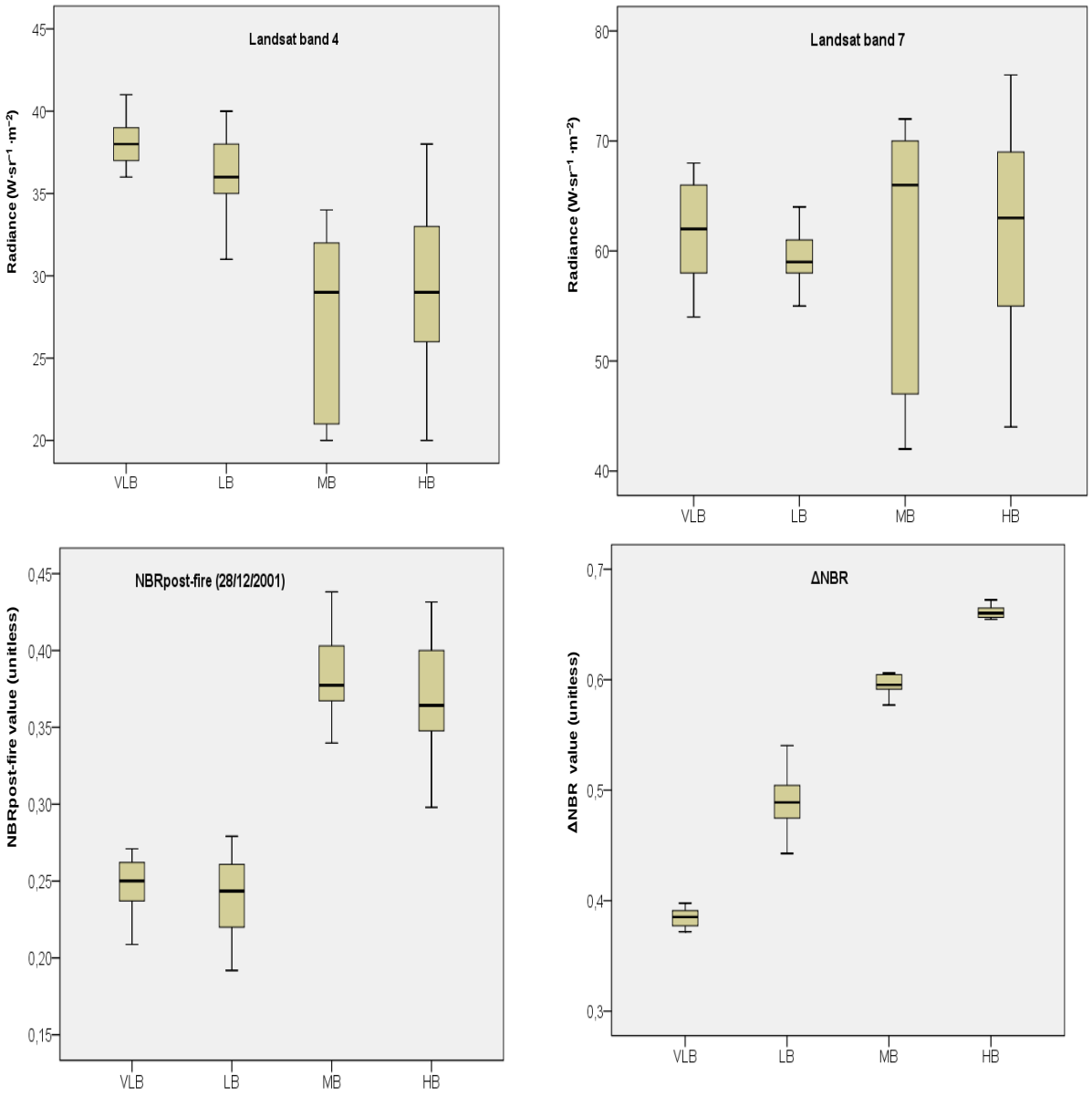

Figure 37: Box plots of the band $4_{post\text{-}fire}$, band $7_{post\text{-}fire}$, $NBR_{post\text{-}fire}$ and $\Delta NBR_{(prefire\text{-}postfire)}$ of Landsat scenes according to burn severity categories (Very low burn: VLB, low burn: LB, moderate burn: MB and high burn: HB) in Bontioli Reserve (Burkina Faso).

What can be seen in figure 37 is that like in Comoé National Park, the burn severity categories are very well separated and distinguished with the ΔNBR index. The median lines are very well distinguished and the variance between the values within every category is very low. In bands 4 and 7 post fire (28/12/2001) and in NBRpostfire, two groups can be distinguished. The first contains very low and low burn severity and the second moderate and

high burn severity. However, there is a great variance between the radiation values and the NBR values within each category, which leads to a great Std.Dev.

5.3.1.2 Pendjari National Park

In this part, mappings obtained from two different satellites will be studied: First, the burned area and burn severity mappings obtained with the Landsat scenes from 25th October 2001 (pre-fire) and 28th December 2001 (post-fire) and second, the burned area and burn severity mapping derived from the ASTER images from 8th December 2007 (pre-fire) and 26th February 2008 (post-fire). The analysis of the latter images will be completed by that of the Landsat images of 5th October 2007 (pre-fire) and 26th February 2008 (post fire) and the results of a field trip to Pendjari in February 2008, which are used for validating the data.

Figure 38 is a subset image of Pendjari National Park acquired from Landsat ETM+ scenes at 30 m resolution. The acquisition day is 2001341, corresponding to 7th December 2001. The old and new burn scars, as well as the unburned area are differentiated by the colours, which were obtained with the spectral channel combination 5 (1.55-1.75 µm), 4 (0.75-0.90 µm) and 3 (0.63-0.69 µm). These bands are respectively shortwave infrared, near-infrared and visible (red) of Landsat ETM+ wavebands. Just like in the above case of Comoé National Park and Bontioli Reserve, the old burn scar is represented by pink to clear purple colours, the new burn scar, which is visible by the dark colours, is characterised by the charcoal and the flaming. The unburned area, corresponding to the green vegetation, is shown in green and the bare soil in white colours.

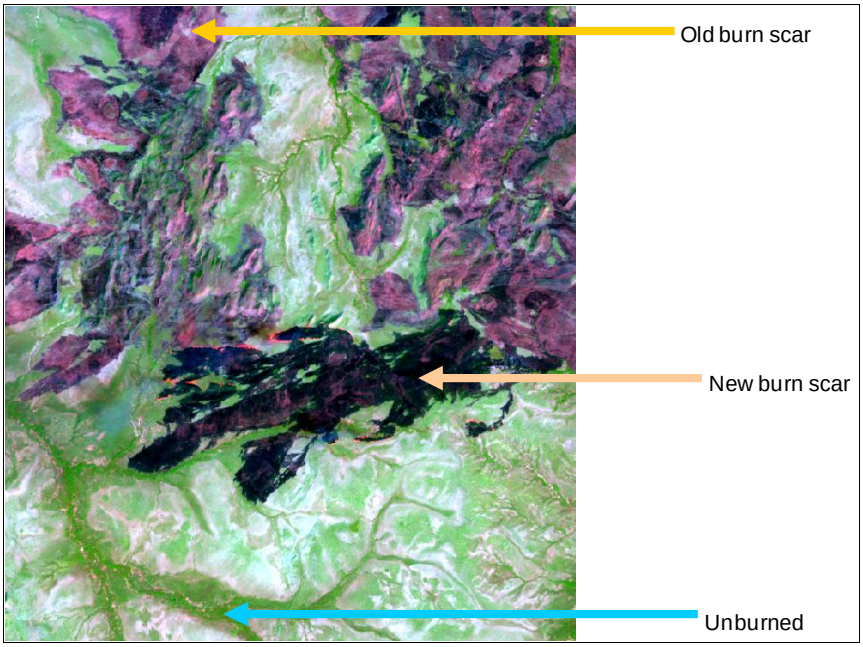

Figure 38: Landsat ETM+ subset image of Pendjari National Park (7/12/2001) using bands 5-4-3.

In the figure 39, the spectral profile of unburned and burned areas (at different times) presented different responses in wavelengths examined. The spectral response of unburned area is high in band 4 (0.75-0.90 µm), whereas that of burned area is low. In band 7 (2.09-2.35 µm), low reflectance of unburned area can be observed, whereas there is a high reflectance from burned area.

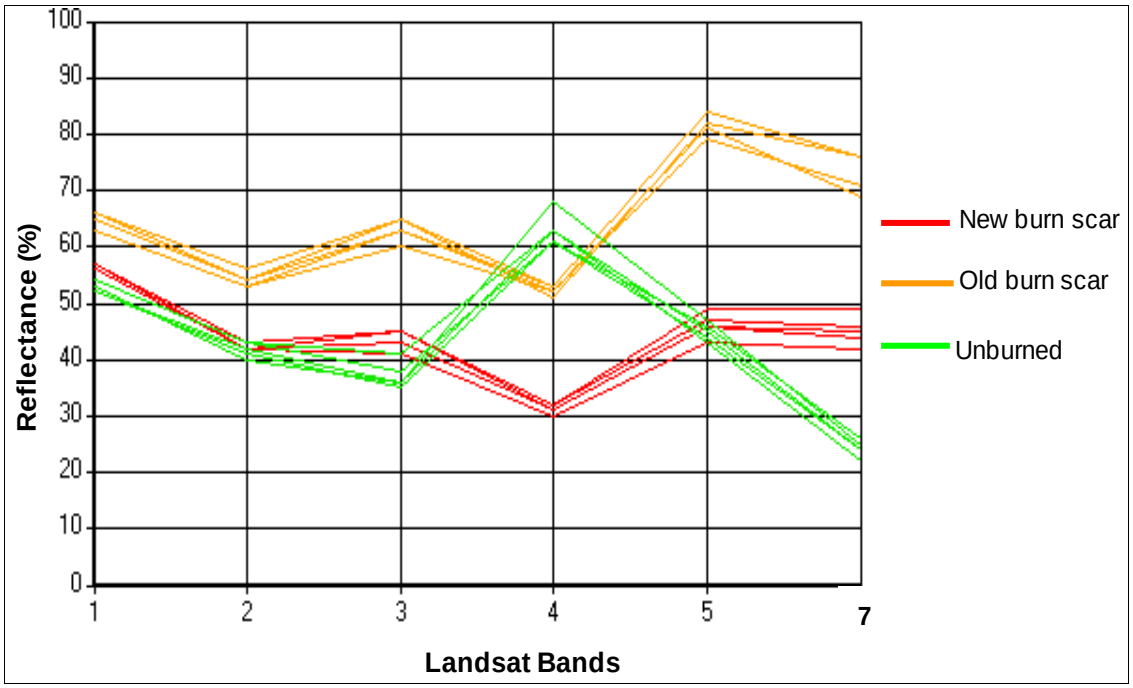

Figure 39: Spectral properties detected in bands 1 to 5 and 7 of Landsat ETM+ of the above subset image of Pendjari National Park (7/12/2001).

The first step of the classification is to create a burn area mapping using also the supervised classification algorithm. This process (figure 40b) yields five classes like in Comoé National Park and Bontioli Reserve.

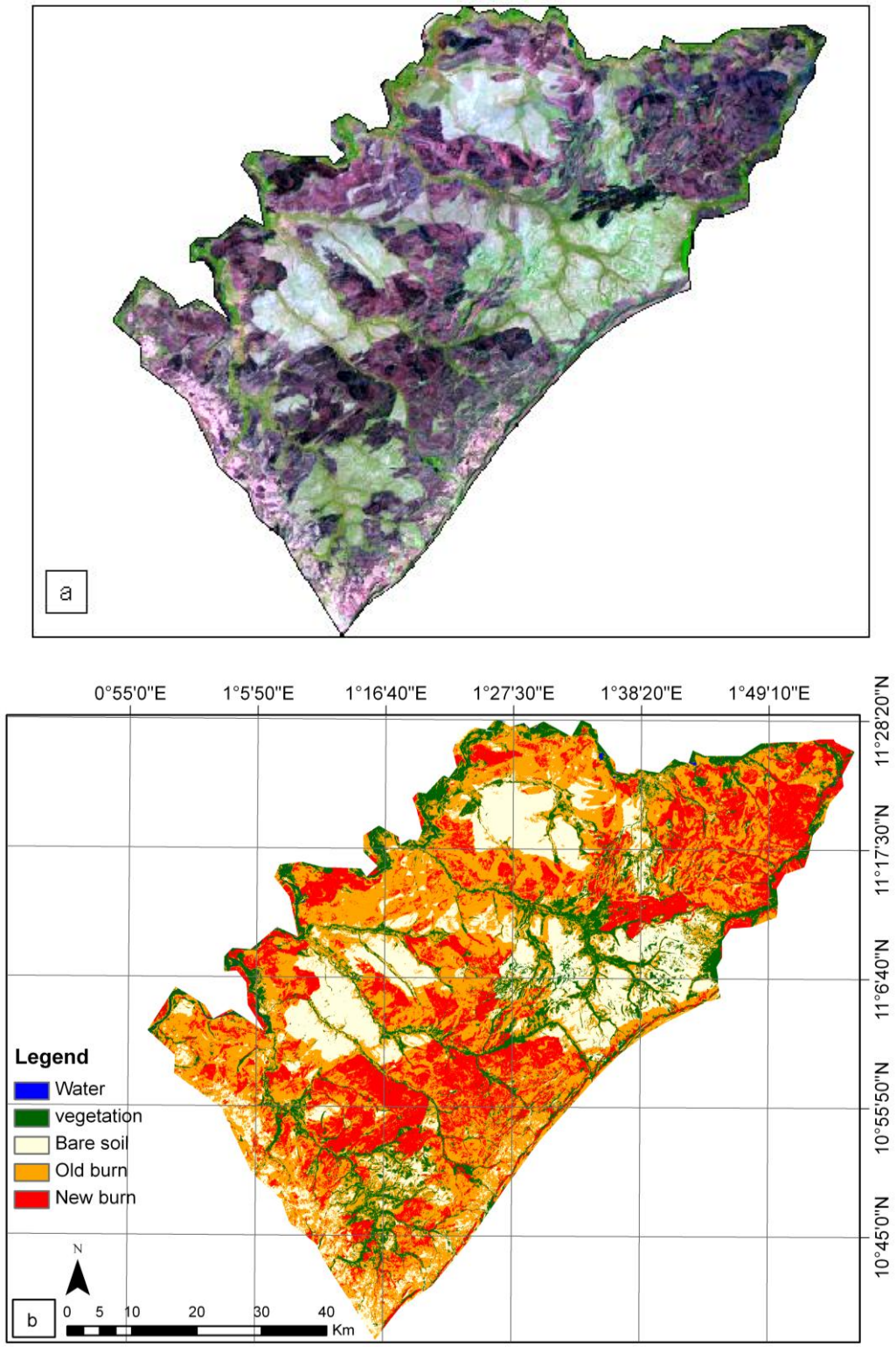

Figures 40: a) Landsat ETM+ subset image (07/12/2001) using bands 5-4-3 and b) Classified image showing burned and unburned areas in Pendjari National Park (Benin).

Like in Comoé National Park and Bontioli Reserve, only new burn scars were considered in the second step of the classification for creating the burn severity mapping (figure 41a). Four burn severity categories were also used here (figure 41b).

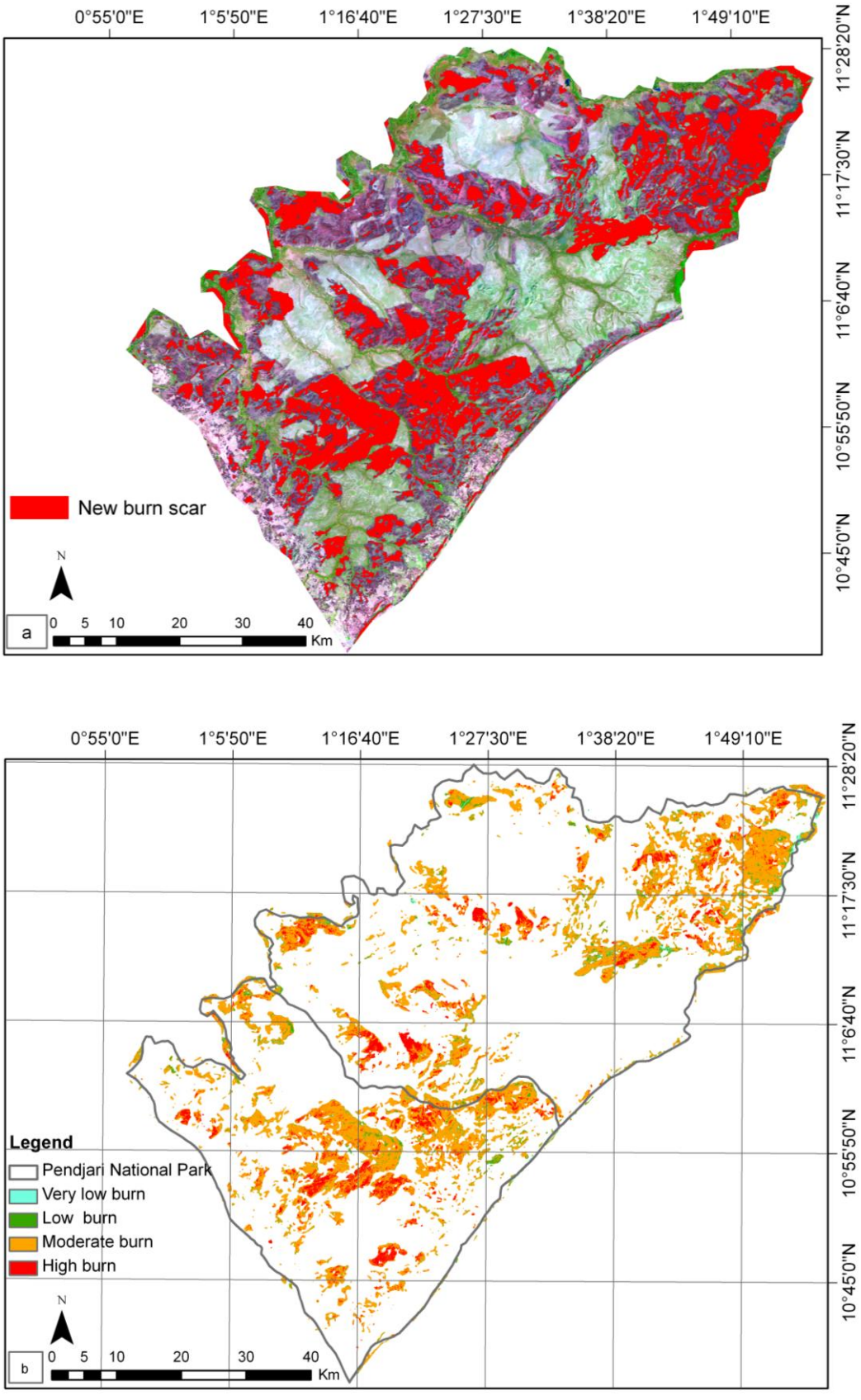

Figures 41: a) New burn scar mask superimposed on the Landsat ETM+ subset image (07/12/2001) of Pendjari National Park and b) Burn severity map using ΔNBR value derived of Landsat ETM+ scenes from pre-fire (2001293) and post-fire (2001341) observation period for Pendjari National Park (Benin).

In figure 41b, the burn severity in Pendjari National Park (including both the hunting zone and the protected area) shows large burn scars from the moderate and high burn severity categories, with scar size for these two severity categories being much larger than that observed both in Comoé National Park and Bontioli Reserve. In Pendjari, the areas belonging to those categories comprise 83,226.7 ha and 16,630.1 ha respectively. The burn scars of very low and low burn severity are small in surface compared to those of moderate and high severity in the park. They comprise 1,588.41 ha and 8,402.94 ha respectively. The burn scars of the four burn severity categories make up around 40 percent of the total surface of the park and cover an area of 109,848.15 ha. In all these data, only the new burn scars were considered.

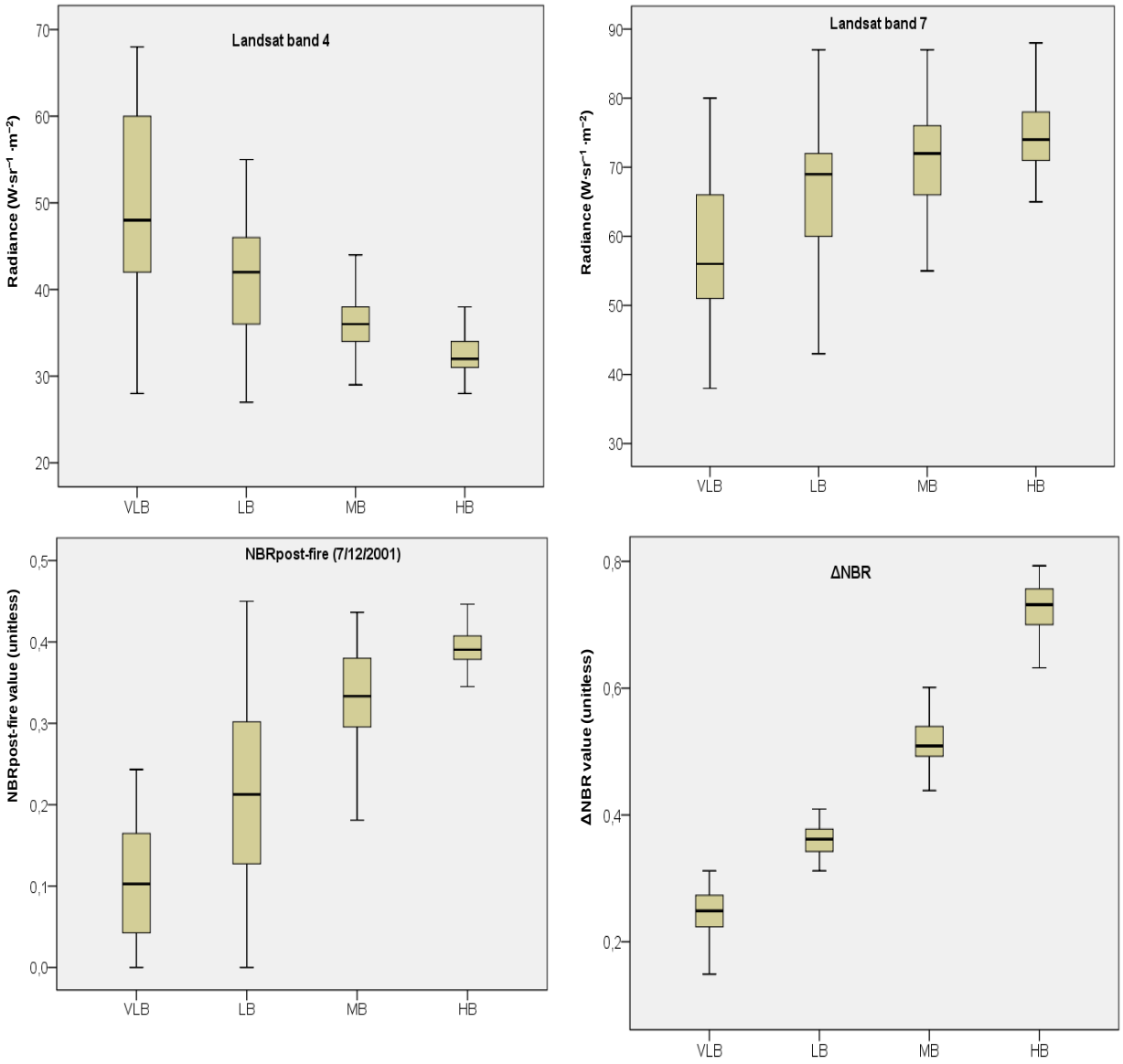

Figure 42: Box plots of the bands $4_{post\text{-}fire}$, band $7_{post\text{-}fire}$, $NBR_{post\text{-}fire}$ and $\Delta NBR_{(prefire\text{-}postfire)}$ of Landsat scenes according to burn severity categories (Very low burn: VLB, low burn: LB, moderate burn: MB and high burn: HB) in Pendjari National Park (Benin).

The figure 42 also shows a very good separation of the burn severity categories with the ΔNBR image of Pendjari National Park which was derived from Landsat ETM+ of NBR 20th October 2001 as pre-fire and 7th December 2001 as post-fire.

5.3.2 ASTER imagery fire mapping

The subset image of a part of Pendjari National Park from ASTER (figure 43) on day 26th February, 2008 only shows 12 GPS points of the 324 points collected in field.

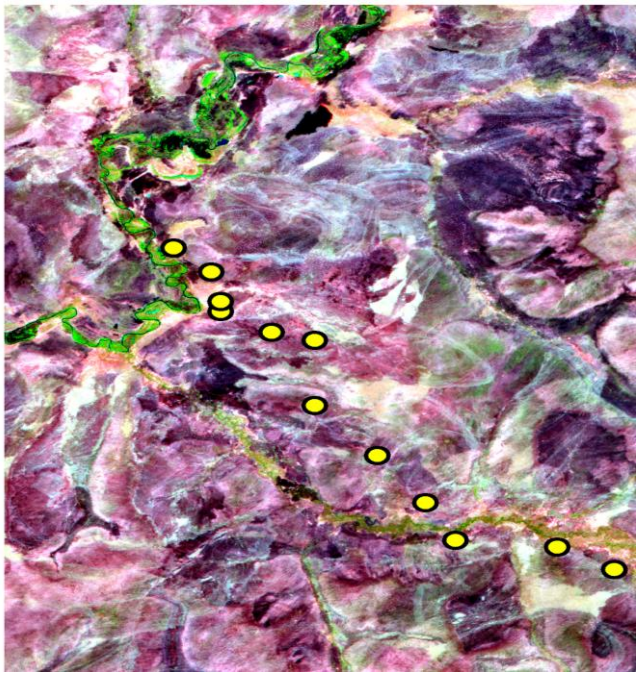

Figure 43: ASTER imagery from 26th February 2008 for part of Pendjari National Park in bands 4-3-2 of ASTER. The 12 GPS sampling points (in yellow) appear in the image. The burn scars are coloured from violet to dark colours, the green colour represents the forest and the gallery forest along Pendjari river.

If only so few points could be observed in the image above (figure 43), this is so because the ASTER images taken pre (8th December 2007) and post fire (26th February 2008) do not have the same centres. Nevertheless, the burned area and burn severity mapping were established by using the part representing the intersection of pre and post fire images. However, due to the very low number of GPS points it was hardly possible to validate the results based on satellite observations with field data by using statistical analyses. This is why the burn severity image results will not be used for the validation of the data.

Therefore, instead of the ASTER images, the Landsat ETM+ scenes from Pendjari National Park were used, which cover the observation period for the field work and have the same acquisition period as the ASTER post fire images used for this study, namely 26/02/2008. Although the Landsat scenes have stripes of missing data due to the problems encountered by Landsat that were already presented in section 2.3.3.1, these images formed

the basis for verifying the remotely sensed results with the field work observations, 149 GPS points could be obtained that are not located within the stripes of missing data. The results of this analysis will be presented after those obtained from the ASTER images.

Like in the different Landsat images, the violet and black colours characterize old and new burn scars respectively (figure 44).

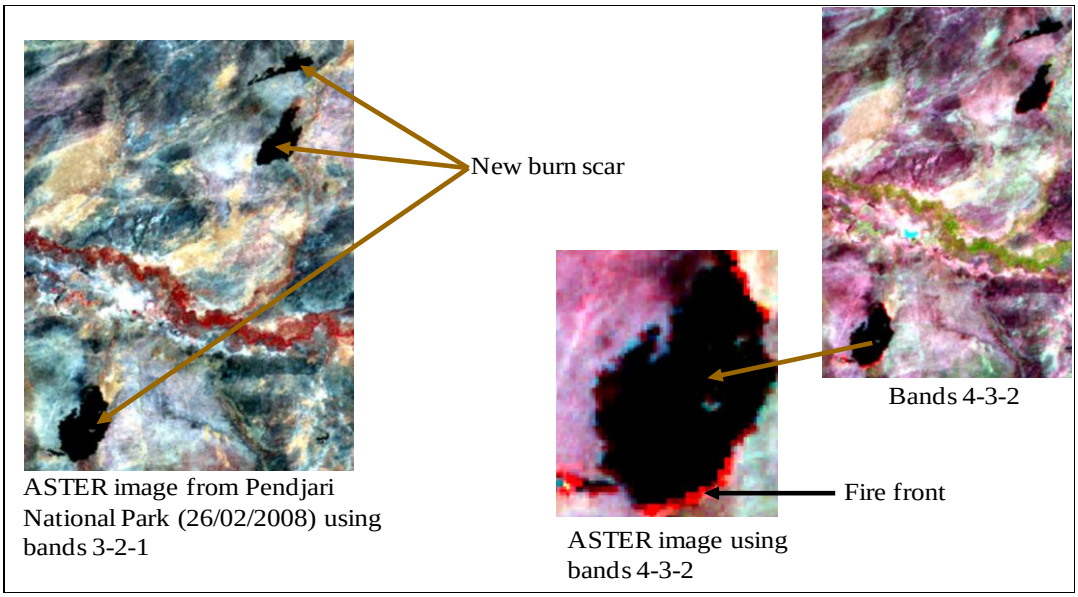

Figure 44: The ASTER image from 26th February 2008 shows new burn scars and a front of fire in Pendjari National Park.

Figure 45 shows 5 classes, namely bare soil, new burn, old burn, vegetation and water. This classification was produced using the supervised classification algorithm.

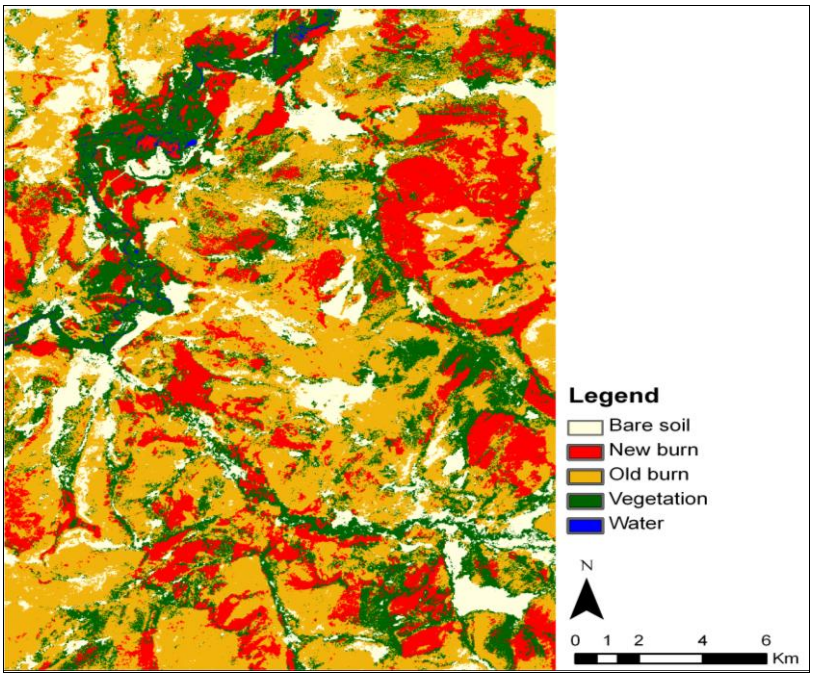

Figure 45: Classified image showing burned and unburned areas on day 2008057 from ASTER in Pendjari National Park (Benin).

The new burn scars (figure 46 on the right) were used to create the four burn severity categories that are shown in figure 47.

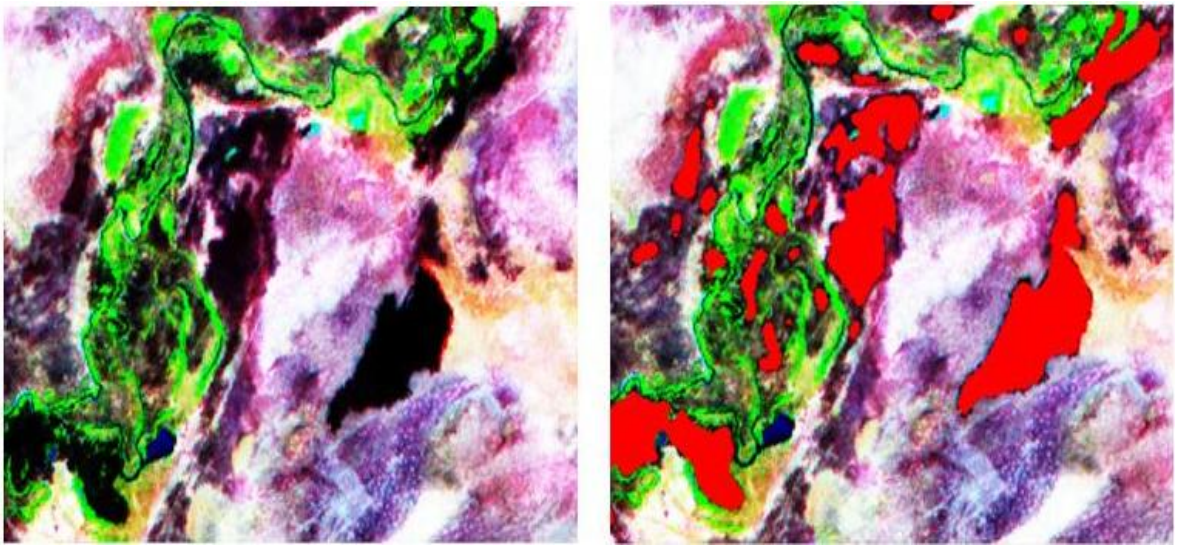

Figure 46: New burn scar mask (in red colour, right image) superimposed on an ASTER subset image of Pendjari National Park (26/02/2008), left image.

In the figure below, areas with very low and low burn severity make up 2,159.9 ha and 2,938.03 ha respectively. Areas of moderate burn severity make up 1,628.66 ha, and the area with high burn severity comprises 625.05 ha.

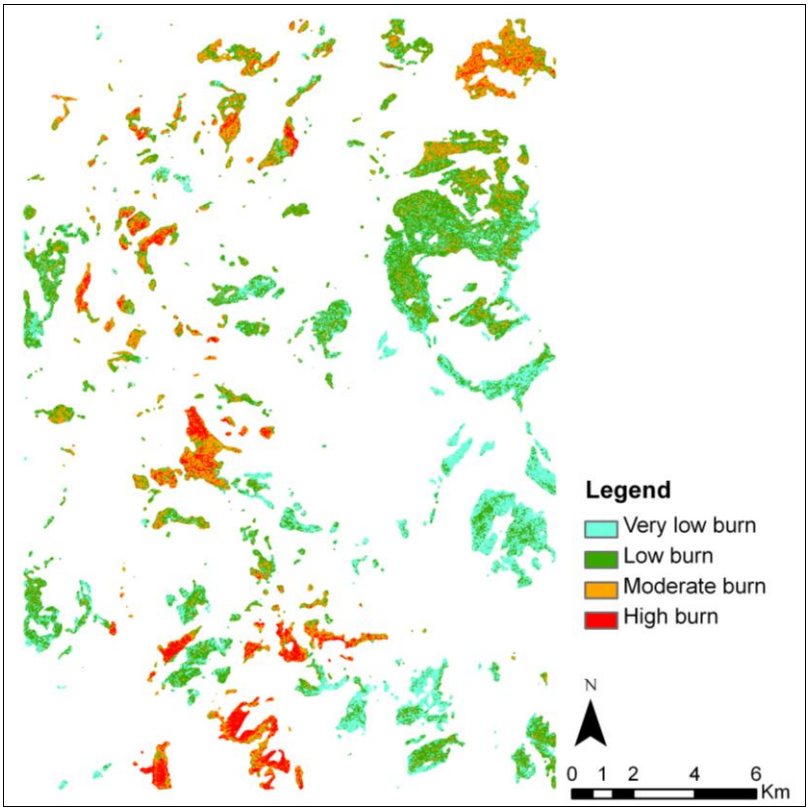

Figure 47: Burn severity map using ΔNBR derived of ASTER image from pre-fire (08/12/2007) and post-fire (26/02/2008) in Pendjari National Park.

In figure 48, the best separation between the 4 burn severity categories can be achieved only with ΔNBR, which shows a very low variance spread within every class, unlike those observed in bands 3N and 8 of ASTER post fire image (26/02/2008) and those of NBR post fire image.

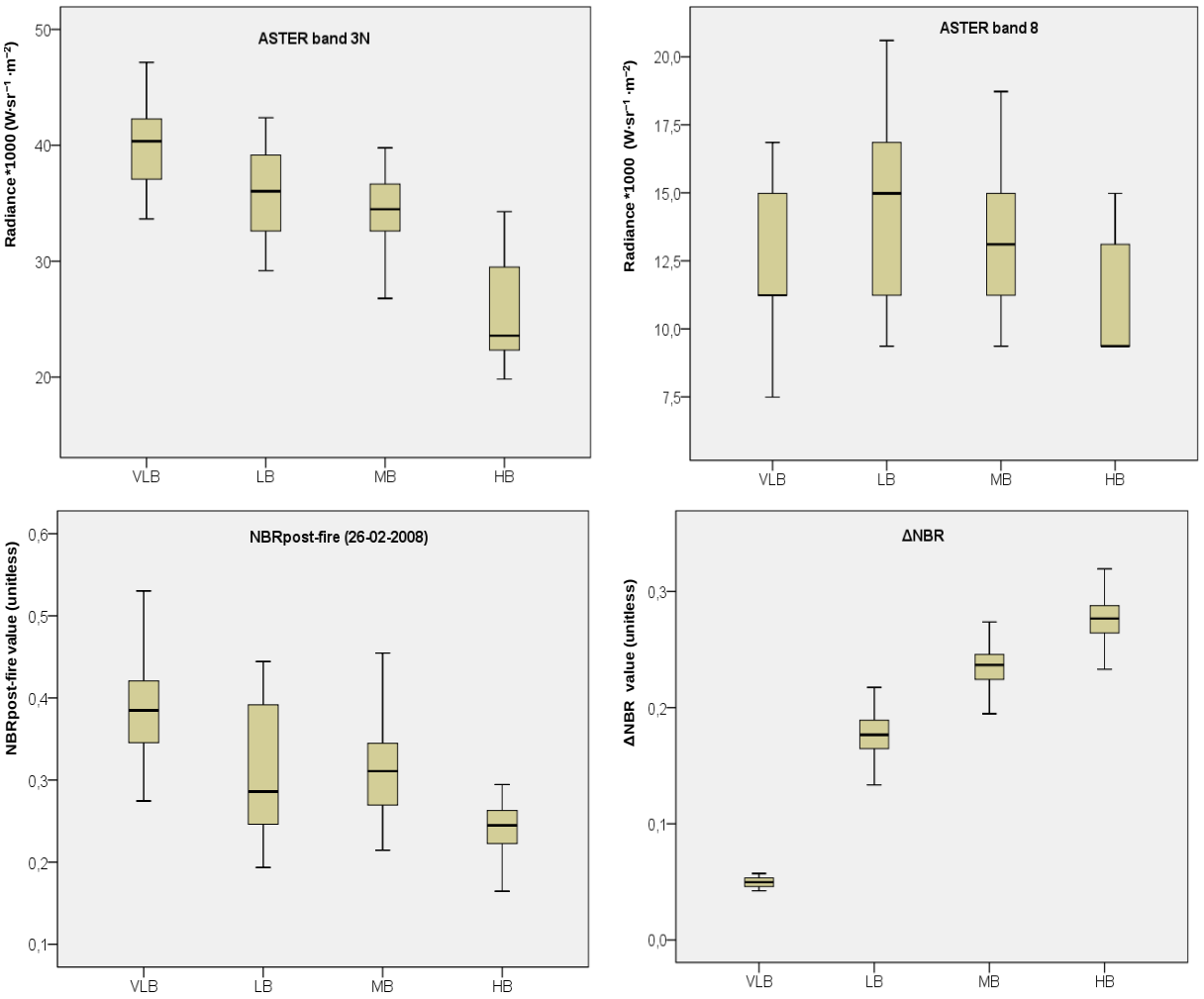

Figure 48: Box plots of the band $3N_{post\text{-}fire}$, band $8_{post\text{-}fire}$, $NBR_{post\text{-}fire}$ and $\Delta NBR_{(prefire\text{-}postfire)}$ of ASTER scenes according to burn severity categories (Very low burn: VLB, low burn: LB, moderate burn: MB and high burn: HB) in Pendjari National Park (Benin).

As mentioned above, the Landsat ETM+ scenes covering Pendjari National park were used for the verification of the burn severity results.

A first, pre-fire image of Landsat was acquired on 5th October 2007, another one (post fire) on 26th February 2008. The results of their analysis are presented below. Figure 49a shows the 149 GPS points collected in Pendjari National park during February 2008. The GPS points are better represented in the park than in the ASTER image above. The stripes to be found in figures 49a and b are data that are missing due to the failure of Landsat's scan line corrector since May 2003.

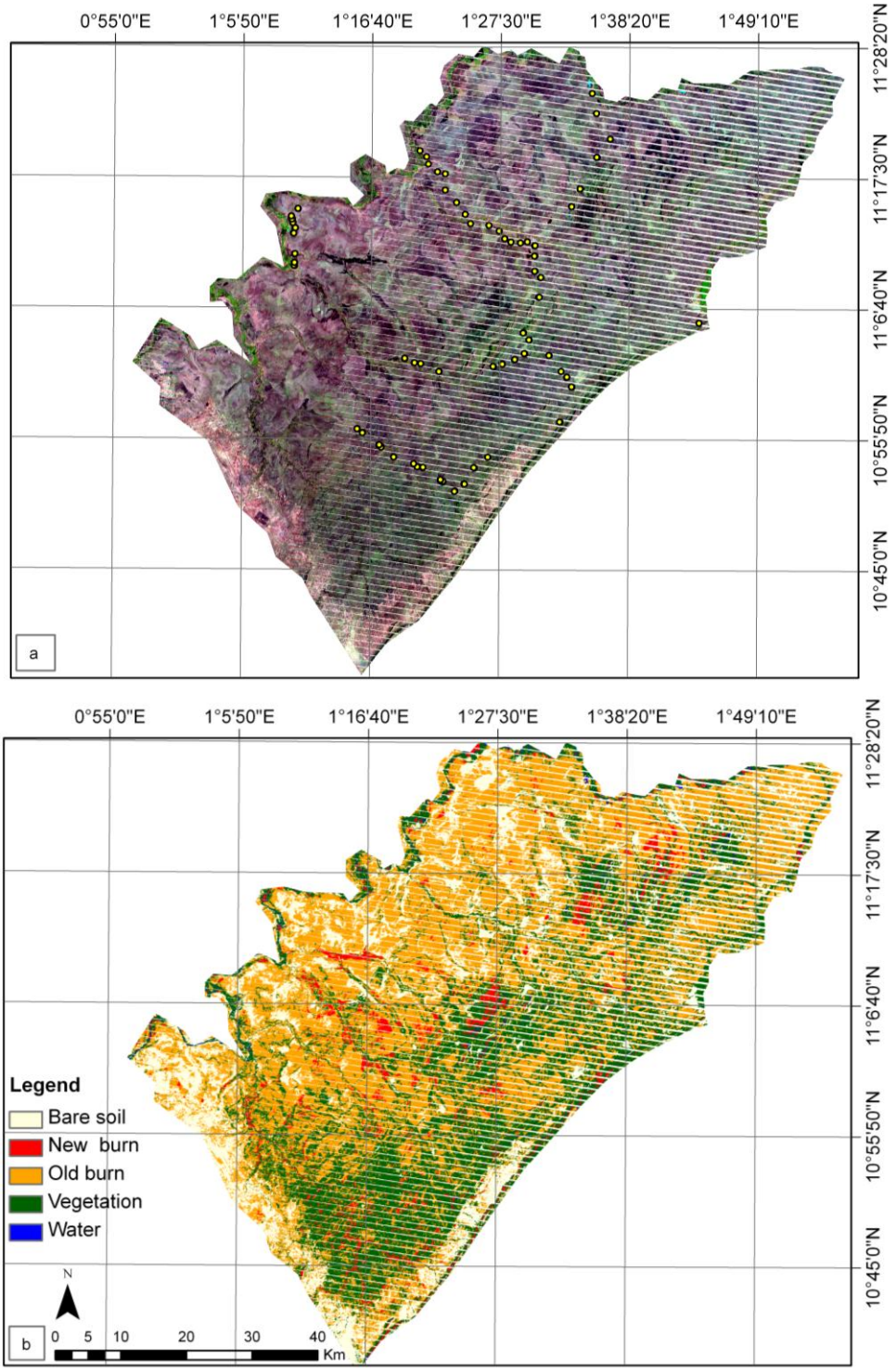

Figures 49: a) Landsat ETM+ subset image on day 26/02/2008 using bands 5-4-3 and GPS sample points collected in the Park in February 2008 and b) Classification of this image showing burned and unburned areas in Pendjari National Park (Benin).

The results of figure 49b were obtained by using the supervised classification algorithm.

The new burn scars were used for the subsequent analyses. It can be seen that the new burn scar mask observed in figure 51 is small in size compared to that obtained with the Landsat image on 07/12/2001 in Pendjari Park (figure 41a). This is so because the picture was taken on 26th February 2008, and as the preceding results of the spatial and temporal analyses

of active fires have shown, fires appearing in February are late season fires, which are much less frequent than those occurring in the early season, i.e. November and December. Towards the end of February, most of the vegetation has already burned, which can be seen from the figure below, where the colours violet and pink prevail. The new burn scars (figure 50) can be observed in the valleys of the small rivers and brooks and, to some extent, along the Pendjari river, where the vegetation was still green and the soil was humid during the passage of the early fires.

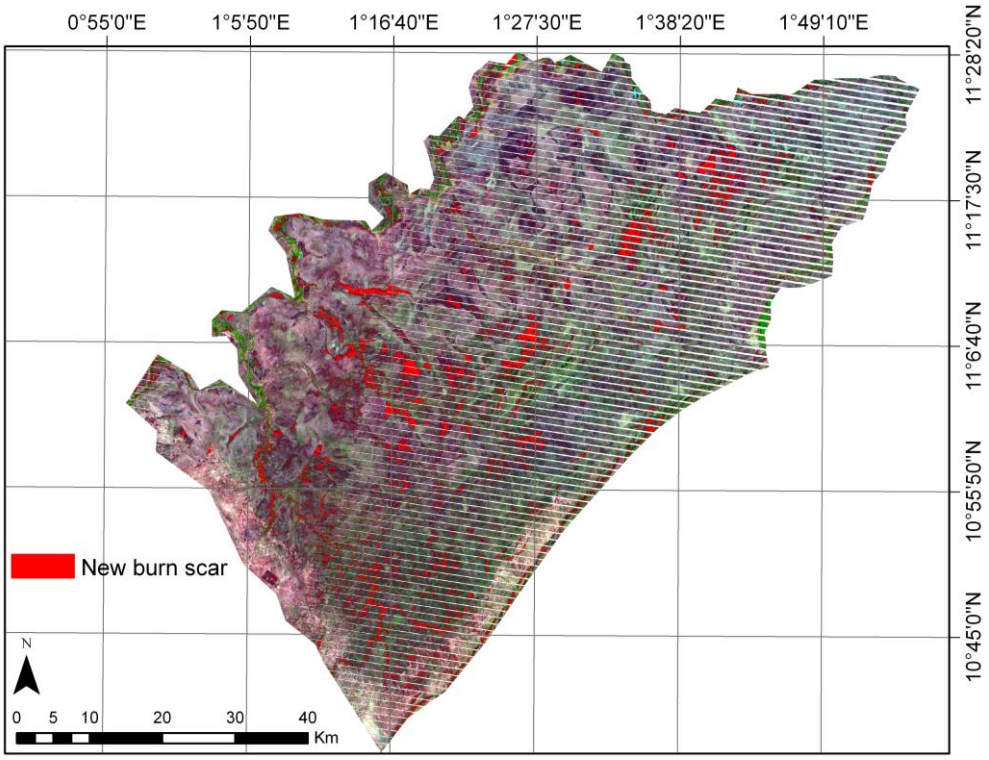

Figure 50: New burn scar mask superimposed on the Landsat ETM+ subset image (26/02/2008) of Pendjari National Park.

In the figure 51, the burn severity value varied from 0 to 1. Burn severity is accordingly classed into four categories, namely very low, low, moderate and high burn severity. To estimate the burn area of each category in hectares, the no gap data was considered. In this analysis, moderate burn severity was most widespread, extending over 8,703 ha, followed by high burn severity with 7,461 ha. Low burn and very low burn severity were found on 486 and 243 ha respectively. Leaving aside the data gaps, the comparison of the areas affected by burn scars of the different severity categories according to the data obtained in February 2008 (figure 51), i.e. in the late fire season, to that observed in December 2001 (figure 41b), i.e. the early fire season in Pendjari National Park, shows that the surface of the areas affected by burn scars of all severity categories in figure 51 is very low. This means that early fires affected larger areas, creating larger burn scars in each burn severity category, whereas late fires affected less surface and created smaller burn scars in all categories. However, whereas

most fires occuring in December were of moderate burn severity, those occurring in late February were quite evenly distributed between the moderate and high burn severity categories.

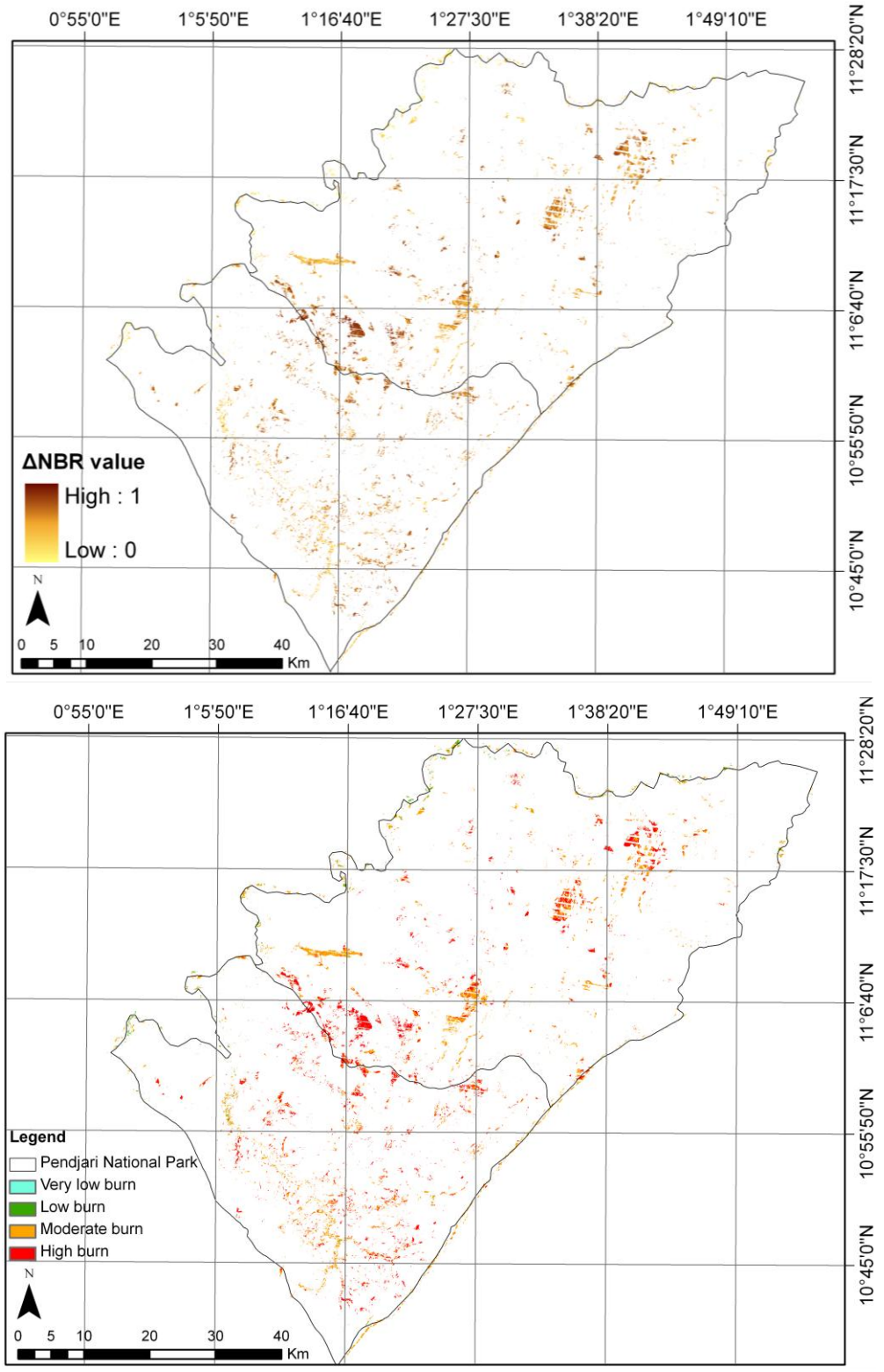

Figure 51: Burn severity map using ΔNBR value derived of Landsat ETM+ scenes from pre-fire (2007278) and post fire (2008057) observation period in Pendjari National Park (Benin). Above, the burn severity is presented by colour graduation, the higher the burn severity the more intense is the colour of the pixel.

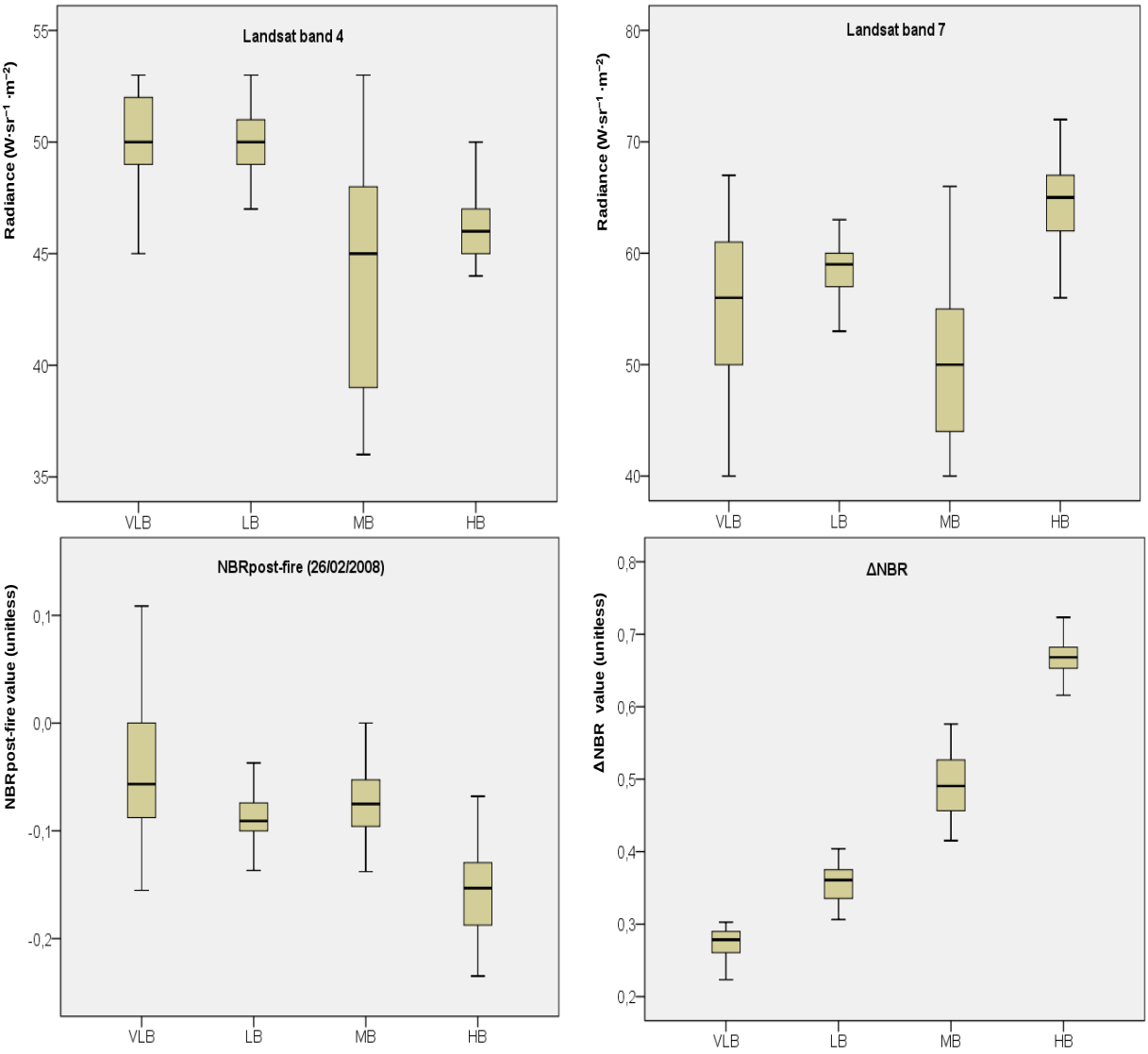

Figure 52: Box plots of the band $4_{post\text{-}fire}$, band $7_{post\text{-}fire}$, $NBR_{post\text{-}fire}$ and $\Delta NBR_{(prefire\text{-}postfire)}$ of Landsat ETM+ scenes according to burn severity categories (Very low burn: VLB, low burn: LB, moderate burn: MB and high burn: HB) in Pendjari National Park (Benin).

Just like with the preceding box plot analyses, only ΔNBR in figure 52 permits to clearly separate the categories, and the variances observed between the values within each category are low.

5.3.3 Verification of ΔNBR derived from Landsat ETM+ with field data

Within the field sampling campaign, the relationship between biomass loss detected by the Landsat imagery and the concurrent biomass loss in burned areas in the field were determined. The ΔNBR value, i.e. the difference between $NBR_{pre\text{-}fire\ (5/10/2007)}$ and $NBR_{post\text{-}fire\ (26/02/2008)}$ from Landsat ETM+ imagery was validated with the estimated biomass combusted by fire as observed in February 2008 in Pendjari National Park. The GPS points in burned area, which had all been attributed a degree of fire-induced biomass loss, which was established by visual estimation, was projected onto the ΔNBR image. The values associated

with every GPS point, namely the estimated biomass loss in percent and the ΔNBR value, are given in appendix 7. This table was used to work out a correlation between the ΔNBR value and the biomass loss in the field. The result of this correlation can be seen in figure 53. It shows the existence of a highly positive logarithmic correlation with R^2 = 0.76. The descriptive statistics show that the estimated biomass loss and ΔNBR had mean values of 55.91 and 0.51 respectively. The Std.Dev.s were 18.41 and 0.08 respectively.

The Pearson and Spearman-Rho correlation tests were used to verify the level of relation existing between the two variables.

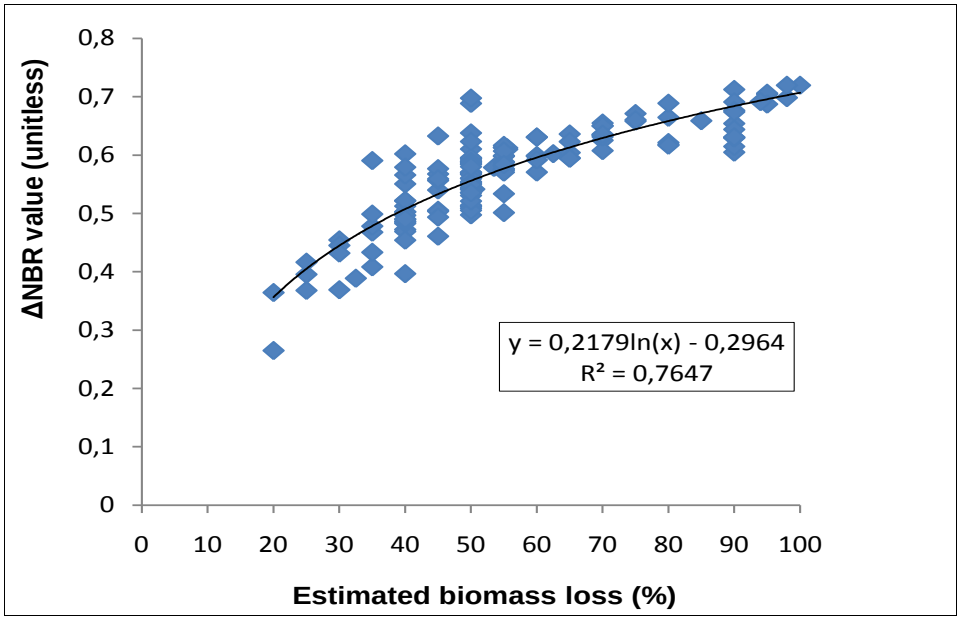

Figure 53: Curve of correlation between $\Delta NBR_{(prefire-postfire)}$ derived from Landsat ETM+ data and the estimated biomass loss (in %) data collected during field trip in Pendjari National Park (Benin).

The results of the statistical analyses of the two variables, as summed up in the tables 12 and 13 show that there is a highly positive relation between estimated biomass loss observed in the field and ΔNBR. The Pearson correlation and Spearman's Rho correlation show a very highly significant relation between the variable data, with r = 0.827 and r = 0.860 respectively. The significance level $P < 0.01$ shows the existence of a highly significant relation between the variables, which means there is a very good positive relation between the ΔNBR derived from Landsat ETM+ imagery and the field data collected in Pendjari National Park. These statistical analyses show that there is a strong link between the ΔNBR values and the percentage of biomass burned in a given area. In this way, the higher the ΔNBR value, the greater the share of biomass that was burned. Conversely, the lower the ΔNBR value, the smaller the biomass loss.

Table 12: Relation between estimated biomass loss (in %) and ΔNBR derived from Landsat ETM+ with the Pearson test.

		Estimated biomass loss (%)	ΔNBR
Estimated biomass loss (%)	**Pearson Correlation (r)**	1	**0.827****
	Sig. (2-tailed)		**0.000**
	Sum of squares and cross-products	50,132.185	185.276
	Covariance	338.731	1.252
	N	149	149
ΔNBR	**Pearson Correlation**	**0.827****	1
	Sig. (2-tailed)	**0.000**	
	Sum of squares and cross-products	185.276	1.002
	Covariance	1.252	0.007
	N	149	149

** Correlation is significant at the 0.01 level (2-tailed).

Table 13: Relation between estimated biomass loss (in %) and ΔNBR derived from Landsat ETM+ with Spearman´s Rho.

			Estimated biomass loss (%)	ΔNBR
Spearman's Rho	**Estimated biomass loss (%)**	**Correlation Coefficient (r)**	1.000	**0.860****
		Sig. (2-tailed)		**0.000**
		N	149	149
	ΔNBR	**Correlation Coefficient (r)**	**0.860****	1.000
		Sig. (2-tailed)	**0.000**	
		N	149	149

** Correlation is significant at the 0.01 level (2-tailed).

5.3.4 Burn severity category verifications through ΔNBR analyses and fields observations

In this part, the photos taken in the field at every GPS point are compared to the correlation between ΔNBR and biomass loss in order to describe the appearance of the vegetation or burned area for each category of burn severity.

The preceding analyses permitted to establish a relationship between the ΔNBR values of each burn severity category and the estimation of biomass combusted.

Very low burn severity has a ΔNBR of between 0 and 0.30 and corresponds to a biomass loss of up 0 to 20 percent. Low burn severity has a ΔNBR of between 0.31 and 0.40; it corresponds to a biomass loss of between 20 percent and 35 percent. Moderate burn severity has a ΔNBR of between 0.41 and 0.60; it corresponds to a biomass loss of between 35 percent and 55 percent. With high burn severity, ΔNBR ranges between 0.61 and 0.99, and biomass

loss can go up to 100 percent. Every burn severity category will now be illustrated by a photograph.

Figure 54: Unburned area near forest island in Pendjari National Park.

Figure 54 represents a plot in a forest island that was observed in the field trip. The tree leaves were green. The grass was a little dry but not burned. Unburned area can also be found in gallery forests, near water bodies as well as on bare soil and rock, which are not presented here.

Figure 55 : A shrubland area with understory grass that was affected by a very low severity fire in Pendjari National Park.

Figure 55 illustrates the passage of a very early season fire, probably lit at the end of the rainy season, i.e. between October and the beginning of November. Some tree leaves were still green, the grasses seem unburned. Here the fire intensity was very low, which is why

very little biomass was burned. Consequently, the loss of biomass was estimated to be lower than 20 percent.

Figure 56: A low severity burn observed in grassland with sparse trees in Pendjari National Park.

Figure 56 shows an area ignited in the early dry season. In the field assessment, the loss of biomass was estimated to be between 20 percent and 35 percent. The tree canopies were not affected by the passage of fire. Grass combustion is largely incomplete and just a few weeks after the fire, regeneration or resprouting processes within a burned area are visible. The fire intensity was low, resulting in a low severity burn.

Figure 57: A moderate severity burn in an open woodland area in Pendjari National Park.

Figure 57 shows a moderately burned area. The tree leaves have remained green, whereas lower parts of the trees were scorched. The shrub and grass layers are completely burnt. The loss of vegetation in this area is high, compared with the loss of vegetation in very low and low fire severity areas. Between 35 percent and 55 percent of biomass were consumed.

Figure 58: High severity burn in a woodland savanna in Pendjari National Park.

Figure 58 shows an area without residual vegetation (high combustion completeness), with a great occurrence of ash and charred matter. The trunk of the tree has been greatly damaged. This fire was observed in the field and was lit in February, which is seen as the month when late fires occur. Here the burn severity is high, which can be seen from higher combustion completeness. The biomass loss in this case can be estimated to be superior to 55 percent and can reach up to 100 percent, which means all grass was combusted by fire and the trunks of trees were greatly scorched by it.

CHAPTER 6: DISCUSSIONS

6.1 Fire seasonality and distribution in West Africa

The fire products derived from MODIS which were used for the analysis were a sample set of data from a total four overpasses per day of Aqua and Terra, corresponding to two overpasses in the morning (01:30 and 10:30) and two overpasses in the afternoon/evening (13:30 and 22:30). It is therefore important to keep in mind that the number of active fires detected in this study is only the result of observations made during the four satellite overpasses and only takes into consideration those fires which occurred in such conditions that MODIS was able to detect them. In fact, fires which only burned outside the overpass times were not dected by MODIS and are therefore not included in the results of this study, just like those which occured when the sky was covered by clouds or by thick smoke, and those which were masked by a canopy of trees. Fires that are thus concealed cannot be detected by MODIS (Giglio 2010). In sum, the fire pixels used in this study are only those which the two sensors of MODIS were able to detect during their passage and which were not masked.

The total number of 1,172,191 active fires detected by MODIS during the observation periods from 2000 to 2009 within the tiles h17v07, h17v08, h18v07 and h17v08 in Western Africa includes the three confidence classes which are assigned to fire pixels. Each confidence class is defined by using a detection algorithm created by Kaufman et al. (1998) and improved by Giglio et al. (2003), Justice et al. (2006) and Giglio (2010) so as to offer a higher sensitivity to small fires, cool fires and a reduction of false alerts due to deserts.

The number of active fires detected in the years 2000 and 2001 is lower than that in 2003. This can be explained by the fact that only MODIS Terra was able to record fires on the earth surface during the first two years. Starting with June 2002, the number of active fires detected began to increase because the number of overpasses of MODIS sensors increased from twice to four times per day. This suggests that Aqua and Terra combined together record more fire than only one sensor, which was confirmed through studies by Hawbaker et al. (2008) in the United States. These studies showed that a detection rate of 82 percent of all active fires was achieved by both Aqua and Terra when they are combined. By contrast, with Aqua and Terra individually, this rate is lower, with respectively 73 percent and 66 percent of active fires detected. The increase in detection rate seems to be even higher in West Africa. Within this study, no direct comparison was made between fires detected by Aqua and Terra, but the finding that Terra and Aqua combined, in 2003, discovered more than double the number of

fires (131,028) than Terra alone in 2001 (63,261) – whereas the number of fires discovered by Aqua and Terra remained relatively stable in the years following 2003 – can best be explained by assuming that Terra and Aqua combined have double the detection rate of Terra alone. If one then assumes that the detection rates of Terra and Aqua are roughly equal (which seems to be confirmed by Hawbaker's findings), both sensors must mostly discover different fires, and there must be few fires that are discovered by both Terra and Aqua, otherwise the detection rate would not double. An explanation of this could be that most fires may be so short that they are only detected by one of the sensors, as they have extinguished when the next sensor passes. This, in turn, could imply that there could be a great number of short fires that flare up after one sensor has passed and go out before the passage of the next one, so they are not detected. What makes this theory plausible is that dry savanna grass burns rapidly, as the author of this study could observe on field trips, so that at least fires in grassland savannas should be of short duration. However, in the framework of this study, the percentage of fires in West Africa that were not detected by the sensors as well as the percentage of false alarms was not assessed, as this would have required further extensive field work on a regional scale.

The great amount of fires detected in the savanna formations between dense forest and steppe can be explained by the intense fire activity in this area in West Africa. This result is confirmed by recent satellite observations of Africa as a whole (NASA 2010a). One reason for this intense activity may be that fires have for decades played an important role in the creation of savannas and in maintaining their dynamics. Another reason may be the high pressure of human activity in these savannas, as described in the literature. Previous studies carried out by Hao & Liu (1994), Dwyer et al. (1998) and Dwyer et al. (2000) found that most fires worldwide occur in African savanna, and most of them are of anthropogenic origin.

The steady increase in the overall number of active fires detected between 2003 and 2008 (the data for 2000, 2001, 2002 and 2009 are incomplete) could also be explained by an increasing population pressure, which may have led to more fires being laid for poaching, converting savannas into agricultural lands and for clearing fields.

The statistical analysis of rainfall and fire detection by MODIS showed a very strong negative correlation ($r = -0.878$) with a high significance of $P < 0.000$. This means that, first, there is a correlation between rainfall amount and active fire detection and, second, this correlation permits to identify the bushfire season. In fact, the analysis shows that the higher the monthly rainfall amount, the lower the number of fires. Conversely, the lower the rainfall, the higher the number of fires. Based on this observation, two seasons were identified in West Africa. One is the dry season which extends over seven months from October to April, where

fire activity is very intense, with more than 98 percent of fires detected taking place in this time, wherefore it is called the fire season, and another season, called rainy season, which lasts for 5 months, from May to September, and which is characterized by a low rate of fires detected (1.34 percent). According to Laris (2002) it is the length of the dry season between 4 and 8 months in West African savanna that makes savannas prone to fire. The comparison of the results of this study to those of another study carried out in South Africa by Roy, Borak, et al. (2002) showed that vegetation burning in Southern Africa occurs in the dry season from approximately May to November.

This difference is explained by the fact that the climatic seasons are opposite, which means that the rainy season in West Africa corresponds to the dry season in South Africa and vice versa. This is so because of the location of these two regions relative to the equator. Southern Africa, below the equator is part of the southern hemisphere, whereas West Africa, above the equator, is located in the northern hemisphere.

Fire density varies within the fire seasonality and it depends on vegetation moisture. Very early fires occur at high latitude and take place in Sahelian and Sahelo-Sudanian areas, whereas very late fires appear at low latitude and are also observed in the forest and especially in the transition zone between the forest and Guinean savannas. This seasonality of fire can be explained by the rainfall gradient, which decreases with latitude getting higher. Therefore, at high latitudes, the plants dry faster after the end of the last rains, which is why the first fires of the season take place there. This result is in accordance with previous observations by Nielsen & Rasmussen (2001) and Devineau et al. (2010). However, the Inner Niger Delta and the irrigated croplands around it, located in the semi-arid Sahel area of central Mali are characterized by very late fires because this area is a wetland, where it takes a long time before the plants have dried, so that fires only occur in the 6^{th} and 7^{th} month of the dry season (Devineau et al. 2010).

Very early fires (making up 3.40 percent of all fires detected) which occur in the very early season indicate the beginning of fire season whereas very late fires (5.47 percent of fire detected) announce the end of the dry season, as most of the fuel has already been consumed by fire. Most fires detected were early and late fires (53.54 percent and 37.57 percent of fires detected), with the peak of activity in December/January. They mainly take place in Sudanian, Sudano-Guinean and Guinean savannas. At this time, a lot of fuel has accumulated in these areas and – due to the lack of rainfall in the previous months - it has dried so much that fires ignite easily and spread rapidly. The reduction of fire activity after this peak can be explained

by the fact that once these great fires, mostly of high intensity, have passed, the fuel that is necessary for further fires has been reduced.

Concerning fire pixel frequency; it is highest in Sudanian, Sudano-Guinean and Guinean savannas, and especially so in the protected areas located in these savanna zones. This corresponds to the observation by Grégoire & Simonetti (2010) that fire density inside parks and reserves is higher than around them. Part of this high fire density and frequency can be explained by conscious use of fire by park management in order to maintain the savanna vegetation structure and avoid bush encroachment, which could mean certain species of plants and animals adapted to the savanna would be displaced by those adapted to the forest. However, part of the high fire intensity seems to be due to poaching by fire or uncontrolled fires lit by the population living next to the proctected areas.

Outside the protected areas and around them, the fire pixel frequency is generally lower than inside. This difference in fire frequency may be due to the presence of fields and villages around the parks, as well as firebreaks between these villages and the parks, which sometimes form physical barriers, leading to a discontinuity or reduction and sometimes lack of biomass which may be the cause of repetitive fires.

6.2 Fire occurrences in land cover classes

The analysis of the occurence of fire and its spatio-temporal distribution within land cover showed that almost all vegetation classes are affected by fire. However, the majority of fires take place in Deciduous woodlands, Deciduous shrubland with sparse trees, Croplands or Croplands mixed with open woody vegetation and mixed Mosaics forests/Croplands.

In the dry season periods from October 2000 to April 2006, the high fire activity in the Deciduous woodlands and Deciduous shrublands (more than 40 percent and 34 percent of the total count of fires detected respectively) were probably related to the ongoing conversion of these natural savannas to agricultural lands and also the high level of fuel and its continuous availability. Across the whole observation period, the annual averages of 37.18 percent and 35.29 percent of the total count of fires being observed within these two areas confirm that the majority of fires occurred in savanna-woodland as shown by previous studies (Nielsen & Rasmussen, 2001; Clerici 2006; Grégoire & Simonetti, 2007).

Another explanation for the high occurrence of fire in these savannas may be the management of tree and shrub height populations. As quoted by Dereix & Amani, (1978) in their study carried out in Kokondékro (in the centre of Ivory Coast), the absence of fires in a savanna formation during several years leads to the appearance of woody vegetation, to the

detriment of the herbaceous and grass layer. Gradually, the savanna is being displaced by woody cover. In this scenario, the savanna will bit by bit turn into a forest, causing a transformation of the ecosystem. As an immediate consequence, certain animals that feed on the herbaceous grass layer will disappear or migrate to other environments, giving way to animals adapted to forest environments. Furthermore, water competition, nutrients and sunlight competition between trees and grass layers will be increased to the detriment of the herbaceous layer. This assertion was confirmed in a previous study carried out in Australian savannas by Dyer et al., (2001).

The need for wood fuels and charcoal may be another reason for highly frequent fires in Deciduous woodland and Deciduous shrubland. In fact, many early season fires of lower intensity 'dry' the shrubs without burning them and make them lose their leaves. People then can cut down these shrubs and use the dry wood as firewood or for making charcoal. The need for firewood and charcoal therefore provides an incentive for lighting bushfires. In the last decades, population increase in West Africa led to a rising demand for charcoal and fuel wood, which is collected almost exclusively from the natural environment. The energy from wood fuel and charcoal is very important both for people living in the countryside and in the cities because it is needed for cooking. As stated by Brocard, Lacaux, & Eva, (1998) and Eva et al. (2006), wood fuel provides between 85 to 99 percent of household energy requirements in Africa with an annual per capital consumption of between 300 and 700 kg of wood.

The fact that in the period between October 2006 and April 2009 the proportion of fire pixels observed sank by 11.17 percent for the Deciduous woodlands and increased by 1.67 percent for the Deciduous shrublands can be explained by the changes in the algorithm used to establish the fire detection confidence. The reason for these changes was to more accurately identify fire pixels (Giglio & Justice 2006), and a consequence of this change is that fewer fires were detected in Deciduous woodlands. It is probably for the same reason that the proportion of fires detected in Mosaic forests/Croplands dropped, whereas the proportion of fires detected in Croplands (>50%) and Croplands with open woody vegetation increased.

According to the observations from 2000 to 2009 made in this study, many fire pixels were found in the different kinds of croplands (about 26 percent on average). This high value can be explained by the fact that after the harvests, farmers frequently use fires to clean their fields, where the remains of crop plants constitute an available fuel.

Lower fire occurrences in other classes (1.82 percent) may be dictated either by low biomass fuel amounts and low fuel continuity in the case of Sahelian vegetation, or by high moisture of fuel in the case of forest vegetation. Landscape discontinuity and expansion of

farm land as well as the expansion of settlements can also limit the spread of fire (Devineau et al. 2010).

Clerici et al. (2004), who studied fire in the dry season October 2002 to April 2003 in West and Central Africa based on MODIS Terra came to results as to distribution of fires across different vegetation classes that are comparable to those in this work: In their study the majority of fires also occurs in Deciduous woodlands (36 percent) and Deciduous shrubland with sparse trees (24 percent), and fires in Croplands with open woody vegetation played an important role (11 percent of fires detected). However, they also found the presence of fires in classes that did not play an important role in this study, such as Mosaic forest/Savanna (13 percent) and Open Deciduous shrubland (6 percent). This may be so because these vegetation forms hardly occur in West Africa, but they do occur in Central Africa, which was also observed by Clerici et al.

6.3 Characteristics of burn severity

The measurement of burn severity with Landsat ETM+ was verified by field observations estimating in percent the quantity of biomass consumption by fire. It should be noted that the quantitative measurement of fuel biomass (g/ha) was not made.

The spectral properties and the Normalised Burn Ratio index permit the highest discrimination between burnt and unburnt area (healthy vegetation) in the NIR band 4 and MIR band 7 of Landsat ETM+ and in the NIR band 3 and MIR band 8 of ASTER. This can be interpreted as being the reflectance change detected by this index, which is a sign of biomass loss increasing the soil exposure. Some literature showed that bands 4 and 7 of Landsat ETM+ as well as bands 3 and 5 to 8 of ASTER are the best discriminators between burned and unburned area (Miller & Yool 2002; Van Wagtendonk et al. 2004; Cocke et al. 2005). In fact, the decrease in reflectance in band 4 correlates to the loss of biomass due to fire. When vegetation has been consumed by fire, less energy is reflected by leaves in this wavelength. The higher reflectance in band 7 correlates with increasing soil exposure after fire, as soil has higher reflectance in this wavelength region than vegetation containing moisture.

As burn severity is contingent on the pre-fire vegetation conditions (Roy & Landmann 2005), the temporal difference between pre and post fire NBR values can be used to estimate the burn severity, especially of new burns (Landmann 2003). The results on ΔNBR in this study that showed the better differentiation of burn severity categories were also confirmed by some previous studies which recommended this variable as an operational index to estimate

burn severity from satellite data (García-Haro et al. 2001; Key et al. 2002; De Santis & Chuvieco 2007).

During the field observations in the Pendjari National Park, the biomass consumed was estimated. A highly significant relation was found between the remotely sensed burn severity and these field assessed data through statistical analyses (Pearson coefficient (r) = 0.827 and Spearman´s Rho coefficient (r) = 0.860). In fact, every category of burn severity corresponded to a quantity of biomass consumed and a certain degree of change in the landscape. This analysis is in agreement with that by Key & Benson (1999), who showed that the higher the positive or negative values of ΔNBR, the higher the degree of change.

It is also evident from the field surveys that the different levels of burn severity are very heterogeneously distributed in the study area. Totally burnt areas can be found next to partially burnt ones and areas with unburnt vegetation. This patchy distribution of burn scars can partly be due to sudden changes of wind direction during combustion, but can often be explained by factors visible in the field, namely by the variable distribution of moisture content of available fuels as well as by gaps in the available fuel continuum and physical barriers such as roads, water bodies, rocks or firewalls which hinder fire spread (Whelan 1995; Williams & Cook 2001; Walz 2004).

In the burn severity analysis in this study, four classes were derived to distinguish between very low, low, moderate and high burn severity. Each of these classes could be matched to vegetation burn characteristics observed during the field trip:

Very low burn severity was found in unburned areas interspersed with areas affected by very low severity ground or surface fires. In these areas where pre-fire vegetation had been forest or shrub, only a small percentage of ground cover (litter) of up to 20 percent had been consumed and vegetation mortality was minimal. Mortality of trees and shrubs was slight because the leaves of trees and shrubs cover remained healthy and green due to the plant moisture. In the field work in Pendjari National Park, some areas characterised as showing very low burn severity were also observed in large coherent areas of rock outcrop or bare soils in the Attacora mountain chain.

Low burn severity (where 20 to 35 percent of vegetation is burned) was found in areas where pre-fire fuels had been sparse or light, namely in grasslands with sparse shrubs and thin litter, and also in areas where smaller but frequent patches of rock outcrop or bare soils contributed to the scarcity of vegetation. The field observations carried out for this study also showed that the small trees and grass were lightly scorched when low burn severity had

occcured. In most areas, just a few weeks after the fire, some grass species like Andropogon and Pennisetum were already sprouting.

Key & Benson (1999) showed in a previous study in North American that fires of this severity have many positive effects which can be summed up as: low loss of biomass, release of nutrients for plants, creation of additional edge habitat and openings, stimulation of some vegetation species which depend on fire.

Moderate burn severity is defined as being that where biomass is consumed between a ratio of 35 and 55 percent. It was found to dominate in woodland areas, in areas of moderately dense to dense shrub communities and grass. The leaves of shrub and grass may be all or partly consumed, with shrub skeletons remaining. In areas where pre-fire vegetation had been made up of woodland, brown leaves remained on trees but much of the litter had been burned. As stated by Key & Benson (1999) the recovery of vegetation cover after moderate burn can be faster if the fires do not occur very frequently. Frequent fires can affect the soil structure because they expose the soil to leaching.

High burn severity was found in woodland, and more extensively in a few alluvial areas where pre-fire vegetation had consisted of dense biomass (trees, shrubs and grasses). In these areas, litter was generally deeper, so fire residence time could be longer, causing a complete consumption of ground fuel biomass, trees, shrubs and grass. The quantity of biomass consumed by the passage of fire is very high because the vegetation is very dry and therefore ignites easily (Landmann 2003). In a late and very late fire season, the effect of this fire on the vegetation is not neglectable. Park managers are very much aware of these damages, so, for example, in Pendjari Park, fires are lit at the beginning of the dry season, which is important for the survival of animals such as herbivores and rodents that are nourished by young regrowth (Tehou 2003; Tehou 2005; Tehou 2006; Tehou 2007). By contrast, very late fires observed in the park were lit by poachers or were uncontrolled fires that originated in fires lit by neighbouring populations (Tehou 2003; Tehou 2005; Tehou 2006; Tehou 2007).

If fires of this severity frequently occur in an area, the continous erosion of organic matter in the soil can be very high because the soil is strongly exposed to the wind and the rain. As a consequence, recovery of vegetation might take a long time. This observation was confirmed by Key & Benson (1999) and Walz et al. (2007).

A comparison of this study's results for burn severity to those found in other areas shows that Walz et al. (2007) obtained burn severity classes of similar characteristics in their study carried out in Jarrah-marri forest (Australia) but the ΔNBR values within each class are different from the ones in this work. In their study, low burn severity was assumed at a

Landsat ΔNBR of between 300 and 650 (>300 to ≤ 650). Moderate burn severity covered the interval from 650 to 1000 (> 650 to ≤ 1000) and for high burn severity, ΔNBR was superior to 1000 (> 1000). In this work, the ΔNBR value for very low and low burn severity was respectively between 0 and 0.30 and between 0.31 and 0.40; the value of moderate burn severity was from 0.41 to 0.60. With the high burn severity, this value ranged from 0.6 to 0.99. These differences observed in the ΔNBR for the two studies can be due to the different vegetal formations, as the study of these authors was carried out in the forest whereas ours had the savanna biomes as its object.

However, the definitions of each burn severity class are almost the same as in this work. Based on field observation, these authors found that low burn severity affected only the understorey of the vegetation. With moderate burn severity, it is the understory and upper understory of vegetation that were affected by fire. With high burn severity, all strata were combusted.

The results in this study can also be compared to those obtained by Key & Benson (1999) and Key (2005) in North America. Although their ΔNBR value range for each burn severity class is different from that in this study, the characteristics of each of these classes are the same as those described in this study. According to this author, the ΔNBR value increases with change levels observed in the landscape, which means that high ΔNBR value correspond to high burn severity and therefore high change within the landscape. In his study, for the low severity class, the ΔNBR values range from 100 to 225, in the Moderate low severity class, they vary from 256 and 410, in the Moderate high class from 411 to 660, while ΔNBR values for high burn severity are superior to 660. Again, the differences observed between their ΔNBR value ranges and those in this study can be explained by the characteristics of the vegetation or the landscape, as these studies were carried out in the pine forests of California, which show a different structure of vegetation and the grass layer than West African savannas.

These are two examples of how the ΔNBR value range for each burn severity class can vary depending on the type of landscape, but the burn severity classes are always connected with roughly the same fire damage characteristics to be observed on the ground.

However, ΔNBR values from studies made in Southern Africa, Australia or California cannot be transferred to West Africa. For every study, burn severity classes need to be defined and the analysis of satellite-based ΔNBR images needs to be connected with observations made on the ground.

Yet, it is safe to assume that the burn severity characteristics established in Pendjari

National Park can be transferred to other areas of West African savanna showing a comparable vegetation structures. This means that the ground observations made in Pendjari National Park which were then used to verify the remotely sensed results for this park can also be seen as validating the results obtained for Comoé National Park and Bontioli Reserve.

The differences in burn scar size of the different severity classes that are observed between the parks can be explained from factors such as park management, intensity of poaching and fires lit in the surrounding areas, as well as the presence of physical barriers hindering the spread of fire.

CHAPTER 7: CONCLUSIONS AND OUTLOOK

This thesis, like some previous studies, has presented satellite data as a tool that scientists can use to study the fire environment on large and fine scales with temporal intervals that were not available before.

This work could just describe some aspects of fire distribution and behaviour in West Africa. It has shown that it is possible to use the Normalised Burn Ratio index for describing the burn severity of fires in West Africa. This index was already used in some previous works, for example in North American forests (Key 2005) and in Australian forests (Walz et al. 2007) to define burn severity.

Concerning the first objective of the study, namely establishing the spatio-temporal distribution of fires on the regional scale by using the MODIS fire product at 1km resolution (with the limitation that only the fires burning during the four daily overpasses of MODIS sensors could be taken into consideration), it was shown that most active fires, namely about 98.75 percent, were detected in the dry season defined to last from October to April and they are located between 5° and 15° N, more specifically in the savanna zones bordering on the dense forest in the south and the steppe in the north. In the rainy season from May to September, very few active fires (1.25 percent of all fires) were detected. Aqua and Terra combined detected more active fires than any single of these satellites. Within the dry season, four fire seasons were determined. Very early fires began at higher latitude around 14°N. These fires occurring in October after the last rainfalls of the rainy season represented only 3 percent of the total count of active fires detected and are often small. They were detected in the Sahelian and Sahelo-sudanian areas. Early fires (November-December) and late fires (January-February) made up 51 percent and 40 percent respectively of the total count of active fires detected. They mostly took place between 12° and 8° N and occurred in Sahelo-Sudanian, Sudanian, Sudano-Guinean and Guinean regions, with their activity peaks in December/January. Very late fires (March-April) take place at the end of the dry season, before the beginning of the rainy season. These fires represented only 6 percent of the total count of fires and mostly took place in the transition zone between the Guinean savanna and the forest. They were also found in the Inner Niger Delta in Mali.

As to the occurrence of fires in the countries which are mostly located in the savanna area, it was found that the higher the savanna surface of a country, the more bushfire activity can be registered in it.

In general, the highest frequency of active fire pixels, with fire pixels detected in 3 to 9 of all the dry seasons, were observed between the Sahelo-sudanian and Guinean areas. This

high frequency was especially observed within the protected areas located in these savannas. In the Sahelian and forest areas, almost only low active fire pixel frequency (from 1 to 2) was observed. This may be so because fires in these areas are comparatively rare and mostly small, due to the lack of fuel in the Sahel area and the great humidity in the forest, so that it is rather improbable for the areas where fires do occur to overlap in consecutive years.

Concerning the second objective of this study, the analysis of the relation between fire occurrences and the land cover classes on a regional scale, the conclusion was reached that fires took place mostly in Deciduous woodlands and Deciduous shrublands with sparse trees (more than 70 percent of total fires detected) and to a lesser extent in Croplands (around 26 percent of total fires detected). Fires showed different seasonalities according to the vegetation in which they occurred.

The third aim of this study was to establish the burn severity in relation to the biomass loss observed in field in Pendjari National Park. The study concluded that ΔNBR is a suitable indicator of burn severity for the West Africa savanna and that field observations are useful to understand this burn severity and to estimate the removal of biomass fuel. Although the NIR and SWIR wavelengths were originally designed to estimate plant water content (Fraser et al. 2000), they have also proven useful to map burn severity (De Santis & Chuvieco 2009). A good correlation was obtained between the field data and the ΔNBR derived from pre and post fire of Landsat ETM+, with $R^2 = 0.76$, which was also confirmed by Key & Benson (1999); Key (2005); Walz et al. (2007); Soverel et al. (2010). The analysis of the correlation coefficient according to Pearson is $r = 0.84$ and according to Spearman-Rho, it is $r = 0.86$. These field observations can therefore be used to verify the remotely-sensed change within savanna biomes. Here, four burn severity classes, namely very low burn, low burn, moderate burn and high burn serverity and their characteristics were determined.

In West Africa savanna, like elsewhere, the loss of biomass increases with burn severity. Very low and low burn severities are characteristic of fires of very low intensity, connected with low biomass removal rates. These fires are less complete and only up to 35 percent of biomass is lost and few weeks after, young shoots appear. They produce a lower effect on the vegetation structure and soil (Key 2005; Walz et al. 2007). Moderate and high burn severities are characteristic of fires which are more complete. Here, 35 to 100 percent of biomass is removed. Damage done by fires of high burn severity is often so great that even the trunks of trees are completely scorched and the soil is completely exposed to sun, wind and rain erosion. This makes vegetation recovery after the fire more difficult (Landmann 2003).

It will be interesting to continue research by using this long times series of active fires to

deepen the analysis of other aspects of fire regime in order to prescribe an optimal fire management for West Africa. The results of this study seem to suggest that lighting fires comparatively early in the dry season is preferable to lighting them late in the fire season. In fact, "very early" and "early" fires seem to be better for savanna vegetation because they are generally of lower severity, so that the biomass of an area is not completely burned and the vegetation can recover after it. Moreover, when a very early or early fire has burned away most of the dry biomass on the ground, there is little fuel left for any late or very late fires of higher burn severity.

Regular observations on fire regimes as spatio-temporal patterns need to continue in remote sensing so that climate change effects on fires and fire regime changes can be monitored.

The areas affected by a high frequency of fire pixels, as observed in this study, must be observed in field studies so as to better understand the long-term impact of fire frequency on biodiversity in a given area.

REFERENCES

Abrams, M., Hook, S. & Ramachandran, B., 1999. *ASTER User Handbook, Version 2*. NASA, Jet Propulsion Laboratory.

Andreae, M.O. & Merlet, P., 2001. Emission of trace gases and aerosols from biomass burning. *Global Biogeochemical Cycles*, 15(4), 955–966.

Arbonnier, M., 2002. *Arbres, arbustes et lianes des zones sèches d´Afrique de l´Ouest. 2eme édition*. CIRAD - MNHN Paris.

BIOTA, 2010. BIOTA West Africa Observatory Information. Available at: http://www.biota-africa.org.

Barbosa, P.M., Grégoire, J.M. & Pereira, J.M., 1999. An algorithm for extracting burned areas from time series of AVHRR GAC data applied at a continental scale. *Remote Sensing of Environment*, 69(3), 253–263.

Barsi, J.A. et al., 2003. Landsat TM and ETM+ thermal band calibration. *Can. J. Remote Sensing*, 29(2), 141–153.

Bartholome, E. & Belward, A.S., 2005. GLC2000: A new approach to global land cover mapping from Earth Observation data. *International Journal of Remote Sensing*, 26(9), 1959–1977.

Baxter, P.W. & Getz, W.M., 2005. A model framed evaluation of elephant effects on tree and fire dynamics in African Savannas. *Ecological Applications*, 15(4), 1331–1341.

Bond, W. & Keeley, J.E., 2005. Fire as a global 'herbivore': the ecology and evolution of flammable ecosystems. *TRENDS in Ecology and Evolution*, 20(7), 387–394.

Bowman, D.M. et al., 2009. Fire in the Earth System. *Science*, 324(5926), 481–484.

Bowman, D.M., 2001. Australian Rainforests: Islands of green in a land of Fire. *Historical Records of Australian Science*, 13(4), 383–437.

Bowyer, P. & Danson, F.M., 2004. Sensitivity of spectral reflectance to variation in live fuel moisture content at leaf and canopy level. *Remote Sensing of Environment*, 92(3), 297–308.

Brewer, C.K. et al., 2005. Classifying and mapping wildfire severity: a comparison of methods. *Photogrammetric Engineering and Remote Sensing*, 71(11), 1311–1320.

Brocard, D., Lacaux, J.P. & Eva, H.D., 1998. Biomass combustion and associated atmospheric emissions in West Africa. *Global Biogeochemical Cycles*, 12, 127–139.

Brown, J., 1995. Fire regimes and their relevance to ecosystem management. In *Proceedings of the society of American Foresters National Convention*. Bethesda (MD): Society of American Foresters, pp. 171–178.

Cahoon, D. et al., 1992. Seasonal distribution of African savanna fires. *Nature*, 359, 812–815.

Carmona-Moreno, C. et al., 2005. Characterizing interannual variations in global fire calendar using data from Earth observing satellites. *Global Change Biology*, 11(9), 1537–1555.

Chandrashekhar, M.B. et al., 2003. Landsat Enhanced Thematic Mapper (ETM+) Mosaic: Nominal 2000´s mosaic for the Limpopo river basin. International Water management Institute (IWMI), Colombo Sri Lanka, 1–9.

Chuvieco, E. et al., 2006. Use of a radiation transfert model to simulate the postfire spectral response to burn severity. *Journal of Geophysical Research*, 111(G04S09), 1–15.

Chuvieco, E., Giglio, L. & Justice, C., 2008. Global characterization of fire activity: Towards defining fire regimes from Earth Observation data. *Global Change Biology*, 14(7), 1488–1502.

Clerici, N. et al., 2004. Assessing vegetation fires activity and its drivers in West-Central Africa using MODIS and TRMM data. In *IEEE International Geosciences and Remote Sensing Symposium*. IEEE International Geosciences and Remote Sensing Symposium, pp. 2087–2090.

Clerici, N., 2006. Monitoring and assessing fire impacts and land-cover change in tropical and subtropical ecosystems using satellite remote sensing and GIS techniques. Ph. D. thesis, Ispra, Italy.

Cocke, A.E., Fulé, P.Z. & Crouse, J.E., 2005. Comparison of burn severity assessments using Differenced Normalized Burn Ratio and ground data. *International Journal of Wildland Fire*, 14, 189–198.

Cole, M.M., 1987. The savannas. *Progress in Physical Geography*, 11(334), 1–23.

Cord, A., 2007. Classifying land cover using FAO-LCCS standards in a tree savannah of Burkina Faso with ASTER and IKONOS Data. Master Thesis, Würzburg, Germany.

Crutzen, P.J. & Andreae, M.O., 1990. Biomass burning in the tropics: Impact on atmospheric chemistry and biogeochemical cycles. *Science*, 250, 1669–1678.

Crutzen, P.J. & Goldammer, G.J., 1993. *Fire in the environment: the ecological, atmospheric and climatic importance of vegetation fires.* New York: John Wiley and Sons.

De Santis, A. & Chuvieco, E., 2007. Burn severity estimation from remotely sensed data: performance of simulation versus empirical models. *Remote Sensing of Environment*, 108(4), 422–435.

De Santis, A. & Chuvieco, E., 2009. GeoCBI: A modified version of the Composite Burn Index for the initial assessment of the short-term burn severity from remotely sensed data. *Remote Sensing of Environment*, 113(3), 554–562.

Defries, R.S. & Townshend, J.R., 1999. Global land cover characterization from satellite data: from research to operational implementation. *Global Ecology and Biogeography*, 8(5), 367–379.

Dereix, C. & Amani, N., 1978. Etude de l´action des feux de brousse sur la végétation. Les parcelles feux de Kokondékro: Résultats après quarante ans de traitement. Bouaké: Centre technique forestier tropical de Côte d´Ivoire.

Devineau, J.L., Fournier, A. & Nignan, S., 2010. Savanna fire regimes assessment with MODIS fire data: their relationship to land cover and plant species distribution in western Burkina Faso (West Africa). *Journal of Arid Environments*, 1–10.

Di Gregorio, A., 2005. *Land Cover Classification System - Classification concepts and user manual for Software version 2*. FAO, Rome, Italy.

Dugué, P., Koné, F.P. & Koné, G., 2003. Natural resource management and evolution of farming systems in the savannahs of Côte d´Ivoire. Consequences for the development of agricultural policies. *Cahiers Agricultures*, 12(4), 267–273.

Dwyer, E. et al., 1999. Characterization of the spatio-temporal patterns of global fire activity using satellite imagery for the period April 1992 to March 1993. *Journal of Biogeography*, 27(1), 57–69.

Dwyer, E., Grégoire, J.M. & Malingreau, J.P., 1998. A global analysis of vegetation fires: spatial and temporal dynamics. *Ambio*, 27(3), 175–181.

Dwyer, E., Pinnock, S. & Grégoire, J.M., 2000. Global spatial and temporal distribution of vegetation fire as determined from satellite observations. *International Journal of Remote Sensing*, 21(6-7), 1289–1302.

Dyer, R. et al., 2001. Using fire to manage savanna. In R. Dyer et al. *Savanna burning*. Darwin: Tropical Savannas CRC, pp. 50–80.

ERDAS Incorporation, 1997. *ERDAS Field Guide, Fourth Edition,* Revised and Expanded. Atlanta.

Epting, J., Verbyla, D. & Sorbel, B., 2005. Evaluation of remotely sensed indices for assessing burn severity in interior Alaska using Landsat TM and ETM+. *Remote Sensing of Environment*, 96(3-4), 328–339.

Eva, H. & Lambin, E.F., 1998. Remote Sensing of Biomass Burning in Tropical Regions: Sampling issues and multisensor Approach. *Remote Sensing of Environment*, 64, 292–315.

Eva, H.D., Brink, A. & Simonetti, D., 2006. Monitoring land cover dynamics in sub-saharan Africa. Ph. D. thesis, Ispra, Italy.

FAO, 2001. State of the world´s forests. Rome, Italy, 13.

Fischer, F. & Linsenmair, K.E., 2001. Decreases in ungulate population densities. Examples from the Comoé National Park, Ivory Coast. *Biological Conservation*, 101, 131–135.

Fraser, R.H., Li, Z. & Cihlar, J., 2000. Hotspot and NDVI differencing synergy (HANDS): a new technique for burned area mapping over boreal forest. *Remote Sensing of Environment*, 74(3), 362–376.

Friedl, M.A. et al., 2002. Global land cover mapping from MODIS: algorithms and early results. *Remote Sensing of Environment*, 83(1-2), 287–302.

Fritz, S. et al., 2004. A new land-cover map of Africa for the year 2000. *Journal of Biogeography*, 861–877.

Fritz, S. et al., 2003. *Harmonisation, mosaicing and production of the Global Land Cover 2000 database (Beta version)*. European communities, Luxembourg.

GLCF, 2010. Global Land Cover Facility. *Available at: http://www.landcover.org/data/.*

García-Haro, F.J., Gilbert, M.A. & Melia, J., 2001. Monitoring fire-affected areas using Thematic Mapper data. *International Journal of Remote Sensing*, 44(4), 533–549.

Giglio, L. & Justice, C., 2006. Collection 5 change summary: MODIS Active Fire Algorithm and Products.

Giglio, L. et al., 2003. An Enhanced Contextual Fire Detection Algorithm for MODIS. *Remote Sensing of Environment*, 87(2-3), 273–282.

Giglio, L., 2005. *MODIS Collection 4 Active Fire Product User's Guide*. NASA, *Science Systems and Applications, Inc., Version 2*.

Giglio, L., 2007. *MODIS Collection 4 Active Fire Product User's Guide*. NASA, *Science Systems and Applications, Inc., Version 2*.

Giglio, L., 2010. *MODIS Collection 5 Active Fire Product User´s Guide*. NASA, *Science Systems and Applications, Inc., Version 2.4*.

Goldammer, G.J. & de Ronde, C., 2004. *Wildland Fire Management, Handbook for Sub-Sahara Africa*. Germany, Global Fire Monitoring Center (GFMC).

Grégoire, J.M. & Simonetti, D., 2007. *Dynamique des brulis dans le Parc Régional du W, le Parc National de la Boucle de la Pendjari et la Réserve d´Arly. Implications pour la gestion de ces aires protégés*. European Communities, Luxembourg.

Grégoire, J.M. & Simonetti, D., 2010. Interannual changes of fire activity in the protected areas of the SUN Network and other parks and reserves of the West and Central Africa region derived from MODIS observations. *Remote Sensing*, 2, 446–463.

Grégoire, J.M., Tansey, K. & Silva, J.M., 2003. The GBA2000 initiative: developing a global burnt area database from SPOT-VEGETATION imagery. *International Journal of Remote Sensing*, 24(6), 1369–1376.

Hansen, M.C. & Reed, B., 2000. A comparison of the IGBP DISCover and University of Maryland 1 km global land cover products. *International Journal of Remote Sensing*, 21(6), 1365–1373.

Hao, W.M. & Liu, M.H., 1994. Spatial and temporal distribution of tropical biomass burning. *Global Biogeochemical Cycles*, 8, 495–503.

Hao, W.M. et al., 1991. Emissions of nitrous oxide from the burning of biomass in an experimental system. *Geophysical Research Letters*, 18(6), 999–1002.

Hawbaker, T.J. et al., 2008. Detection rates of the MODIS active fire product in the United States. *Remote Sensing of Environment*, 112, 2656–2664.

Herold, M. et al., 2008. Some challenges in global land cover mapping: An assessment of agreement and accuracy in existing 1 km datasets. *Remote Sensing of Environment*, 112, 2538–2556.

Houghton, R., Hackler, J.L. & Lawrence, K.T., 1999. The U. S. carbon budget: contributions from land-use change. *Science*, 285, 574–578.

Jensen, J.R., 2005. *Introductory digital image processing: a remote sensing perspective*, 3 ed., New York, Prentice Hall.

Jensen, J.R., 2000. *Remote sensing of the environment: an earth resource perspective*. U.S.A, Prentice Hall.

Joyce, R.J. et al., 2004. CMORPH: A Method that Produces Global Precipitation Estimates from Passive Microwave and Infrared Data at High Spatial and Temporal Resolution. *Hydrometeorology, 5*, 487–503.

Justice, C. et al., 2006. *Algorithm technical background document: MODIS Fire products. MODIS ATBD. Version 2.*

Justice, C.O. et al., 2002. An overview of MODIS Land data processing and product status. *Remote Sensing of Environment*, 83(1-2), 3–15.

Justice, C.O. et al., 2000. The MODIS fire products. *Remote Sensing of Environment*, 83(1-2), 244–262.

Justice, C.O. et al., 1998. The Moderate Resolution Imaging Spectroradiometer (MODIS): Land remote sensing for Global Change Research. *IEEE Transactions on Geosciences and Remote Sensing*, 36(4), 1228–1249.

Kassa, D.B., 2008. Ecologie, éthologie, utilisation de l´espace et dynamique des populations de Waterbuck (Kobus ellipsiprymnus defassa) dans la réserve de Biosphére de la Pendjari, Benin. Ph. D. thesis, Abomey Calavi, Benin.

Kauffman, J. et al., 1998. Smoke, clouds and radiation-Brazil (SCAR-B) experiment. *Journal of Geophysical Research*, 103(D24), 31,783–31,808.

Kauffman, J.Y., Tucker, C.J. & Fung, Y.I., 1989. Remote sensing of biomass burning in the tropics. *Adv. Space Res.*, 9(7), (7)265– (7)268.

Kaufman, Y.J. et al., 1998. Potential global fire monitoring from EOS-MODIS. *Journal of Geophysical Research*, 103, 32215–32238.

Keeley, J.E., 2009. Fire intensity, fire severity and burn severity: a brief review and suggested. *International Journal of Wildland Fire*, 18(1), 116–126.

Keene, W.C. et al., 2006. Emissions of major gaseous and particulate species during experimental burns of southern African biomass. *Journal of geophysical research*, 111, 1–18.

Kerr, J.T. & Ostrovsky, M., 2003. From space to species: ecological applications for remote sensing. *TRENS in Ecology and Evolution*, 18(6), 299–305.

Key, C.H. & Benson, N.C., 1999. Measuring and remote sensing of burn severity: the CBI and NBR. In *Poster abstract. In L. F. Neuenschwander and K. C. Ryan (Eds.), Proceedings Joint Fire Fire Science Conference and Workshop, Vol.II, Boise; id; 15-17 June 1999*. University of Idaho and International Association of Wildland Fire, pp. 284.

Key, C.H. et al., 2002. The normalized burn ratio and relationships to burn severity: Ecology, remote sensing and implementation. In J. D. Greer *In: Rapid Delivery of Remote Sensing Products; Proceedings of the Ninth Forest Service Remote Sensing Applications Conference*. San Diego: American Society of Photogrammetry and Remote Sensing, Bethesda, MD.

Key, C.H., 2005. Remote sensing sensitivity to fire severity and fire recovery. In *In J. de la Riva and E. Chuvieco, eds.2005. Proceedings of the 5th International Workshop on remote sensing and GIS applications to forest fire management: Fire effects assessment*. Spain: 29-39 Universidad de Zaragoza.

Kokaly, R.F. et al., 2007. Characterization of post-fire surface cover, soils, and burn severity at the Cerro Grande Fire, New Mexico, using hyperspectral and multispectral remote sensing. *Remote Sensing of Environment*, 106(3), 305–325.

Lacaux, J. et al., 1992. Biogenic emissions and biomass burning influences on the chemistry of the fogwater and stratiform precipitations in the African equatorial forest. *Atmospheric Environment*, 26A(4), 541–551.

Lalayé, P., 2001. La faune halieutique de la riviére Pendjari. CENAGREF, Projet Pendjari/GTZ, Cotonou, Benin.

Landmann, T., 2003. A case study for Skukuza: Estimating biophysical properties of fires using EOS-MODIS satellite data. Ph. D. thesis, Göttingen, Germany.

Landsberg, R., 1997. The use of fire as a management tool in the semi-arid tropics: a producer´s perspective. In B. J. McKaige, R. J. Williams, & W. M. Waggitt *In Bushfire´97*. Darwin: CSIRO, pp. 221–226.

Laris, P., 2002. Burning the Seasonal Mosaic: Preventative burning strategies in the Wooded Savanna of Southern Mali. *Human Ecology*, 30(2), 1–32.

Latifovic, R. et al., 2004. Land cover mapping of North and Central America: Global land cover 2000. *Remote Sensing of Environment*, 89(1), 116–127.

Lerebours, A.P. & Ménager, M.T., 2001. *Africa Atlases: Burkina Faso. 2nd edition.* Paris: Les éditions J.A aux éditions du Jaguar.

Lillesand, T.M. & Kiefer, R.W., 2000. *Remote sensing and image interpretation. 4th edition.* New York: John Wiley & Sons, Inc.

Lillesand, T.M., Kiefer, R.W. & Chipman, J.W., 2004. *Remote sensing and image interpretation. 5th edition.* United States of America: John Wiley & Sons.

Loveland, T.R. et al., 2000. Development of a global land cover characteristics database and IGBP DISCover from 1 km AVHRR data. *International Journal of Remote Sensing*, 21(6), 1303–1330.

Lu, D. & Weng, Q., 2007. A survey of image classification methods and techniques for improving classification performance. *International Journal of Remote Sensing*, 28(5), 823–870.

Mayaux, P. et al., 2003. *A land cover map of Africa/Carte de l´occupation du sol de l´Afrique*, Luxembourg: European Commision Joint Research Centre.

Menaut, J.C. et al., 1991. Biomass burning in West African savannas. In J. S. Levine *Global Biomass Burning*. Cambridge: MIT-Press, pp. 133-143.

Mensah, G. et al., 2006. Inventaire des mammifères rongeurs et des reptiles dans la Réserve de Biosphère de la Pendjari. Rapport technique final. DPNP/ProCGRN/GTZ, Benin.

Mensah, G. et al., 2007. Inventaire des mammifères rongeurs et des reptiles dans la Réserve de Biosphère de la Pendjari. GFA/GTZ/ProCGRN, Benin.

Miller, H.J. & Yool, S.R., 2002. Mapping forest post-fire canopy consumption in several overstory types using multi-temporal Landsat TM and ETM data. *Remote Sensing of Environment*, 82(2-3), 481–496.

Monnier, Y., 1990. *La poussière et la cendre : Paysages, dynamique des formations végétales et stratégies des sociétés en Afrique de l´Ouest.* 2eme édition., Paris, Ministère de la coopération et du Développement.

Morisette, J., Privette, J.L. & Justice, C.O., 2002. A framework for the validation of MODIS Land products. *Remote Sensing of Environment*, 83(1-2), 77–96.

NASA, 2010. ASTER. Available at: http://asterweb.jpl.nasa.gov/.

NASA, 2010. LANDSAT 7. Available at: http://geo.arc.nasa.gov/sge/landsat/l7.html.

NASA, 2010. MODIS Rapid Response System Global Fire Maps. Available at: http://rapidfire.sci.gsfc.nasa.gov/firemaps/.

NASA, 2010. USGS Global Visualization Viewer. Available at: http://glovis.usgs.gov/.

NASA, 2010. Warehouse Inventory Search Tool (WIST). Available at: https://wist.echo.nasa.gov/~wist/api/imswelcome/.

Nago, S.G., Rodel, M. & Sinsin, B., 2006. Etablissement d´une base de données d´utilisation des amphibiens. *Pendjari*, 1, 13–14.

Nielsen, T.T. & Rasmussen, K., 2001. Utilization of NOAA AVHRR for assessing the determinants of savanna fire distribution in Burkina Faso. *International Journal of Wildland Fire*, 10(2), 129–135.

N´Klo, O., 2001. Situation des ressources génétiques forestiéres de la Côte d´Ivoire (zone de savanes). 1–47.

Ouédraogo, P., 1999. Inventaire de la diversité biologique du Sahel Burkinabè. Maitrise, Ouagadoudou, Burkina Faso

Paeth, H. & Hense, A., 2005. Mean versus extreme climate in the Mediterranean region and its sensitivity to future global warming conditions. *Meteorologische Zeitschrift*, 14(3), 329–347.

Paré, E., 1992. Maitriser les feux : Tous les feux n´ont pas la même signification. *Agripromo*, 76, 11–12.

Roques, K., O´Connor, T. & Watkinson, A.R., 2001. Dynamics of shrub encroachment in an African savanna: relative influences of fire, herbivory, rainfall and density dependence. *Journal of Applied Ecology*, 38(2), 268–280.

Roy, D.P. & Landmann, T., 2005. Characterizing the surface heterogeneity of fire effects using multi-temporal reflective wavelength data. *International Journal of Remote Sensing*, 26(19), 4197–4218.

Roy, D.P. et al., 2002. The MODIS land product quality assessment approach. *Remote Sensing of Environment*, 83(1-2), 62–76.

Roy, D.P., Boschetti, L. & Trigg, S.N., 2006. Remote sensing of fire severity: Assessing the performance of the Normalized Burn Ratio. *IEEE Geosciences and Remote Sensing Letters*, 3(1), 112–116.

Roy, D.P., Lewis, P.E. & Justice, C.O., 2002. Burned area mapping using multi-temporal moderate spatial resolution data—a bi-directional reflectance model-based expectation approach. *Remote Sensing of Environment*, 83(1-2), 263–286.

Sankaran, M., Ratnam, J. & Hanan, N.P., 2004. Tree–grass coexistence in savannas revisited – insights from an examination of assumptions and mechanisms invoked in existing models. *Ecology Letters*, 7(6), 480–490.

Schmitz, A., 1996. *Controle et utilisation du feu en zones arides et subhumides africaine.* Cahier FAO: Conservation.

Scholes, R. & Archer, S., 1997. Tree-grass interactions in savannas. *Forest Science*, 28, 517–544.

Scott, A.C. & Glasspool, I.J., 2006. The diversification of Paleozoic fire systems and fluctuations in atmospheric oxygen concentration. *PNAS*, 103(29), 10861–10865.

Shaner, J. & Wrightsell, J., 2000. *Editing in ArcMap*, United States of America: ESRI.

Sonko, I., 2000. Etude des effets de différents regimes de feux sur la dynamique de la flore et de la végétation ligneuses des plateaux du Parc National du Niokolo-Koba (Sud-Est du Sénégal). Ph. D. thesis, Dakar, Senegal.

Soverel, N.O., Perrakis, D.D. & Coops, N.C., 2010. Estimating burn severity from Landsat dNBR and RdNBR indices across western Canada. *Remote Sensing of Environment*, 114(9), 1896–1909.

Stott, P., 1991. Recent trends in the ecology and management of the world´s savanna formations. *Progress in Physical Geography*, 15(18), 1–12.

Tansey, K. et al., 2004. Vegetation burning in the year 2000: Global burned area estimates from SPOT VEGETATION data. *Journal of Geophysical Research*, 109(D14S03), 22.

Tehou, A., 2007. Evaluation: Campagne d´incinération 2006-2007. Pendjari, Benin.

Tehou, A., 2003. Evaluation: Rapport de la campagne d´incinération 2002-2003. Pendjari, Benin.

Tehou, A., 2005. Evaluation: Rapport de la campagne d´incinération 2004-2005. Pendjari, Benin.

Tehou, A., 2006. Evaluation: Rapport de la campagne d´incinération 2005-2006. Pendjari, Benin.

Thonicke, K. et al., 2001. The role of fire disturbance for global vegetation dynamics: coupling fire into a dynamic global vegetation model. *Global Ecology and Biogeography*, 10, 661–677.

Tilman, D. et al., 2000. Fire suppression and ecosystem carbon storage. *Ecology*, 81(10), 2680–2685.

Traoré, N., 2009. *Etude sur le cadre de gestion environnementale et sociale (CGES). Abidjan, Ministère des mines et de l´énergie*.

Trollope, W., De Ronde, C. & Geldenhuys, C.J., 2004. Fire behaviour. In J. G. Goldammer & C. De Ronde *Wildland fire management: Handbook for Sub-Sahara Africa*. Global Fire Monitoring Center (GFMC), pp. 27–59.

UNESCO, 2010. List of World Heritage in Danger. *UNESCO Publishing*. Available at http://whc.unesco.org/en/danger/.

Van Der Werf, G. et al., 2003. Carbon emissions from fires in tropical and subtropical ecosystems. *Global Change Biology*, 9, 547–562.

Van Wagtendonk, J.W., Root, R.R. & Key, C.H., 2004. Comparison of AVIRIS and Landsat ETM+ detection capabilities for burn severity. *Remote Sensing of Environment*, 92(3), 397–408.

Walz, Y. et al., 2007. Classification of burn severity using Moderate Resolution Imaging Spectroradiometer (MODIS): A case study in the jarrah-marri forest of southwest Western Australia. *Journal of Geophysical Research*, 112(G02002), 1–14.

Walz, Y., 2004. Measuring burn severity in forests of south-west western Australia Using MODIS. Master-Thesis, Würzburg, Germany.

Ward, D.E. et al., 1996. Effect of fuel composition on combustion efficiency and emission factors for African savanna ecosystems. *Journal of Geophysical Research*, 101(D19), 23569–23576.

Whelan, R.J., 1995. *The Ecology of fire. 1st edition*. United Kingdom, USA: Cambridge University Press.

Williams, D. & Cook, G., 2001. Savanna landscapes. In R. Dyer et al. *Savanna burning*. Darwin: Tropical Savannas CRC, pp. 5–14.

Yahmed, D., 2005. *Atlas de l´Afrique: Atlas du Burkina Faso*. Paris, Les éditions J.A aux éditions du Jaguar.

Zhu, Z. et al., 2006. Evaluate sensitivities of burn severity mapping algorithms for different ecosystems and fire histories in the United States. Final Report to the Joint Fire Science Program.

APPENDIX

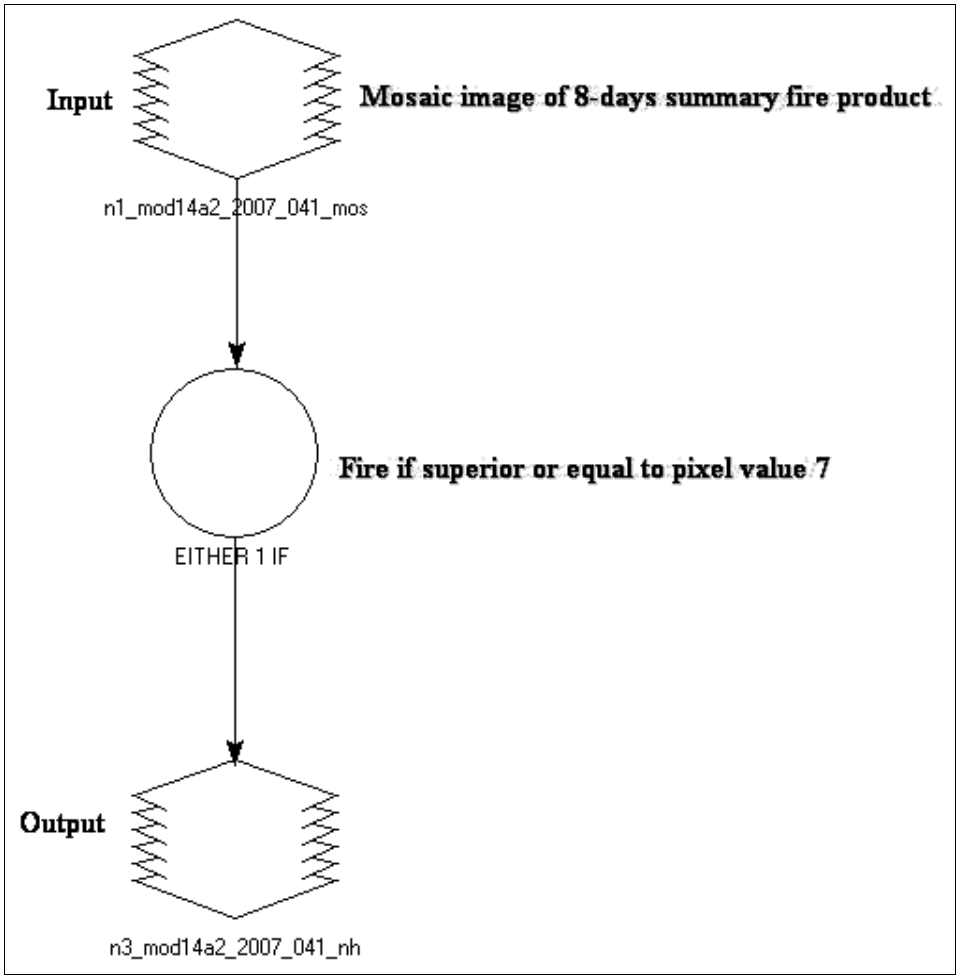

Appendix 1: Model of extraction of three confidence classes of fire pixels: Low-nominal and high confidence levels detected by MODIS.

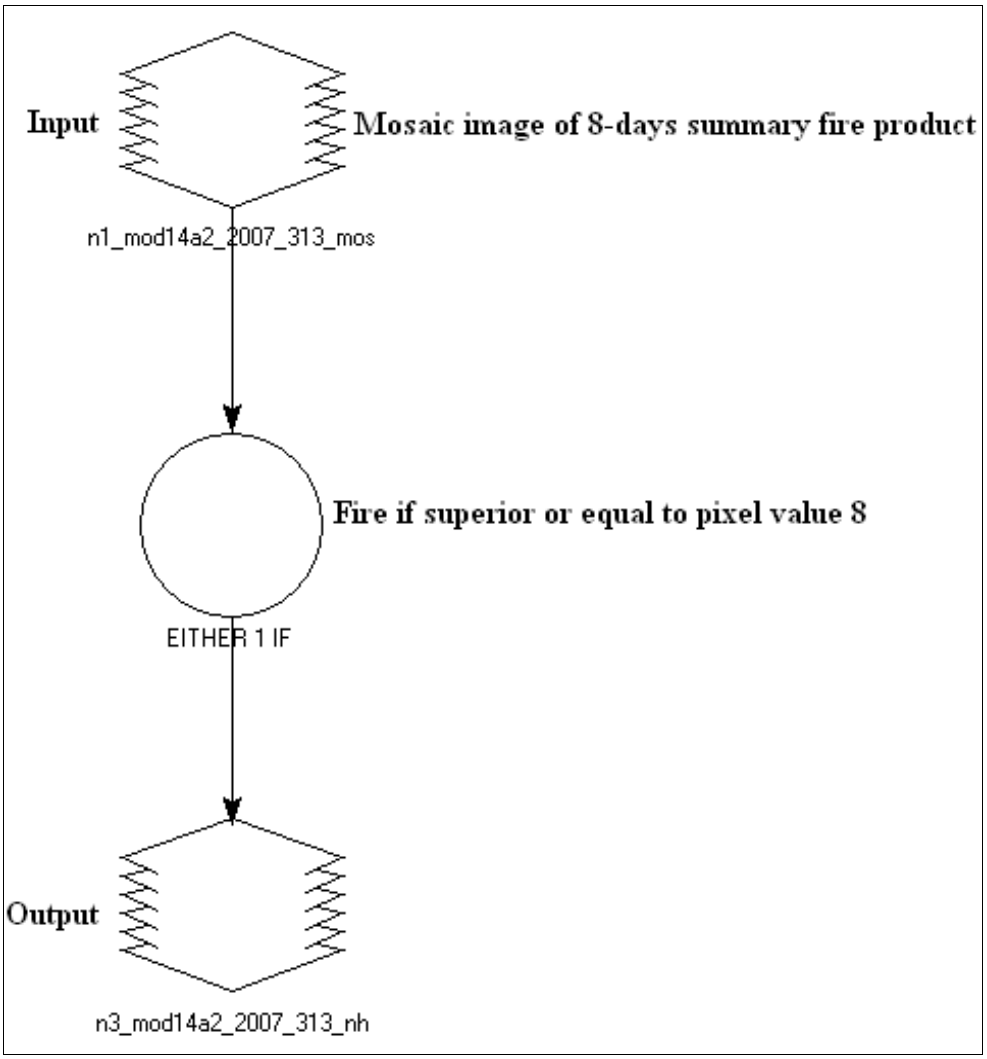

Appendix 2: Model for the extraction of two confidence classes of fire pixels: Nominal and high confidence levels detected by MODIS.

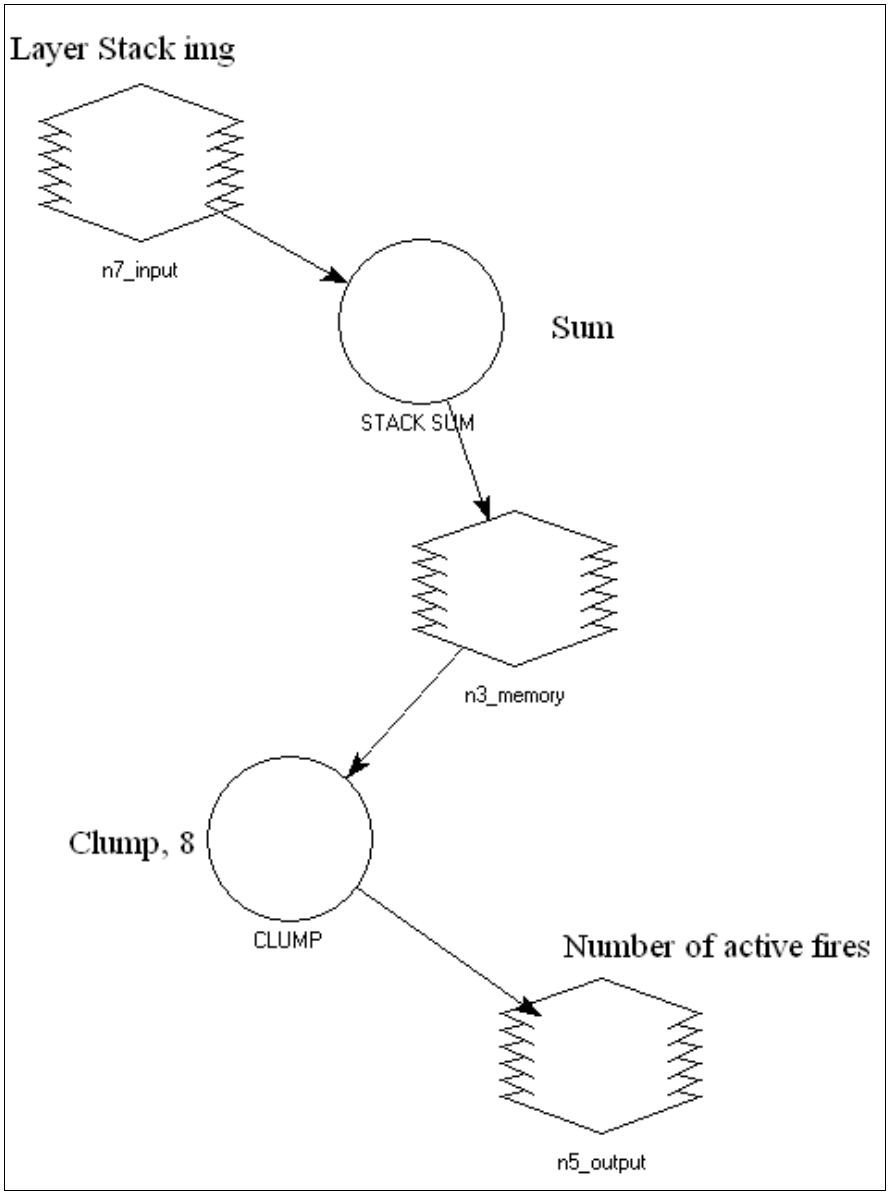

Appendix 3: Model for the extraction of the Number of active fires detected by MODIS.

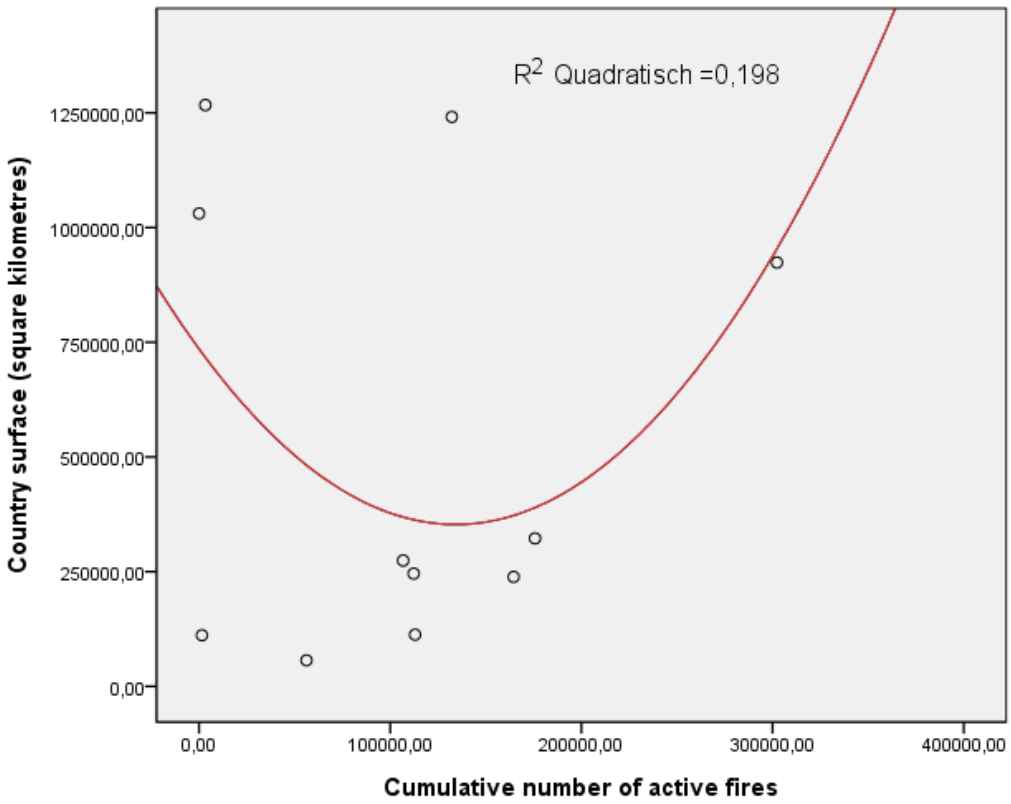

Appendix 4: Curve of correlation between the surface of the country (in km^2) and the cumulative number of fires detected during the observation period (2000-2009).

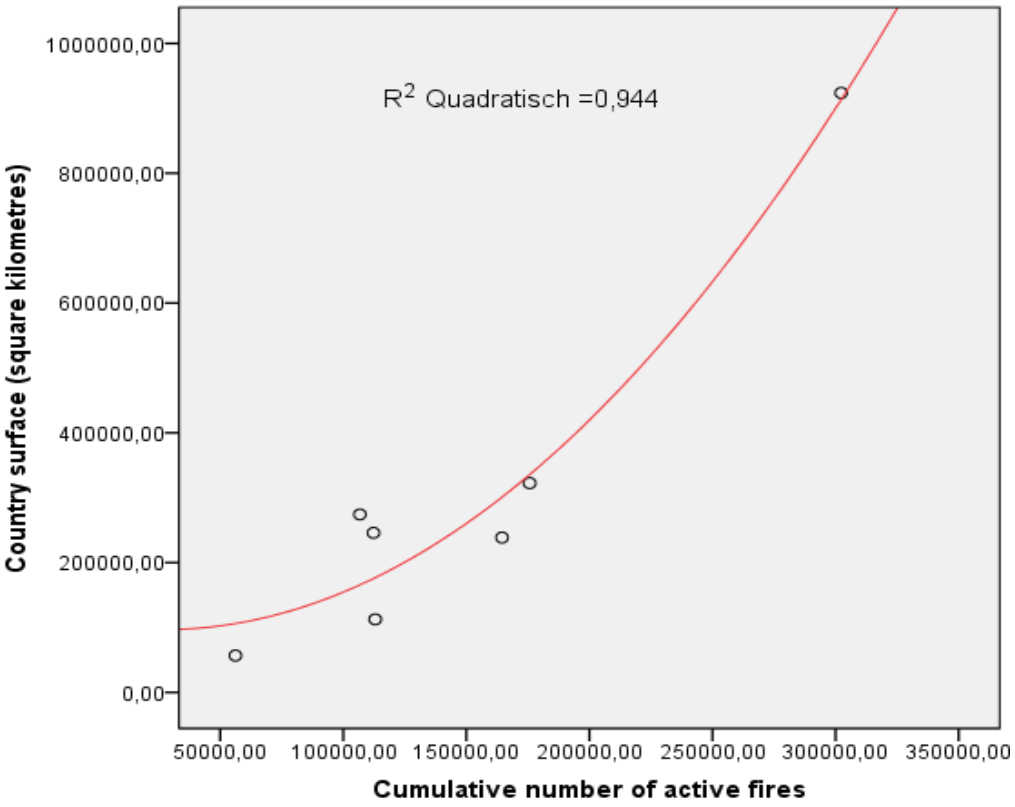

Appendix 5: Curve of correletion between the countries of which 2/3 of the surface are located in savanna zones and the cumulative number of fires detected in them during the observation period (2000-2009).

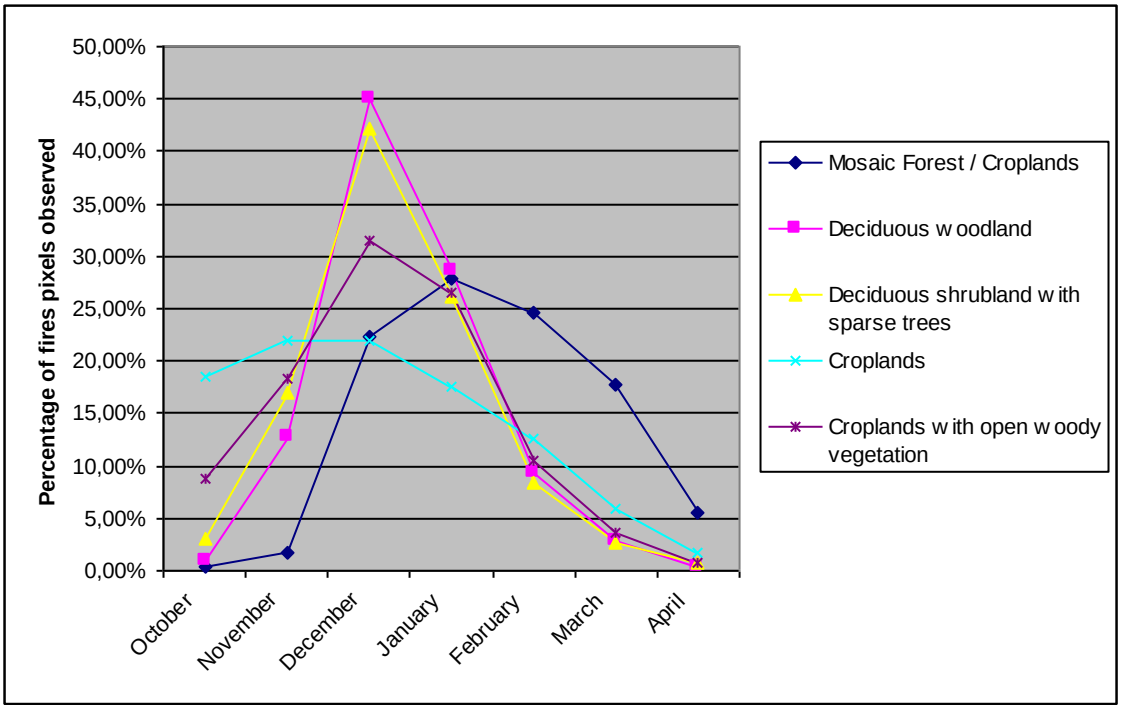

Appendix 6: Seasonal distribution of fire pixels in vegetation types mainly affected by fire occurrence, as detected by MODIS sensors (2000-2009).

Appendix 7: GPS sampling points and the descriptions of the field observations in Pendjari National Park related to ΔNBR value. The ΔNBR image was derived from Landsat ETM+ scenes (Pendjari National Park) of NBR 5th October 2007 as pre-fire and 26th February 2008 as post-fire. The visually assessed combusted biomass in field varied between 0% (no burn) and 100% (no vegetation remained after the passage of the fire). In this table, for every waypoint, identified by a number and its location (latitude and longitude), the estimated biomass loss in the immediate surroundings of this point is given. These waypoints are projected onto the ΔNBR image in order to compare the ΔNBR value and the estimated biomass loss for each point.

TYPE	IDENT	LATITUDE	LONGITUDE	Estimated biomass loss (%)in field	ΔNBR value
Waypoint	1	10,905805	1,442072	80	0.617898
Waypoint	2	10,905747	1,44225	70	0.65
Waypoint	5	10,890769	1,423497	55	0.588235
Waypoint	6	10,891	1,423229	62.5	0.602035
Waypoint	8	10,891302	1,422772	70	0.624966
Waypoint	13	10,86878	1,409008	40	0.472126
Waypoint	14	10,868679	1,409332	50	0.56875
Waypoint	15	10,868583	1,409521	35	0.408103
Waypoint	16	10,868387	1,409756	40	0.46875
Waypoint	21	10,858892	1,396428	50	0.541597
Waypoint	23	10,858544	1,396156	55	0.597619
Waypoint	24	10,858319	1,395939	53.5	0.578476
Waypoint	25	10,871191	1,379348	70	0.654503
Waypoint	26	10,871479	1,379377	80	0.664316
Waypoint	27	10,87172	1,379417	90	0.712092
Waypoint	28	10,872188	1,37965	95	0.704031

Waypoint	29	10,873665	1,375751	100	0.719298
Waypoint	30	10,873896	1,375958	95	0.705656
Waypoint	31	10,874175	1,376048	98	0.698028
Waypoint	32	10,874482	1,376228	98	0.719298
Waypoint	34	10,891009	1,351059	60	0.630339
Waypoint	35	10,891217	1,351186	60	0.598843
Waypoint	36	10,891466	1,35146	50	0.593337
Waypoint	37	10,892839	1,34412	90	0.690759
Waypoint	38	10,89259	1,343908	95	0.686959
Waypoint	39	10,892269	1,343709	94	0.691256
Waypoint	40	10,89209	1,343551	90	0.67619
Waypoint	43	10,89612	1,338338	50	0.688214
Waypoint	44	10,896291	1,338405	50	0.697298
Waypoint	45	10,905518	1,310477	55	0.501045
Waypoint	46	10,905261	1,310506	90	0.604545
Waypoint	53	10,919359	1,292956	70	0.633691
Waypoint	55	10,918983	1,292675	90	0.65384
Waypoint	56	10,918833	1,29255	55	0.598673
Waypoint	57	10,922115	1,28939	50	0.593616
Waypoint	59	10,921789	1,28952	70	0.634273
Waypoint	60	10,922261	1,290055	80	0.621118
Waypoint	65	10,939188	1,266752	55	0.581436
Waypoint	66	10,938981	1,266601	50	0.570378
Waypoint	67	10,938677	1,266343	60	0.597701
Waypoint	70	10,944572	1,259318	65	0.603994
Waypoint	71	10,944352	1,259206	50	0.569817
Waypoint	72	10,944236	1,258844	60	0.63063
Waypoint	81	11,197973	1,506411	50	0.559569
Waypoint	83	11,198168	1,506816	65	0.635781
Waypoint	84	11,198218	1,507144	70	0.649572
Waypoint	89	11,183914	1,507078	45	0.567346
Waypoint	90	11,18384	1,506832	45	0.576391
Waypoint	92	11,18374	1,506454	50	0.586666
Waypoint	97	11,162749	1,507344	85	0.658496
Waypoint	98	11,16266	1,507114	75	0.657864
Waypoint	99	11,162668	1,506827	75	0.670814
Waypoint	100	11,162723	1,506616	75	0.660053
Waypoint	101	11,153929	1,514744	50	0.535374
Waypoint	102	11,153991	1,515019	90	0.614502
Waypoint	104	11,154205	1,515482	55	0.587254
Waypoint	109	11,126953	1,512627	35	0.43307
Waypoint	110	11,126941	1,512932	40	0.489639
Waypoint	111	11,126906	1,513202	50	0.511431
Waypoint	112	11,126946	1,513467	40	0.485074
Waypoint	117	11,077987	1,491403	50.5	0.541321
Waypoint	118	11,077662	1,491501	55.5	0.609519
Waypoint	120	11,077414	1,491045	55.5	0.612092
Waypoint	121	11,067931	1,499498	40	0.601767
Waypoint	122	11,067812	1,499175	40	0.550313
Waypoint	130	11,046708	1,527458	45	0.632352
Waypoint	131	11,046554	1,527301	35	0.590253
Waypoint	133	11,016394	1,55216	55	0.533399
Waypoint	134	11,016559	1,552317	55	0.612825

Waypoint	136	11,01683	1,552691	55	0.573913
Waypoint	146	10,954708	1,543152	40	0.50238
Waypoint	147	10,954748	1,543042	40	0.50238
Waypoint	148	10,954819	1,54271	45	0.539823
Waypoint	149	11,003095	1,559646	50	0.589552
Waypoint	152	11,003367	1,558979	50	0.583869
Waypoint	153	11,024419	1,544366	50	0.497136
Waypoint	161	11,048666	1,493251	25	0.36772
Waypoint	162	11,048857	1,492982	30	0.368851
Waypoint	163	11,049133	1,492881	32.5	0.388574
Waypoint	164	11,049252	1,492612	40	0.396424
Waypoint	169	11,040216	1,479007	90	0.629006
Waypoint	170	11,040473	1,479152	50	0.637592
Waypoint	172	11,040787	1,479435	50	0.610109
Waypoint	177	11,035137	1,461656	65	0.622742
Waypoint	178	11,034899	1,461786	65	0.594888
Waypoint	180	11,034346	1,461874	65	0.594043
Waypoint	181	11,030562	1,449569	90	0.643638
Waypoint	182	11,030766	1,449323	90	0.673675
Waypoint	183	11,031003	1,449088	90	0.630066
Waypoint	185	11,041165	1,325116	60	0.570475
Waypoint	186	11,041419	1,325055	50	0.566662
Waypoint	188	11,041869	1,325044	40	0.512298
Waypoint	190	11,035878	1,33857	60	0.591393
Waypoint	192	11,03561	1,338755	80	0.616484
Waypoint	196	11,034666	1,347717	50	0.554096
Waypoint	197	11,023949	1,373625	55	0.612605
Waypoint	198	11,023753	1,37338	50	0.595311
Waypoint	199	11,023507	1,373258	55	0.616218
Waypoint	204	11,408603	1,586362	30	0.454263
Waypoint	205	11,380979	1,592464	35	0.467502
Waypoint	213	11,345557	1,611708	40	0.521155
Waypoint	214	11,34565	1,611985	40	0.521825
Waypoint	217	11,320114	1,593602	50	0.588766
Waypoint	219	11,320274	1,593182	45	0.556125
Waypoint	220	11,320425	1,592937	45	0.505079
Waypoint	224	11,276831	1,570054	40	0.482628
Waypoint	225	11,252355	1,557928	40	0.56554
Waypoint	226	11,252202	1,558108	45	0.558823
Waypoint	227	11,252105	1,558346	50	0.584565
Waypoint	261	11,09191	1,737483	50	0.56018
Waypoint	264	11,203206	1,496279	55	0.606603
Waypoint	265	11,201675	1,486644	40	0.578947
Waypoint	266	11,202769	1,473292	50	0.508586
Waypoint	267	11,2073	1,46463	80	0.688533
Waypoint	268	11,218073	1,456746	50	0.544459
Waypoint	269	11,225639	1,442336	50	0.542748
Waypoint	270	11,227936	1,416599	50	0.552514
Waypoint	271	11,240826	1,408953	20	0.264705
Waypoint	272	11,257028	1,396693	50	0.54074
Waypoint	273	11,274173	1,380807	90	0.630512
Waypoint	274	11,296651	1,380742	45	0.460575
Waypoint	275	11,299393	1,369867	50	0.550766

Waypoint	277	11,309943	1,356845	40	0.453853
Waypoint	278	11,320112	1,354487	25	0.395284
Waypoint	279	11,328358	1,344924	25	0.364093
Waypoint	288	11,169101	1,169914	50	0.513688
Waypoint	290	11,169141	1,169451	40	0.496471
Waypoint	291	11,169226	1,16923	40	0.486333
Waypoint	293	11,172938	1,170343	50	0.505038
Waypoint	294	11,173193	1,169999	35	0.477894
Waypoint	295	11,173276	1,169755	50	0.530443
Waypoint	300	11,1853	1,170108	45	0.503418
Waypoint	302	11,185532	1,17059	50	0.520839
Waypoint	304	11,213931	1,168052	55	0.576193
Waypoint	305	11,213806	1,16832	55	0.570318
Waypoint	306	11,213774	1,168664	55	0.583424
Waypoint	308	11,221114	1,170179	50	0.622962
Waypoint	309	11,221147	1,170451	50	0.549045
Waypoint	310	11,221298	1,170716	50	0.579822
Waypoint	313	11,228498	1,16774	70	0.607323
Waypoint	314	11,228315	1,167575	70	0.631028
Waypoint	315	11,228287	1,16732	70	0.635386
Waypoint	316	11,233381	1,166681	30	0.44488
Waypoint	317	11,233241	1,166371	30	0.431629
Waypoint	318	11,233225	1,16622	25	0.416128
Waypoint	321	11,23743	1,165571	50	0.535344
Waypoint	324	11,237293	1,165019	40	0.490068
Waypoint	326	11,247639	1,174791	45	0.493325
Waypoint	328	11,248007	1,174512	35	0.498539

ERKLÄRUNG

Hiermit versichere ich, dass ich die vorliegende Dissertation „Satellitengestützte Kartierung der Verteilung von Buschfeuern und ihrer Auswirkung auf die Vegetation in Westafrika“ selbständig verfasst habe und keine anderen als die von mir vollständig angegebenen Quellen und Hilfsmittel benutzt habe. Sie wurde an keiner anderen Hochschule als Dissertation eingereicht und wurde auch nicht an anderer Stelle veröffentlicht.

Zudem erkläre ich, daß diese Dissertation weder in gleicher noch in anderer Form bereits in einem Prüfungsverfahren vorgelegen hat.

Ich habe früher außer den mit dem Zulassungsgesuch urkundlich vorgelegten Graden keine weiteren akademischen Grade erworben oder zu erwerben versucht.

Würzburg, den 30.09.2010 Noëllie Rüth geb. Yao